DISSERTATION

ARCTIC TUNDRA SHRUB INVASION AND SOOT DEPOSITION: CONSEQUENCES FOR SPRING SNOWMELT AND NEAR-SURFACE AIR TEMPERATURES

Submitted by

John E. Strack

Graduate Degree Program in Ecology

In partial fulfillment of the requirements

For the Degree of Doctor of Philosophy

Colorado State University

Fort Collins, Colorado

Summer 2006

COLORADO STATE UNIVERSITY

May 1, 2006

WE HEREBY RECOMMEND THAT THE DISSERTATION PREPARED UNDER OUR SUPERVISION BY JOHN E. STRACK ENTITLED **ARCTIC TUNDRA SHRUB INVASION AND SOOT DEPOSITION: CONSEQUENCES FOR SPRING SNOWMELT AND NEAR-SURFACE AIR TEMPERATURES** BE ACCEPTED AS FULFILLING IN PART REQUIREMENTS FOR THE DEGREE OF DOCTOR OF PHILOSOPHY.

Committee on Graduate Work

Dr. Michael B. Coughenour

Dr. Richard E. Eykholt

Dr. Glen E. Liston

Dr. Roger A. Pielke Sr., **Adviser**

Dr. Daniel E. Binkley, **Department Head**

ABSTRACT OF DISSERTATION

ARCTIC TUNDRA SHRUB INVASION AND SOOT DEPOSITION: CONSEQUENCES FOR SPRING SNOWMELT AND NEAR-SURFACE AIR TEMPERATURES

Invasive shrubs and soot pollution both have the potential to alter the surface energy balance and timing of snow melt in the Arctic. Shrubs reduce the amount of snow lost to sublimation on the tundra during the winter leading to a deeper end-of-winter snowpack. The shrubs also enhance the absorption of energy by the snowpack during the melt season, by converting incoming solar radiation to longwave radiation and sensible heat. This results in a faster rate of snow melt, warmer near-surface air temperatures, and a deeper boundary layer. Soot deposition lowers the albedo of the snow allowing it to more effectively absorb incoming solar radiation and thus melt faster.

This study uses the Colorado State University Regional Atmospheric Modeling System version 4.4 (CSU-RAMS 4.4), equipped with an enhanced snow model, to investigate the effects of shrub encroachment and soot deposition on the atmosphere and snowpack in the Kuparuk Basin of Alaska during the May-June melt period. The results of the simulations suggest that a complete invasion of the tundra by shrubs leads to a 1.5°C warming of 2-m air temperatures, 17 W m^{-2} increase in surface sensible heat flux,

and a 108 m increase in boundary layer depth during the melt period. The snow free-date also occurred 11 days earlier despite having a larger initial snowpack. The results also show that a decrease in the snow albedo of 0.1, due to soot pollution, caused the snow-free date to occur five days earlier. The soot pollution caused a 0.5°C warming of 2-m air temperatures and a 2 W m^{-2} increase in surface sensible heat flux. In addition, the boundary layer averaged 25 m deeper in the polluted snow simulation.

John E. Strack
Graduate Degree Program in Ecology
Colorado State University
Fort Collins, CO 80523
Summer 2006

ACKNOWLEDGEMENTS

I would like to thank my advisor Dr. Roger Pielke Sr. for his expert guidance during the course of this research. I would also like to thank the other members of my committee, Dr. Glen Liston, Dr. Michael Coughenour, and Dr. Richard Eykholt for their helpful suggestions and comments. Dr. Christopher Hiemstra and Dr. Jeffrey Welker deserve thanks for their help with the FLOSS vegetation measurements. Finally, gratitude is extended to Dr. Larry Mahrt for access to the FLOSS flux data. This work was funded by NASA Fellowship Grant No. NGT5-30527, and NSF Grant No. 0229973.

TABLE OF CONTENTS

LIST OF FIGURES

LIST OF TABLES

Chapter 1

INTRODUCTION

There is growing evidence that the size and number of deciduous shrubs (dwarf birch '*Betula nana*', willow '*Salix* sp.', and green alder '*Alnus crispa*') in arctic Alaska is increasing due to the recent warming in this region (Tape et al. 2006; Sturm et al. 2001a). Through an analysis of numerous aerial photograph pairs similar to the one shown in Figure 1.1, Tape et al. (2006) found an average relative increase in shrub coverage of 33% and 160% for slopes and river terraces/floodplains, respectively, over the past 50 years. In addition, Goetz et al. (2005) have used satellite data to detect an increase in photosynthetic activity in Alaskan and Canadian tundra over the past 22 years.

The coverage of shrubs in this region is very important because of their strong impact on snow distributions. Snow depth is increased significantly in the presence of these shrubs because they reduce the wind speed, which leads to local accumulation of blowing snow. In addition, since snow particles that are captured in these shrub regions are less likely to become airborne, sublimation losses are reduced. Observations by Sturm et al. (2001b) illustrate the effect shrubs have on snow accumulation in the Arctic. The authors took observations of leaf area index (LAI), stem diameter, canopy height, elevation, and snow depth near Happy Valley, Alaska located in the Arctic about half

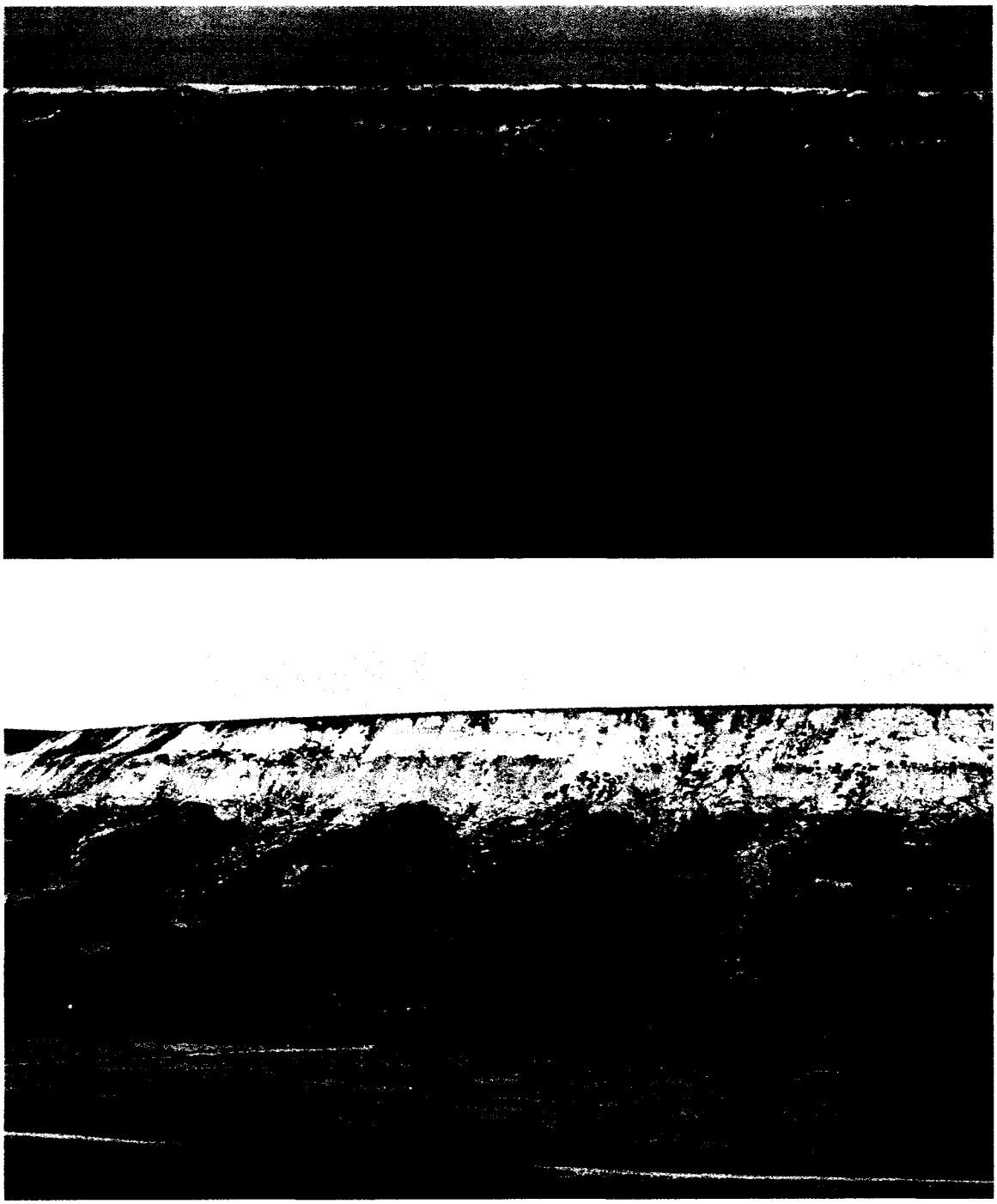

Figure 1.1: Photographic example of shrub expansion on bluffs near Sagwon, Alaska (Latitude: 69.41°N, Longitude 148.61°W). Top photo was taken circa 1950 and bottom photo was taken at same location in 2002 (Sturm and Racine 2005).

way between the Brooks Range and Prudhoe Bay. The snow properties were measured in April 1996 and the vegetation parameters were measured the following July. More details of how the measurements were made can be found in Sturm et al. (2001b). Their analysis showed that the greatest snow depth occurs downwind of the maximum shrub height, while the snow depth was noticeably less in areas removed from shrubs. These results suggest that increasing the area covered by shrubs in arctic Alaska would increase the mass of snow retained through the winter. An example of snow collecting downwind of shrubs at a mid-latitude site is shown in Figure 1.2. Not only do patches of shrubs produce the snow fence effect described above, but large areas of shrubs also trap more snow in their interior due to the general reduction of wind speed beneath the canopy.

Figure 1.2: Snow drifting downwind of shrubs near Saratoga, WY (photo courtesy of Chris Hiemstra).

Some additional light has been shed on the significance of increased shrubs in the Arctic by Liston et al. (2002). They used a blowing snow model along with a simple surface energy balance model to show that increased shrubs over a 4 km^2 domain in arctic Alaska led to significant decreases (68%) in sublimation losses and therefore increases in end-of-winter snow depth. The greater amount of snow retained through the winter then leads to larger runoff magnitudes during the melt period.

Although the effects of increased shrubs on snow distributions and properties has been looked at fairly extensively through both observational and modeling studies very little has been done to investigate the effects on the Arctic atmosphere during the spring melt season. Liston et al. (2002) did not utilize an atmospheric model and so nothing could be determined about the influence of increased shrubs on air temperature and precipitation. Also, the simple surface energy budget model used was not able to represent the shading, longwave, and sensible heat emission effects of the shrubs during the melt season. Emission of longwave radiation and turbulent sensible heat by the shrubs during the spring could cause the snow to melt more rapidly even though it is deeper, which would have a strong impact on the surface energy budget.

There has been a considerable amount of research illustrating how snow can significantly reduce daytime temperatures by as much as 10°C on time scales of days to months (Namias 1985; Cohen and Rind 1991; Baker et al. 1992; Leathers and Robinson 1993; Ellis and Leathers 1998). Snow cover reduces daytime temperatures by increasing the net surface albedo and reducing the maximum attainable surface temperature. First of all, the higher surface albedo reduces the amount of incoming solar radiation that can be absorbed, meaning less energy will be available to heat the surface and nearby air.

Secondly, the temperature of the snow is limited to 0°C or less. Once the snow temperature reaches 0°C the remaining energy can only be used for melting. These two effects combine to produce a surface that is significantly cooler than its snow-free counterpart under the same ambient conditions.

Strack et al. (2003) found, using the Colorado State University Regional Atmospheric Modeling System version 4.3 (CSU-RAMS 4.3.0), that daytime near-surface air-temperatures over snow were increased when the quantity of vegetation protruding through ephemeral snow cover in the Texas Panhandle was increased. The authors of that study found that protruding vegetation increased sensible heat fluxes as much as 80 W m^{-2} and daytime temperatures by as much as 6°C. In addition, they found that afternoon boundary layer height increased as much as 200-300 m.

Sturm et al. (2005) measured incoming and reflected solar radiation over shrubs of various heights during two winter seasons in western Alaska. In order to prevent disturbing the shrubs and vegetation, they mounted pyranometers on 50 m long cables strung across each measurement site. The pyranometers were than pulled back and forth along the cables to obtain average values of incoming and reflected solar radiation for each site. Their observations suggest shrubs protruding through a tundra snowpack reduce the net surface albedo by as much as 30% and can increase absorbed solar radiation up to 75% during the snow season. They mention that this is approximately two thirds as strong as the increase that would be associated with tundra to forest transition.

In addition to examining the effects of shrub increases, the influence of black carbon deposition on spring snow melt is also examined. Black carbon lowers the albedo of the snowpack leading to enhanced absorption of solar radiation. Black carbon

deposition in the Arctic has the potential to increase in future years due to increased human activity (energy extraction and ocean shipping) in the region (Hansen and Nazarenko 2004). Since there has already been pronounced warming at high latitudes, and future warming is expected to be most extreme in these regions, it is of utmost importance to develop a thorough understanding of the processes governing Arctic climate. The modeling work described in this dissertation helps to show the significance of the shrub and black carbon effects at a regional scale. By showing the importance of these processes with relatively little computational expense at the regional scale the importance of including such effects in long-term global climate simulations can be determined.

In order to examine the effects of the shrubs and black carbon, two modeling systems were used in tandem to simulate the accumulation and melt of snow during the winter and spring, as well as atmospheric temperatures during the spring melt period, for three fall-winter-spring seasons in the Kuparuk Basin of Alaska. The blowing snow model, SnowTran-3D (Liston and Sturm 1998a), was utilized to simulate the accumulation period (September-April). The spring melt period (May-June) was simulated using the CSU-RAMS version 4.4 (Cotton et al. 2003), equipped with a modified snowpack model described in more detail in the next chapter.

Before describing in detail the design of the experiment and model configurations, a description of the modified snow model used in RAMS for this study will be given. In addition, descriptions of the testing of this new snow model are included. Chapter 2 contains the new snow model description and the testing of its ability to simulate snow depths. The ability to simulate snow depths is important for this study since snow depth

must be known accurately in order to realistically simulate the amount of protruding shrub. The experiment described in Chapter 2 will show how well the model can simulate snow depth when forced with observed meteorological parameters offline from RAMS. This method removes potential errors introduced from the atmospheric component of RAMS and thus allows for better testing of the snow model component.

Chapter 3 describes a test of the sensible and latent heat fluxes simulated by the new model. The accuracy of these fluxes is important since they communicate the land-surface changes to the atmosphere. The experiment in Chapter 3 will show how well the RAMS land-surface parameterization, equipped with the new snow model, can simulate these fluxes when driven with observed meteorological parameters offline from RAMS. Again, the offline simulation will enable better checking of the land-surface model without the introduction of potential errors from the atmospheric model.

After the new snow model has been described and tested detailed explanations of the project's experimental design, model configurations, and results are given in Chapter 4. Finally, in Chapter 5 a summary and suggestions for future work are given.

Chapter 2

MODIFICATIONS TO THE RAMS SNOW MODEL

2.1 Introduction

The contents of this chapter were previously published in Strack et al. (2004) and have been copyrighted by the American Meteorological Society. Snow cover can significantly influence energy and moisture fluxes between the Earth's surface and the atmosphere. Snow-covered surfaces absorb much less solar radiation than most other natural surfaces. For example, the typical albedo of snow for shortwave radiation ranges from 0.6–0.9, while the albedo for most soils and vegetation is typically less than 0.3 (Pielke 2002). In addition, snow-covered surfaces are limited to a maximum temperature of 0°C. Finally, due to its low thermal conductivity, snow acts as an insulating blanket that decouples the soil and atmosphere.

The strength of these effects depends on the degree to which snow is able to mask the underlying surface (Liston 1995; Strack et al. 2003). When tall vegetation such as shrubs or trees protrude through the snowpack, it absorbs more solar radiation and warms relative to the surrounding snow, thus providing a boundary layer heat source (see Figure 2.1). To determine the degree of masking by snow, both vegetation height and snow depth must be known. Knowing the correct snow depth is most critical for regions where fluctuations in snow depth lead to significant fluctuations in the amount of protruding

vegetation. This occurs when the winter snowfall leads to snow accumulations that are comparable to the vegetation height. Snow depth is not as important in forests since the depth seldom, if ever, approaches the height of a typical tree and thus depth has proportionally less influence on the amount of protruding vegetation. Likewise, snow depth is not critical in regions of very short grass or bare ground, since any significant snowpack will immediately mask such surfaces. Shrubs and grass, having heights from 0.15–1.0 m, are the primary land-cover types where snow depth changes can lead to significant fluctuations in the amount of protruding vegetation. Approximately 68% of the Northern Hemisphere land area that experiences snow (excluding Greenland) is covered with shrubs and grass (Liston 2004). Due to the widespread prevalence of the shrub and grass land-cover types it is important that weather and climate models accurately estimate the degree to which they are masked by snow. Since snow depth is one of the parameters this masking is dependent on, it must be simulated as accurately as possible.

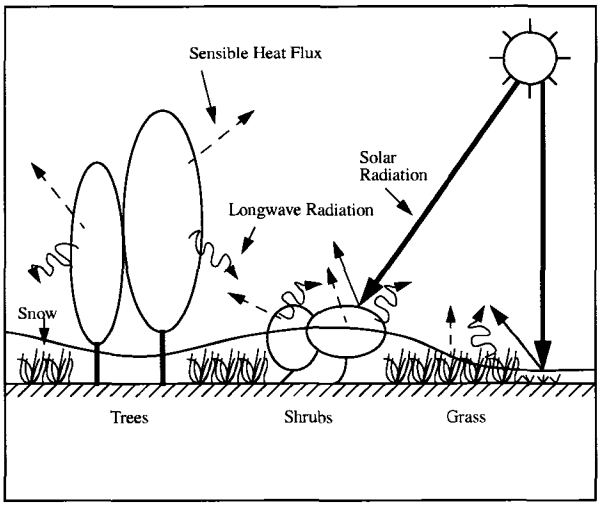

Figure 2.1: Schematic showing vegetation of various heights protruding through a snowpack.

In recent years a number of sophisticated snow models have been introduced. Essery et al. (1999) describe a comparison to observations of several snow models including the Interactions between Soil, Biosphere, and Atmosphere (ISBA) scheme used in the Météo-France ARPEGE GCM (Douville et al. 1995a,b), the CROCUS snow scheme used for avalanche forecasting (Brun et al. 1989), and the INM scheme used for hydrological forecasting (Fernandez 1998). SNTHERM is a sophisticated physically based one-dimensional snow energy and mass balance scheme (Jordan 1991) that has recently been used to simulate snow processes in the boreal forest (Hardy et al. 1998) and on sea ice (Jordan et al. 1999). Jin et al. (1999) tested a simplified version of SNTHERM against observations of snow depth at a grassland site in the French Alps as well as at the Boreal Ecosystem-Atmosphere Study (BOREAS) Southern Study Area Old Aspen site. In addition, Link and Marks (1999) tested ISNOBAL, a two-layer snow mass and energy transfer scheme, against observations gathered during the BOREAS campaign. In yet another study, Yang et al. (1997) successfully tested the simple snow model of the Biosphere-Atmosphere Transfer Scheme (BATS) against observations taken at grassland sites in the former Soviet Union.

The purpose of the work described in this chapter was to determine how well an upgraded version of the RAMS snow model simulates the time evolution of snow depth when driven with observed atmospheric forcing data. Here we describe modifications to the snow model used by RAMS version 4.4 that allow snow depth (in addition to snow water equivalent simulated by the original model) to be predicted each time step. In addition, we discuss how the modified model was run in a single column mode for several of the BOREAS stations (Sellers et al. 1997), and compare the results with

observations. Even though the taiga region is not very representative of areas where vegetation protrusion is an issue, these stations are still adequate for testing how well the model can simulate the basic snowpack thermodynamic properties.

2.2 Experimental Design

In this section the modifications to the snow model are described in detail, as well as the data used to drive the model offline for testing. A few of the key equations used by the model are included in the model description subsection. The data description sub-section lists the input variables required by the model and the stations where they were collected. Finally, the last subsection explains how the offline model was configured for the test runs described later in the text.

2.2.1 Model Description

The model used in this study is similar to the original LEAF-2 land-surface scheme contained in RAMS and described by Walko et al. (2000). Four basic components, canopy air, vegetation, temporary surface water (snow), and soil, comprise the model. The canopy air is defined to be the air below the defined vegetation height when vegetation is present. When no vegetation is present the "canopy" air is defined to be the air in the laminar sublayer. At each time step, energy and moisture balances are carried out for each of these components. The turbulent sensible and latent heat fluxes between vegetation and canopy air are proportional to the fraction of total leaf area index (LAI) that protrudes above the snowpack. Similarly, the emission and absorption of longwave radiation and the absorption of shortwave radiation are proportional to the portion of the vegetation fraction that protrudes above the snow. The vegetation fraction is considered to be the fraction of the ground/snow that is obscured by vegetation when viewed directly

from above. This protruding LAI fraction and vegetation fraction decreases linearly to zero as the snow depth approaches the vegetation height.

The main differences between this offline model and the original model are: 1) the snowpack treatment has been improved, and 2) soil moisture is forced from observations instead of predicted. Six major changes have been made to the snow component of the offline model. These changes include snow depth prediction, prediction of the falling snow density, addition of a new snowpack compression rate, a new age-based snow albedo formulation, addition of a blowing snow sublimation sink, and prediction of the snow skin-temperature.

The new model keeps track of snow depth in addition to the liquid water equivalent. Depth gains and losses are calculated with simulated snow densities. The density of newly fallen snow is calculated from (Anderson 1976),

$$\rho_s = 50 + 1.7(T_{wb} - 258.16)^{1.5} \tag{2.1}$$

where ρ_s is the snow density in kg m^{-3} and T_{wb} is the wet-bulb temperature of the near-surface air in Kelvin. This equation is used to calculate precipitation density if the air temperature is less than or equal to 0°C, otherwise the precipitation is assumed to be rain and the density is set to the liquid water value. The snow is allowed to compress with time at a rate adapted from the INM model described in Fernandez (1998) and is given by,

$$\rho_s(t+\delta t) = \rho_s(t)\{1 + a\delta t \exp[-b(T_o - T_s) - c(\rho_s(t) - \rho_d)]\} \tag{2.2}$$

where t is time, $a = 2.8 \times 10^{-6}$ s^{-1}, $b = 0.02$ K^{-1}, $\rho_d = 250$ kg m^{-3}, $T_o = 273.15$ K, T_s is the snow temperature, and δt is the time increment. The constant c takes the value of 0 when $\rho_s \leq \rho_d$ and 460 m^{3}kg^{-1} when $\rho_s > \rho_d$. The maximum snow density is capped at a typical

value (Liston et al. 1999a) for each of the snow-type categories in the Sturm et al. (1995) snow-classification system. Finally, in addition to the influence of changing snow density, depth changes due to sublimation and melting are calculated from the mass losses due to these processes.

The new cold snow albedo is calculated using (Douville et al. 1995a),

$$\alpha_s(t+\delta t) = \alpha_s(t) - \tau_a \frac{\delta t}{\tau_1} \tag{2.3}$$

where α_s is the snow albedo, τ_a = 0.008, and τ_1 = 86 400 s. For melting snow the albedo is calculated using (Douville et al. 1995a),

$$\alpha_s(t+\delta t) = (\alpha_s(t) - \alpha_{\min})\exp\left(\tau_f \frac{\delta t}{\tau_1}\right) + \alpha_{\min} \tag{2.4}$$

where α_{min} = 0.5 and τ_f = 0.24. New snow is assigned an albedo of 0.85, and the albedo of an old snowpack is reset to 0.85 after 0.003 SWE has fallen. Equations 2.3 and 2.4 gradually decrease the albedo to a minimum of 0.5 as the snow ages. This is an improvement over the original RAMS scheme where the albedo was not allowed to exceed 0.5. However, it should be noted that we did not account for the effects of forest litter which can significantly lower snow albedo in some cases.

The offline model has also incorporated the blowing snow sublimation scheme from SnowTran-3D (Liston and Sturm 1998a). This scheme calculates the loss of snow due to sublimation of saltating and suspended particles. Since the runs described in this paper were carried in a single column manner, the snow transport features of SnowTran-3D could not be utilized. In order to get around this difficulty, it was assumed that any loss of snow due to horizontal transport of saltating and suspended particles was exactly offset by gains from the same process each time step. This implies that a relatively

homogeneous snow surface existed around the stations at all times. In addition, it was assumed that at all times a sufficient fetch existed in the upwind direction for the concentration of saltating particles to be equal to the maximum equilibrium concentration as described in Liston and Sturm (1998a).

Finally, the new version of the model was improved by the addition of a snow skin-temperature calculation. In the original model, the longwave radiation emission and sensible heat flux were calculated from the temperature of the top snow layer. This is not realistic since only a very thin layer at the surface actually responds directly to the atmosphere. The flow of heat between the bulk of the snow and this thin surface layer (skin) is much slower than the flow between the skin and the atmosphere. The skin temperature is calculated each time step by setting the sum of the terms of the surface energy balance to zero as shown below.

$$H_{ss} - SH_{sc} - LH_{sc} + LW_{sa} + LW_{sv} = 0 \tag{2.5}$$

All of the terms in the above equation were computed as they are in LEAF-2 with the exception that the snow skin-temperature is used in place of the top layer bulk snow temperature. In Equation 2.5 H_{ss} is the conduction of heat between the top snow layer and the snow skin and is given by,

$$H_{ss} = K\frac{T_s - T_{skin}}{0.5d} \tag{2.6}$$

where K is the thermal conductivity of the snow, T_s is the top layer snow temperature, T_{skin} is the snow skin-temperature, and d is the thickness of the top snow layer. The SH_{sc} term is the turbulent sensible heat flux given by,

$$SH_{sc} = c_p \rho_a \frac{T_{skin} - T_c}{r_d} \tag{2.7}$$

where c_p is the specific heat of air at constant pressure, ρ_a is the density of air, T_c is the canopy air temperature, and r_d is the aerodynamic resistance between the snow and the canopy air as defined in Appendix D of Pielke (2002). The LH_{sc} term is the turbulent latent heat flux given by,

$$LH_{sc} = L_s \rho_a \frac{r_{sat} - r_c}{r_d} \tag{2.8}$$

where L_s is the latent heat of sublimation, r_{sat} is the saturation water vapor mixing ratio at the snow skin-temperature, and r_c is the water vapor mixing ratio of the canopy air. The LW_{sa} term is the net longwave radiation absorbed by the snow from the atmosphere and is given by,

$$LW_{sa} = \varepsilon_s (1 - \Gamma_s)(R_a - \sigma T_{skin}^4) \tag{2.9}$$

where σ is the Stefan-Boltzmann constant, ε_s is the emissivity of snow, R_a is the longwave radiation emitted by the atmosphere, and Γ_s is the portion of the vegetation fraction which protrudes above the snow. This exposed vegetation fraction is given by,

$$\Gamma_s = \max\left[0, \Gamma\left(1 - \frac{z_s}{z_v}\right)\right] \tag{2.10}$$

where Γ is the vegetation fraction when the snow depth is equal to zero, z_s is the snow depth, and z_v is the height of the vegetation. The net longwave radiation absorbed by the snow from the vegetation, LW_{sv}, is given by,

$$LW_{sv} = \sigma \varepsilon_s \varepsilon_v \Gamma_s (T_v^4 - T_{skin}^4) \tag{2.11}$$

where ε_v is the emissivity of the vegetation and T_v is the temperature of the vegetation.

All incoming solar radiation passes completely through the skin and is steadily attenuated as it passes through each of the snow layers below. The remaining solar

radiation at the bottom of the snowpack is absorbed by the soil. When the snow skin-temperature is predicted to be greater than 0°C, the surface energy balance is then solved with the skin temperature set to 0°C and the resulting flux is defined as the energy available for melting. The melt flux is then used to melt a portion of the top snow layer. This method for calculating the snow skin-temperature is very similar to that described in Liston et al. (1999b).

2.2.2 Data Description

The data needed to drive the model included: above-canopy air temperature, atmospheric pressure, water vapor mixing ratio, precipitation, wind speed, soil moisture, soil temperature, incoming solar radiation, and downward atmospheric longwave radiation. Since the model required downward longwave radiation, only stations that were augmented with "suite B" observations could be used. These stations were: Saskatoon, SK (52.2°N, 106.6°W), the Old Aspen site in Prince Albert National Park, SK (53.6°N, 106.2°W), the Old Jack Pine site near Nipawin, SK (53.9°N, 104.7°W), the Old Jack Pine site near Nelson House, MB (55.9°N, 98.6°W), and Flin Flon, MB (54.7°N, 101.7°W). The locations of these stations are shown in Figure 2.2. All of the stations, except Saskatoon, were situated in the forest. Saskatoon was located in a grassland setting. All of the variables mentioned above, except for precipitation, were recorded as 15-minute averages of 5-second observations. The precipitation measurements were recorded every hour. In addition, the snow depth, measured by an ultrasonic sensor, was recorded every hour. We have not made any wind corrections to the precipitation observations. Short periods, typically a few days or less, of missing data, were filled in using the interpolation scheme developed by Liston and Elder (2006). At each of the

forest stations the above-canopy air temperature, relative humidity, wind speed, and radiation sensors were located on towers extending several meters above the canopy. The longwave sensors at all of the stations except Nelson House were located within 1 km of the suite A tower. The longwave radiation sensor for Nelson House was located about 15 km from the suite A tower. The precipitation and snow depth gauges were located in nearby clearings. More information on the BOREAS surface mesonet can be found in Shewchuk (1997).

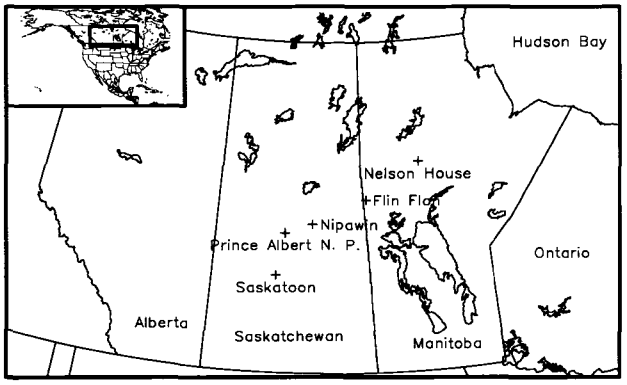

Figure 2.2: Map showing the locations of the BOREAS surface mesonet stations.

2.2.3 Model Configuration

The offline snow model was used to simulate snow depth over the 1995–96 winter at the five BOREAS surface mesonet stations. The vegetation was defined as short grass with a LAI of 1.0, vegetation fraction of 0.98, albedo of 0.2, and a canopy height of 5 cm. These vegetation parameters were used for the forest sites since the precipitation and snow depth gauges were located in clearings. The model was run at the snow depth gauge location in single column mode, ignoring the forest canopy.

One, 5 cm thick soil layer, and a maximum of six snow layers were used. The number of snow layers was automatically adjusted by the model based on the total snow mass present. The observed 10 cm depth soil temperature was used as the lower boundary for the soil heat conduction equation, and the soil moisture was forced by the value observed at 10 cm depth. The meteorological tower observations were used to drive the offline simulations; the model was run on a 15 s time step and the driving variables were updated every 15 min. The observed above-canopy air temperature and mixing ratio communicated with the canopy air through fluxes computed from similarity theory as described for LEAF-2 in Appendix D of Pielke (2002). The turbulent sensible heat flux between the canopy air and the air at observation height is given by,

$$SH_{ca} = c_p \rho_a \frac{T_c - T_{obs}}{r_a} \tag{2.12}$$

where T_{obs} is the observed above-canopy temperature and r_a is the aerodynamic resistance, corrected for stability, between the canopy air and the observation height. The turbulent moisture flux between the canopy air and the air at observation height is given by,

$$E_{ca} = \rho_a \frac{r_c - r_{obs}}{r_a} \tag{2.13}$$

where r_{obs} is the water vapor mixing ratio at the observation height.

2.3 Results

The following sections contain descriptions of the simulation results for each of the BOREAS stations. The modeled snow depth and time of snow-free date are compared with the observed values and some discussion of differences is given. Plots of observed

air temperature and wind speed are also displayed. The stations modeled were Nipawin, Prince Albert, Nelson House, Flin Flon, and Saskatoon.

2.3.1 Nipawin

Due to the large amount of missing data in November and December of 1995 at the Nipawin station, the simulation was started at 0600 UTC 2 January 1996. The simulation terminated at 0000 UTC 30 May 1996. The model was initialized with 89.3 kg m^{-2} of snow on the ground in six layers. The initial snow mass on the ground was determined from the observed snow depth and an estimated density of 225 kg m^{-3} (Liston et al. 1999a) for the taiga snow classification (Sturm et al. 1995). The top snow layer temperature was set equal to the air temperature, and the temperatures of successively lower layers were increased linearly to the value of the soil temperature at the bottom layer. This method was used to initialize snow temperature for all the stations where snow existed at the start of the simulation. Simulations were also run where the initial snow temperature was set isothermally to either the soil or the air temperature. Virtually no differences were found between these simulations and the simulations with the linear profiles, suggesting little sensitivity to the initial snow temperature profile. The above-canopy air temperature, wind speed, and relative humidity were measured at 20.7 m above the ground for this station. Time series of air temperature and wind speed during the times of the simulations for all stations are shown in Figure 2.3 and Figure 2.4, respectively. During the period of the simulation, the air temperature and wind speed averaged -8.5° C and 2.0 m s^{-1} respectively at Nipawin.

Figure 2.5a shows the time evolution of the simulated (thin line) and observed (bold line) snow depth during the course of the simulation. It can be seen from Figure 2.5a that

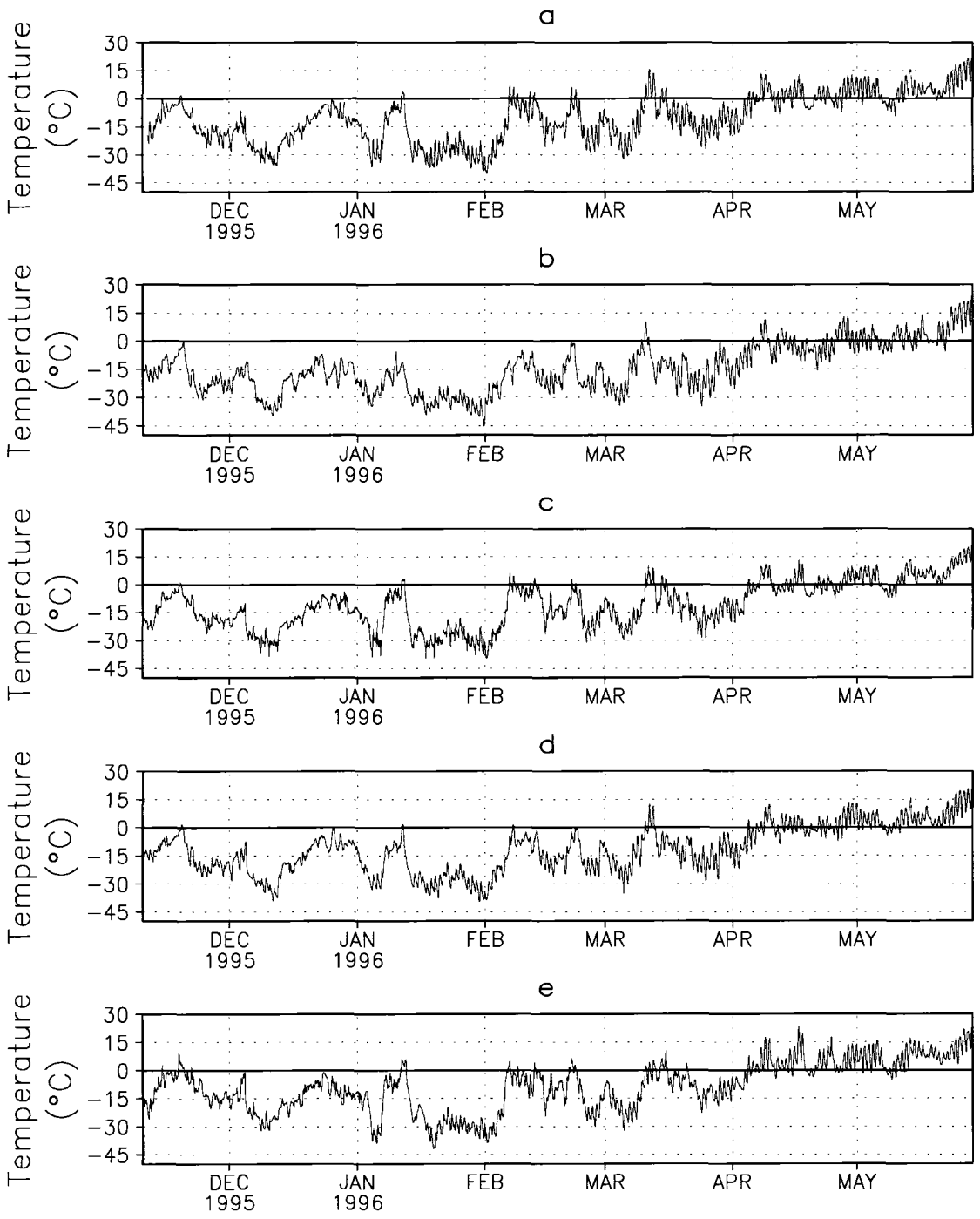

Figure 2.3: Observed air temperature at (a) Nipawin, (b) Nelson House, (c) Prince Albert, (d) Flin Flon, and (e) Saskatoon.

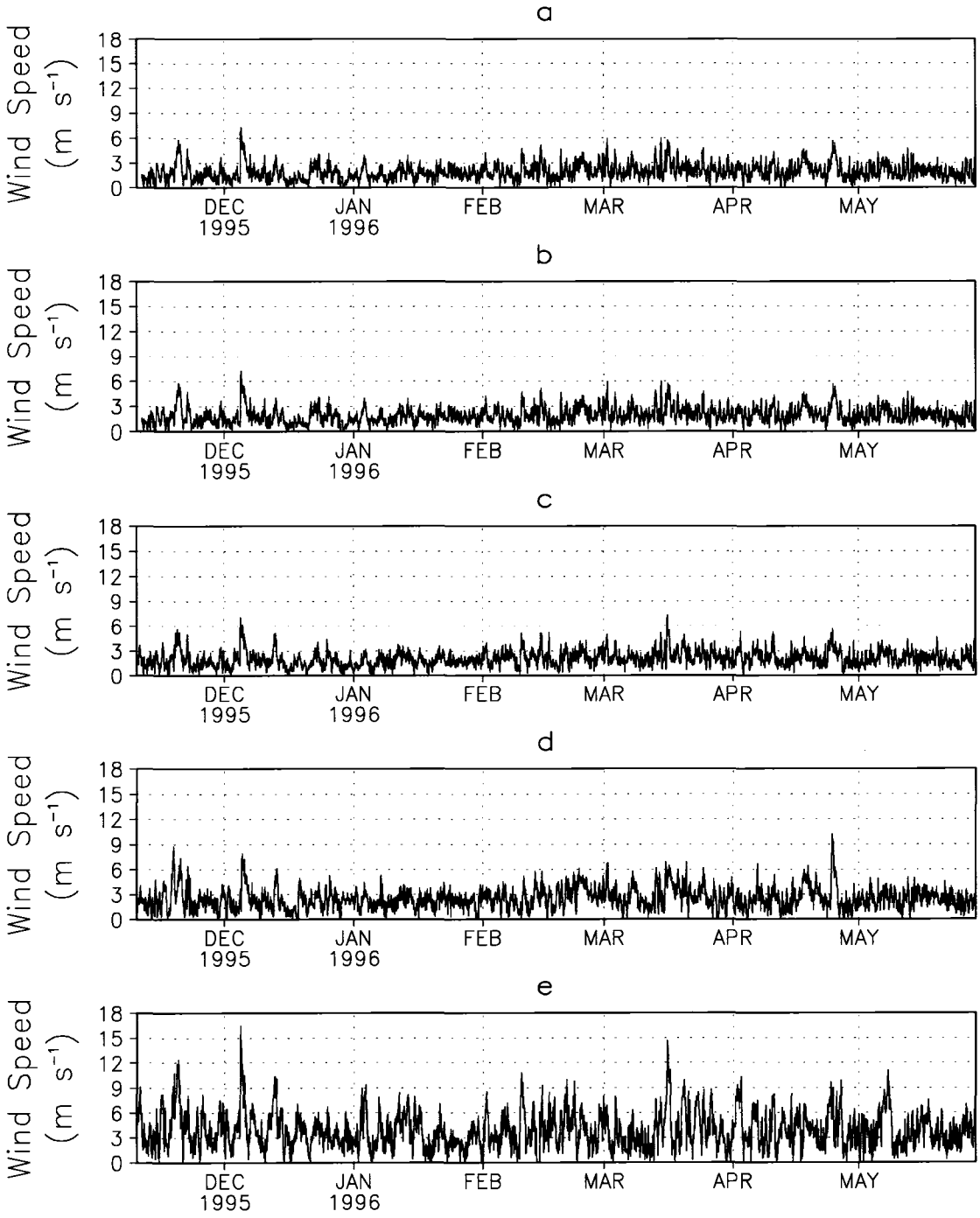

Figure 2.4: Observed wind speed at (a) Nipawin, (b) Nelson House, (c) Prince Albert, (d) Flin Flon, and (e) Saskatoon.

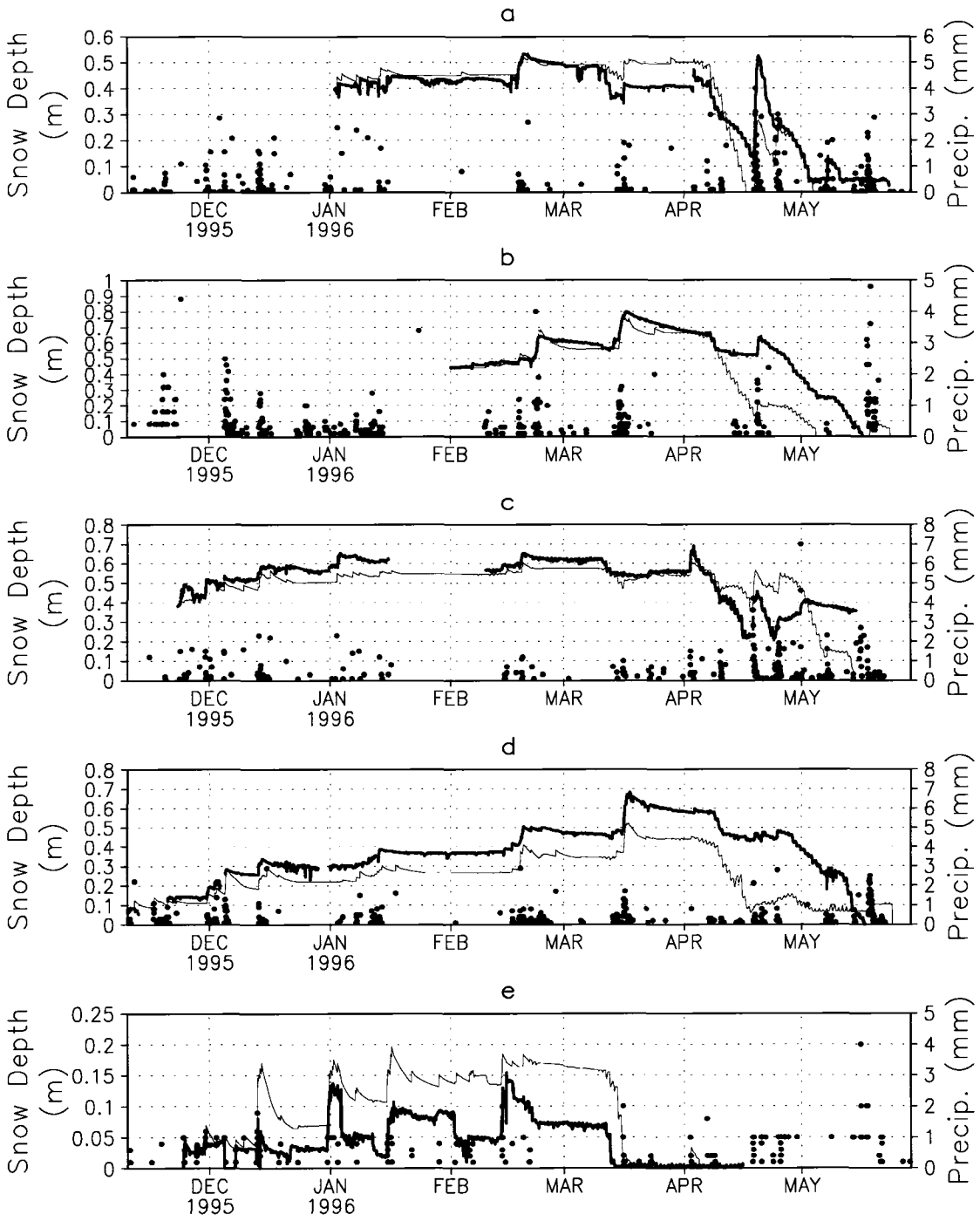

Figure 2.5: Time evolution of observed (bold line) and simulated (thin line) snow depth and observed hourly precipitation (solid circles) for (a) Nipawin, (b) Nelson House, (c) Prince Albert, (d) Flin Flon, and (e) Saskatoon.

the model tended to overestimate the snow depth by amounts as great as 20 cm, but generally less than 10 cm. The average absolute difference between the two was 0.05 m, or 26% of the observed. Even though precipitation errors are to be expected in this type of experiment, due to the difficult nature of measuring solid precipitation and the simple equation used to calculate precipitation density, the model did well at simulating the snow depth increases due to the precipitation events (solid circles in Figure 2.5a) in mid-February, mid-March, and mid-April. The small melt event that occurred in mid-March was captured by the model, although its magnitude was underestimated. The large melt event that occurred in early April was overestimated and the snow melted away entirely by mid-April before returning during the late April accumulation event. The model reproduced the early May final snow-free date fairly well. The period of near constant snow with depth of about 0.05 m during the first half of May is believed to be erroneous since the temperatures during this time (Figure 2.3a) were above freezing.

An average snow density of 152 kg m^{-3} was measured on 5 March near the Nipawin station (Hardy and Davis 1998). This density combined with a depth of 0.45 m yields a SWE of 0.069 m, which is significantly less than the simulated SWE of 0.110 m. The simulated SWE is larger than the observed SWE since we initialized the snow mass based on the "typical" taiga density of 225 kg m^{-3} which appears to be greater than the observed values. Two percent of the simulated snowpack at Nipawin was lost to sublimation. Finally, Figure 2.6 shows the evolution of the modeled snow albedo during the simulations for all of the stations. It ranges from a maximum of 0.85 immediately following snow events to a minimum of 0.5 during periods between snow accumulation events.

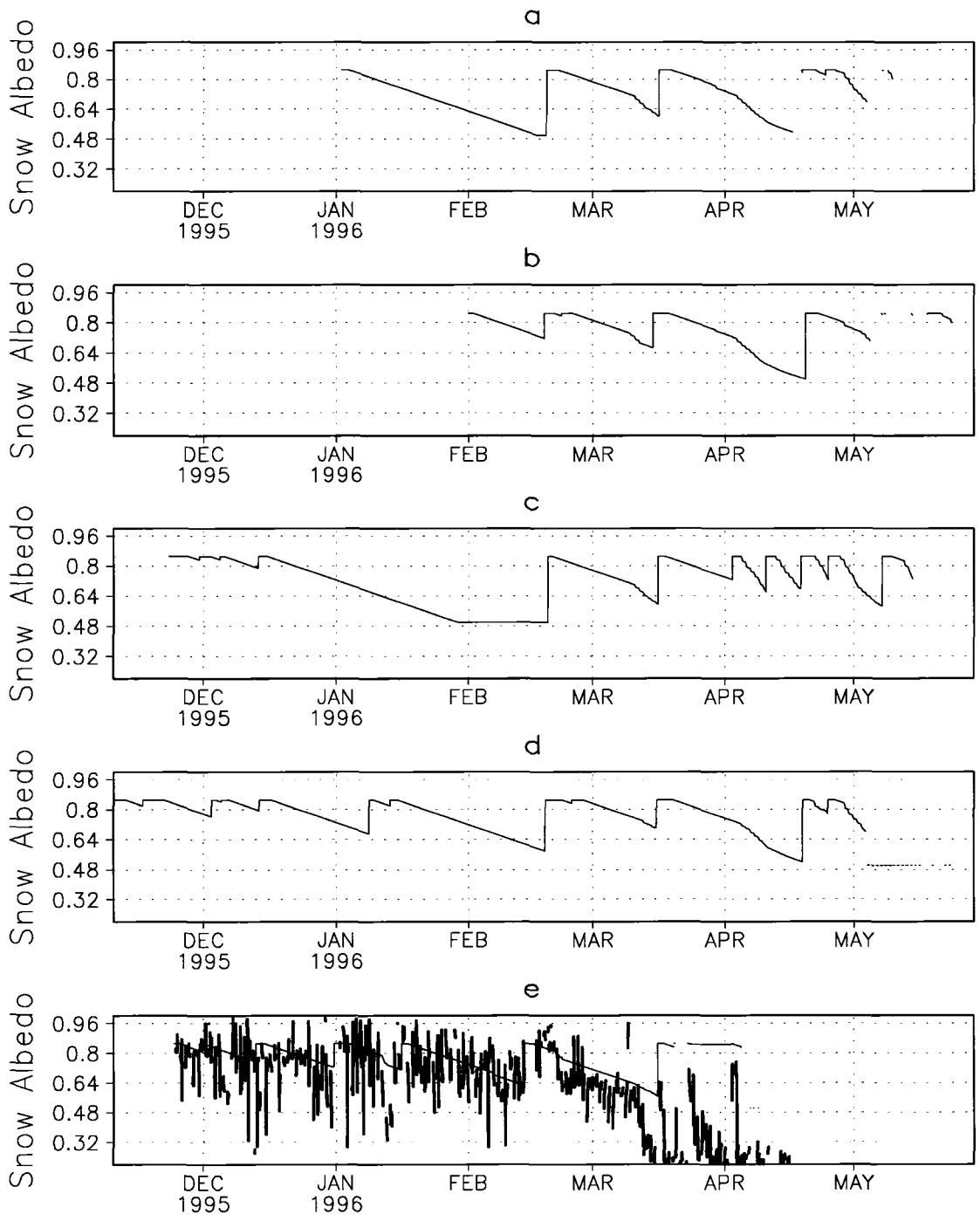

Figure 2.6: Simulated snow albedo at (a) Nipawin, (b) Nelson House, (c) Prince Albert, (d) Flin Flon, and (e) Saskatoon. The bold line in panel e represents the observed net surface albedo computed from the incoming and reflected solar radiation.

2.3.2 Nelson House and Prince Albert

The simulation for Nelson House was started at 0000 UTC 01 February 1996 and terminated at 0000 UTC 30 May 1996. The long period of missing data spanning the entire month of January prevented an earlier start time. Air temperature, relative humidity, and wind speed were measured at 15.8 m and 23.7 m above the ground, at Nelson House and Prince Albert, respectively. The average air temperature and wind speed at Nelson House were -8.4° C and 2.5 m s^{-1} respectively. The model was initialized, using the same method discussed above, with 99.4 kg m^{-2} of snow in six layers. The simulation for Prince Albert was started at 0000 UTC 23 November 1995 and terminated on 0000 UTC 30 May 1996. Again, long periods of missing data prevented an earlier start date. Average air temperature and wind speed at Prince Albert were -10.9° C and 2.1 m s^{-1} respectively. An initial snow mass, spread over six layers, of 85.5 kg m^{-2} was used.

Figures 2.5b and 2.5c show the simulated and observed snow depth evolution for the Nelson House and Prince Albert stations. The difference between observed and simulated snow depths at Nelson House was generally 0.1 m or less for most of the simulation, with the exception of the end-of-season melt period in late April and early May when the difference reached a peak of 0.5 m (Figure 2.5b). The average absolute difference between the simulated and observed snow depths was about 0.10 m, or 28% of the observed value. The end-of-season melt-off during late April and early May was handled poorly, with the simulated snow-free date occurring 12 days ahead of the observed. The inability of the model to represent snowpack shading by the surrounding forest is a possible explanation for the simulated snow melting much faster during the last half of April. The snow depth sensor was located in a forest clearing, while the

radiometer, used to drive the incoming solar radiation in the model, was located above the forest canopy. During the morning and evening hours when the sun was relatively low in the sky, the forest likely produced shadows across the clearing. Link and Marks (1999) ran similar simulations at Nipawin and Nelson House with the ISNOBAL model for the 1994-95 winter. They used a canopy radiative transfer scheme to simulate the sub-canopy radiation and were better able to simulate the snow-free dates. Three percent of the simulated snowpack at Nelson House was lost to sublimation.

Figure 2.5c shows that the model overestimated the snow depth at Prince Albert by 0.05 to 0.1 m during December. A string of missing snow depth data extending from about mid-January to mid-February inhibits any conclusion on the models ability during that time. From mid-February to March the model did fairly well while the melting events during mid-April were generally underestimated. During the last few days of April the simulated snowpack began to ablate while the observed snow depth increased slowly. This could be due to the model predicting rain when wet snow was actually falling. For simplicity, the model defines precipitation as snow when the air temperature is at or below 0°C, but in reality snow can fall when the temperature near the surface is as much as 5°C above freezing (Auer 1974). During the first half of May the simulated snowpack melts away rapidly and is completely gone by 15 May, while the observed snow depth appears to be 0.35 m. However, Hardy et al. (1998) found, through an examination of the net surface albedo, that the snow actually melts off by 29 April, meaning the snow in our model took 16 days longer to melt off. Hardy et al. (1998) were able to simulate this snow-free date quite well with SNTHERM. An average snow density of 159 kg m^{-3} was measured on 4 March near the Prince Albert station (Hardy and Davis 1998). This

density combined with a depth of 0.62 m yields a SWE of 0.099 m, which is significantly less than the simulated SWE of 0.130 m. Again, the simulated SWE is larger than the observed SWE since we initialized the snow mass based on the "typical" taiga density of 225 kg m^{-3} which is greater than the observed values. The extra SWE may explain the delayed snow-free date in this case. The average absolute difference between the observed and simulated snow depths at Prince Albert was 0.07 m or 18% of the observed value. Four percent of the simulated Prince Albert snowpack was lost to sublimation.

2.3.3 Flin Flon

The simulation for Flin Flon began at 0000 UTC 10 November 1995 and ended 0000 UTC 30 May 1996. Air temperature, relative humidity, and wind speed were measured at 17.9 m above the ground. The average air temperature and wind speed during the period of the simulation were -11.3° C and 2.5 m s^{-1} respectively. The model was initialized with 15.8 kg m^{-2} of snow. Figure 2.5d shows the time series of simulated and observed snow depths at this station. The absolute difference between the simulated and observed snow depths was 0.13 m, or 34% of the observed. The model appeared to compress the snow too quickly during the month of December. The erroneously fast compression leads to a general underestimation of the snow depth from mid-December through mid-April. The accumulations in mid-February and mid-March appear to be well simulated. The simulated snowpack completely melts by 4 May, while the observed snow lingered until 17 May. The more rapid melt of the simulated snowpack could again be due to the lack of shading in the model. Ten percent of the simulated snowpack sublimated.

Since the soil was saturated during much of April and May, the melted snow formed 0.1 m deep standing water in the model during the first half of May (Figure 2.5d). It should be noted that the Figure 2.5 snow depth plots show the total surface water depth including both liquid and frozen fractions. So, even though it appears snow existed during the first half of May, an inspection of the snow liquid water fraction (not shown) reveals only standing liquid water existed during this time period. In the model, the snowpack was not allowed to have more than 10% of its mass in the form of liquid water. Any amount that exceeded this limit percolated into the soil, unless the soil was saturated as in the case mentioned above.

2.3.4 Saskatoon

As a grassland site instead of in a forest clearing, Saskatoon was significantly different than the other stations. The temperature and relative humidity sensors were located at 1.7 m and the wind speed sensor was at 10.0 m. The average air temperature and wind speed during the period of the simulation were -13.4° C and 3.9 m s^{-1} respectively. The simulation was started at 0000 UTC 24 November 1995 and terminated at 0000 16 April 1996. No snow was present at the beginning of the simulation.

The model overestimated the snow depth during much of the simulation (Figure 2.5e). The average absolute difference between the observed and simulated snow depths was 0.05 m or 132% of the observed. The model captured the accumulation events around the first and middle parts of January, however, the mid-December and mid-February events were overestimated and underestimated, respectively. The lack of wind-driven horizontal snow transport in the model is a likely reason for these errors. Since this station was located on the prairie where the peak winds were stronger (Figure 2.4e),

transport is expected to be a larger factor than in the forest clearings. In addition, the lack of a wind-dependent new-snow density algorithm might be another reason for the overestimation of snow depth since new-snow density in windy areas is often greater than that predicted by temperature alone. The influence of wind at Saskatoon was evident in the much larger sublimation flux simulated by the model there. At Saskatoon 43% of the simulated snowpack was lost to sublimation (13% during blowing snow events) compared to less than 5% (with no blowing snow) in most of the forest clearings. Finally, Figure 2.6 shows a plot of the modeled snow albedo (thin line) along with the observed ratio of reflected shortwave radiation to incoming shortwave radiation (bold line) which represents the net surface albedo. Since the primary vegetation at the Saskatoon site is short grass we can assume this quantity closely approximates that of the snow albedo. An examination of the figure shows that the modeled albedo is fairly close to the observed value until early March. Starting in early March the observed net surface albedo drops below the simulated snow albedo. This is likely due to patches of grass emerging as the snow begins to melt.

2.4 Discussion

Averaged over the winter, the modeled snow depth at the four low-wind stations was within 0.09 m of the observations and the average percent error was 27%, while the one wind-blown station, Saskatoon, was considerably worse. The average depth error at all five stations was ±0.08 m. In order to gain some idea of how significant these errors would be to the calculation of the turbulent sensible and longwave radiative heat fluxes from protruding vegetation, a simple conceptual model of a shrub patch partially buried in snow was developed. This model was used to simulate the change in turbulent sensible

and longwave radiative heat fluxes from the shrubs as a function of snow depth. The heat fluxes generated by the shrub were calculated for hypothetical atmospheric conditions as the snow depth was varied from 0 m to the 1.0 m shrub height. The turbulent sensible and longwave radiative fluxes were calculated with the same equations used by LEAF-2. The sensible heat flux is calculated using,

$$SH_{vc} = 2.2\gamma_s c_p \rho_a \frac{(T_v - T_c)}{r_b} \tag{2.14}$$

where the portion of the LAI that protrudes above the snow, γ_s, is,

$$\gamma_s = \max\left[0, \gamma\left(1 - \frac{z_s}{z_v}\right)\right] \tag{2.15}$$

and the resistance between the vegetation and the canopy air, r_b, is,

$$r_b = \frac{(1 + 0.55\gamma_s)}{0.01}\left[\max(0.1, u_*)116.6\right]^{\frac{-1}{2}} \tag{2.16}$$

The friction velocity, u_*, is calculated from surface similarity theory (Louis et al. 1981) and is dependent upon the net surface roughness, z_o,

$$z_o = zo_{\text{veg}} \max\left(0, 1 - \frac{z_s}{z_v}\right) + zo_{\text{snw}} \min\left(1, \frac{z_s}{z_v}\right) \tag{2.17}$$

The variables T_v and T_c represent vegetation and canopy air temperatures respectively. The longwave radiation emitted by the vegetation to the snow is,

$$LW_{vs} = \Gamma_s \varepsilon_s \varepsilon_v \sigma T_v^4 \tag{2.18}$$

Table 1 lists the remaining variables in these equations that have not been defined. The vegetation and canopy air temperatures were set to 268 K and 267 K respectively and the 10 m wind speed was set to 5 m s^{-1}.

Symbol	Description	Value
γ	Leaf area index	2
σ	Stefan-Boltzmann constant	5.67 X 10^{-8} W m^{-2} K^{-4}
Γ	Vegetation fraction	0.8
ε_s	Snow emissivity	0.99
ε_v	Vegetation emissivity	0.96
c_p	Specific heat of air at constant pressure	1004 J kg^{-1} K^{-1}
zo_{snw}	Snow roughness length	0.001 m
zo_{veg}	Vegetation roughness length	0.05 m
z_s	Snow depth	0.01–1.0 m
z_v	Vegetation height	1 m
ρ_a	Air density	1.3 kg m^{-3}

Table 1: Values of vegetation and atmospheric parameters used in the heat flux sensitivity experiments.

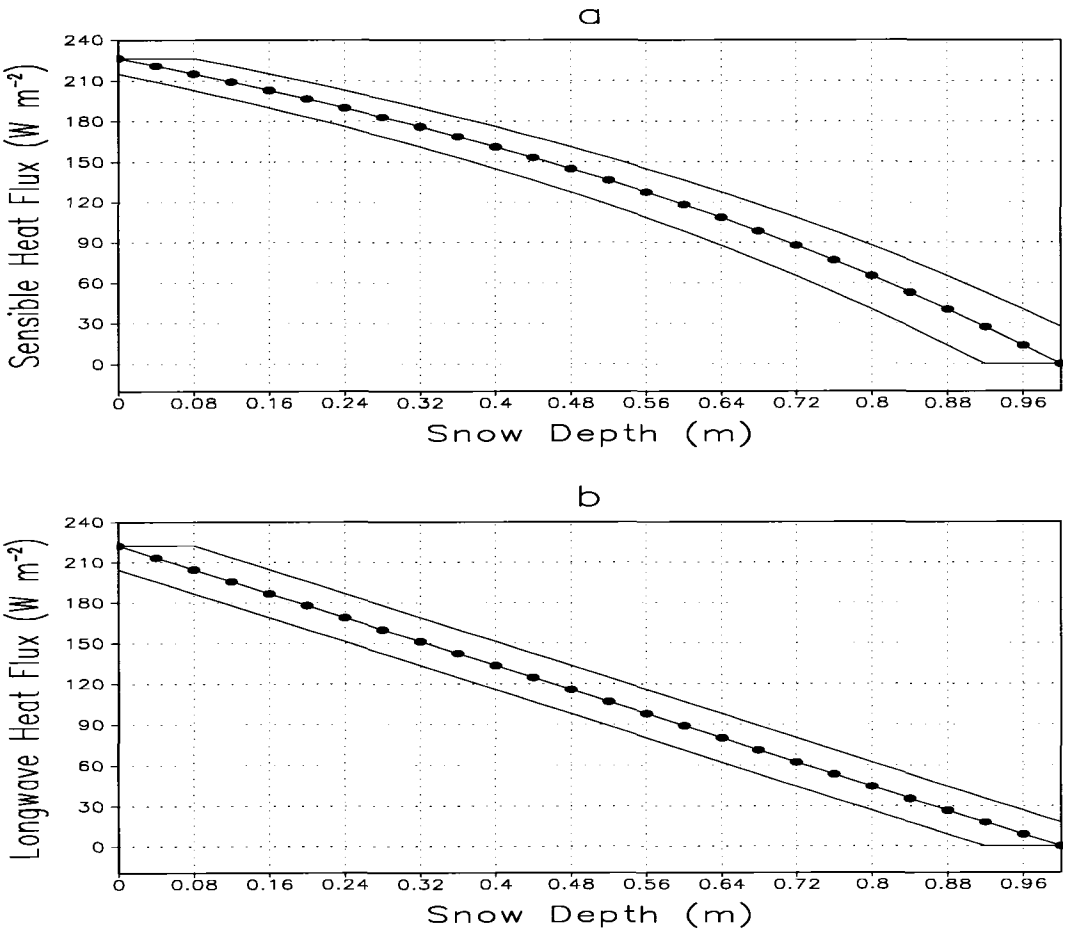

Figure 2.7: (a) Simulated sensible heat flux emission from a hypothetical 1 m tall shrub patch with varying snow depth. The line with solid circles represents the sensible heat flux at each snow depth. The upper and lower thin solid lines represent the heat flux for snow depth error of -0.08 m and +0.08 m respectively. (b) Same as in (a) except for longwave radiative flux.

Figure 2.7a shows the variation in sensible heat flux with changing snow depth. The line with solid circles represents the heat flux simulated at each snow depth and the thin solid lines represent 0.08 m deviations from the actual snow depth. The average error of 0.08 m in snow depth produced an average 17 W m^{-2} sensible heat flux error. Figure 2.7b shows similar longwave radiative heat flux variation with snow depth. The average longwave radiative flux error was also 17 W m^{-2}. The conceptual model discussed above assumes that the vegetation fraction and LAI will decrease linearly as the snow approaches the height of the shrub. One should note that this assumption itself could lead to heat flux errors of a similar magnitude to those produced by incorrect snow depth. However, the focus of this paper is improving the accuracy of the simulated snow depths.

Chapter 3

TESTING THE LEAF-2 SENSIBLE AND LATENT HEAT FLUXES

3.1 Introduction

After the snow depth model was tested, attention was focused on the quality of the turbulent surface sensible and latent heat fluxes simulated by LEAF-2. Since many of the effects of increased shrubs and black carbon pollution on the Arctic atmosphere are directly communicated through alterations in these surface fluxes, it is important to make an assessment of their accuracy before drawing any conclusions from the sensitivity simulations. No measurements of surface sensible and latent heat fluxes exist for the times and location of the Arctic simulations, so data from the North Park region of Colorado is used instead.

North Park is a high altitude, approximately 2,450 meters above sea-level, valley located in north central Colorado between the Medicine Bow and Park Range mountains. The vegetation is dominated by sage '*Artemisia tridentata*' and various graminoids. The fact that North Park is often snow-covered with protruding shrubs during the winter months makes it a reasonable location to test LEAF-2's ability to simulate turbulent heat and moisture fluxes over snow-covered shrublands.

In this chapter, the ability of a modified version of the LEAF-2 (Land Ecosystem-Atmosphere Exchange Feedback) model (Walko et al. 2000) to simulate sensible and

latent heat fluxes from a snow-covered mixture of shrubs and grass at North Park Colorado is discussed. The fluxes computed by the model using similarity theory (Equations 2.12 and 2.13) were compared to those measured by tower-mounted eddy-covariance instruments that were installed at North Park during the 2002-2003 winter for the FLuxes Over Snow Surfaces (FLOSS) project.

When measuring sensible and latent heat flux from a tower within a heterogeneous landscape, one must consider which part of the landscape influences the flux sampled by the instruments. This variable landscape fraction, known as a footprint, is dependent upon wind direction, wind speed and atmospheric stability (thermal and mechanical). In this study a very simple formulation was used, based only on wind direction, to estimate the upwind area sensed by the tower-mounted eddy-covariance instruments. The modified version of LEAF-2 was then used to simulate the fluxes of sensible and latent heat from this region of influence, and the results were compared to those observed at the tower.

3.2 Experimental Design

The modified offline version of LEAF-2 used in this flux study was the same model used in the snow depth study described in the previous chapter. The idea was to drive the model with observations and test the accuracy of the simulated sensible and latent heat fluxes. In this section a description of the data used to drive the model is given, followed by a discussion of the model configuration.

3.2.1 Data Description

All of the meteorological parameters needed to drive the model were collected at a 34 m tower erected for the FLOSS campaign during the winter of 2002-2003. The following parameters from the tower were utilized: incoming solar radiation, incoming

longwave radiation, air temperature, relative humidity, wind speed, atmospheric pressure, and soil temperature. The tower is located at 40° 39' 32" N and 106° 19' 26" W and at an elevation of approximately 2476.5 m. All of the variables used to drive the model were 5 min averages of the actual tower observations. The sensible and latent heat fluxes simulated by the model were compared with those measured at 10 m height on the tower by sonic anemometers and krypton hygrometers.

The vegetation was determined from a 1 m resolution color orthophoto derived dataset. This dataset was a 1 km square box centered on the tower and defines the vegetation as either shrub or grass. The average height of the grass was determined from magnaprobe observations taken along the same transects and grids as the snow observations described below. The average leaf area index (LAI) of the shrubs was estimated from measurements made with a Delta-T Sunscan Canopy Analysis System during April of 2003. This system estimates the LAI from the extinction of light through the vegetation canopy. A random sample of 234 shrubs was taken around the tower site. The heights of these shrubs were also recorded with a magnaprobe.

The average snow depth was determined from magnaprobe observations upwind of the tower every ten days. Two grids were setup in shrub patches upwind of the tower and the snow depth was measured at 1 m intervals. In addition, 11 radial transects extending approximately 300 m from the tower were sampled by an observer every 2.5 strides. The vegetation type at each of the snow depth measurements along the radial transects was determined from the 1 m vegetation data set mentioned above. From this data, average depths for the shrub and grass areas were calculated for each day the model was run. The

snow density was determined from sipre tube measurements taken at several locations near the tower on the observation days.

3.2.2 Model Configuration

The offline snow model was used to simulate surface sensible and latent heat fluxes for seven individual days at the FLOSS tower site in much the same way it was used to simulate snow depths at the BOREAS stations. The model setup for these simulations was different from the BOREAS runs in three major ways. First of all, the model was run for seven 24-hour days ranging from 13 January 2003 to 13 March 2003 when all necessary data were available, instead of for the entire winter season.

Secondly, the snow depth was initialized from the observations around the tower and held constant during the course of each 1-day simulation. The snow depth observations around the tower were grouped according to vegetation type, i.e., grass or shrub, and then an average depth for each type was calculated. Furthermore, the fraction of snow-free ground in each vegetation type was calculated by dividing the number of zero depth points by the total number of observation points. The canopy air over each vegetation type "patch" received the area-weighted average sensible and latent heat fluxes from the snow-covered and snow-free portions of the patch. The soil temperature in each vegetation patch was updated from the area-weighted average radiative, conductive, and turbulent fluxes from the snow-covered and snow-free areas.

The third major difference was the use of two vegetation patches whose relative coverage varied with time according to wind direction. The tower instruments were assumed to sense a 1 km fetch bounded by plus or minus the standard deviation of the hourly mean wind azimuth most strongly; see Figure 3.1. The footprint was calculated

every five minutes based on the average wind direction and standard deviation during the preceding hour. The sensible heat flux was then calculated for both the grass and shrub areas within the footprint and the area-weighted average compared to the flux observed at the tower. A similar calculation was done for latent heat flux.

Figure 3.1: Schematic of the simple tower footprint.

In these simulations the grass was assigned an LAI of 1.0, vegetation fraction of 0.9, albedo of 0.25, and a canopy height of 0.05 m. The shrubs were assigned an LAI of 2.0, vegetation fraction of 0.75, albedo of 0.2, and a canopy height of 0.47 m.

One 0.03 m thick soil layer was used in the model and the observed 0.05 m depth soil temperature was used as the lower boundary for the soil heat conduction equation. The soil moisture was set at 33% saturation and held constant for the simulations. The

meteorological tower observations were used to drive the offline simulations; the model was run on a 15 s time step and the driving variables were updated every five minutes.

3.3 Results

The following subsections contain descriptions of the simulated sensible and latent surface heat fluxes and net radiation for the seven days examined. The sensible and latent heat fluxes are defined as positive upward while the net radiation is defined to be positive downward.

3.3.1 January 13, 2003

Figure 3.2 shows the simulated sensible and latent heat fluxes, red dashed lines, and the observed sensible and latent heat fluxes, black solid lines, for 13 January 2003. The average observed snow depths in the shrubs and grass were 0.13 and 0.10 m respectively. Average snow density in the shrubs and grass were 181 and 169 kg m^{-3} respectively. Finally, the fractions of shrub and grass areas covered with snow were 97 and 88% respectively. The sensible heat flux on this day showed little if any diurnal variation and remained mostly negative. The model appeared to underestimate the sensible heat flux most of the day. The average absolute difference between modeled and observed sensible heat fluxes was 18 W m^{-2} and the average percent difference was 71%. Figure 3.2 shows that the latent heat flux exhibited a mid-day peak of 90 W m^{-2} and fell to near 0 W m^{-2} during the nighttime hours. The model tended to overestimate the latent heat flux during the night and underestimate it during the day. The average absolute difference between modeled and observed latent heat fluxes was 9 W m^{-2} and the average percent difference was 93%.

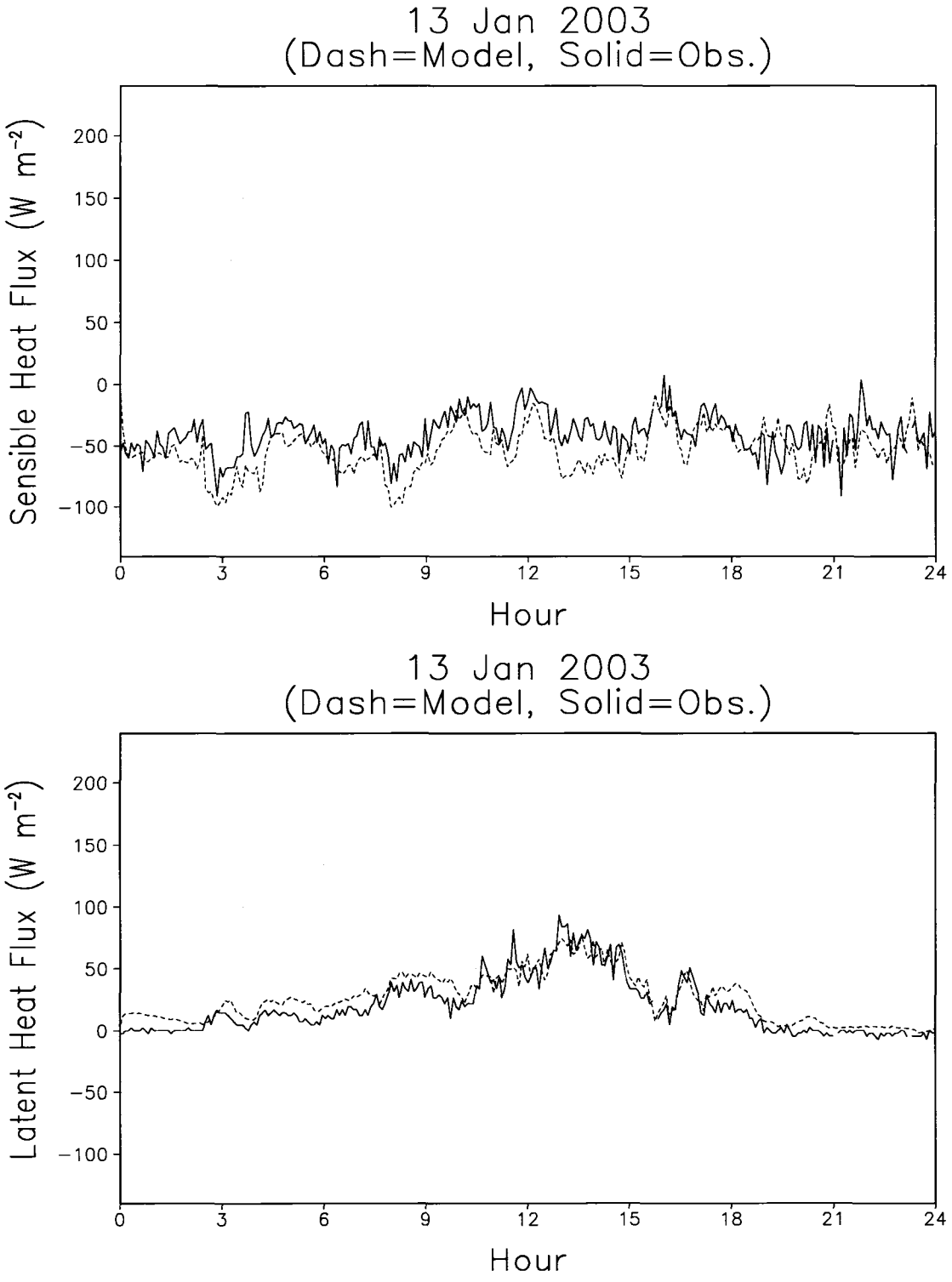

Figure 3.2: Modeled (red dashed line) and observed (black solid line) sensible and latent heat fluxes at the FLOSS tower on 13 January 2003.

Figure 3.3 shows plots of the modeled canopy air temperatures in the grass and shrub patches as well as the 10 m air observed air temperature for 13 January 2003. Also shown in Figure 3.3 is a plot of the observed and modeled net radiation. The "canopy" temperature over the grass, which was mostly buried by snow on that day, was several degrees Kelvin lower than the 10-m height temperature. On the other hand, the canopy air temperature over the shrub patch exceeded the 10 m air temperature for a brief period around mid-day. This was possible since the shrubs protruded through the snowpack and warmed the nearby air. As can be seen from Equation 2.12, whenever the canopy air temperature exceeds the 10 m air temperature the turbulent sensible heat flux becomes positive and the flow of heat is upward from the surface. Even though the shrub patch produced a positive heat flux during the middle of the day, the average flux over both the grass and shrub patches remained negative since the grass patch covered a larger area.

The bottom panel of Figure 3.3 shows the simulated, red dashed line, and observed, solid black line, net radiation. The net radiation ranged from -50 and -100 W m^{-2} during the night to a maximum between 100 and 150 W m^{-2} during the middle of the day. The model tended to slightly overestimate the upward flux at night and the downward flux during the day. The average absolute difference between modeled and observed net radiation was 5 W m^{-2} and the average percent difference was 34%.

3.3.2 January 22, 2003

Figure 3.4 shows the sensible and latent heat fluxes for 22 January 2003. The average observed snow depths in the shrubs and grass were 0.13 and 0.08 m respectively. Average snow density in the shrubs and grass were 233 and 182 kg m^{-3} respectively. Finally, the fractions of shrub and grass areas covered with snow were 88 and 70%

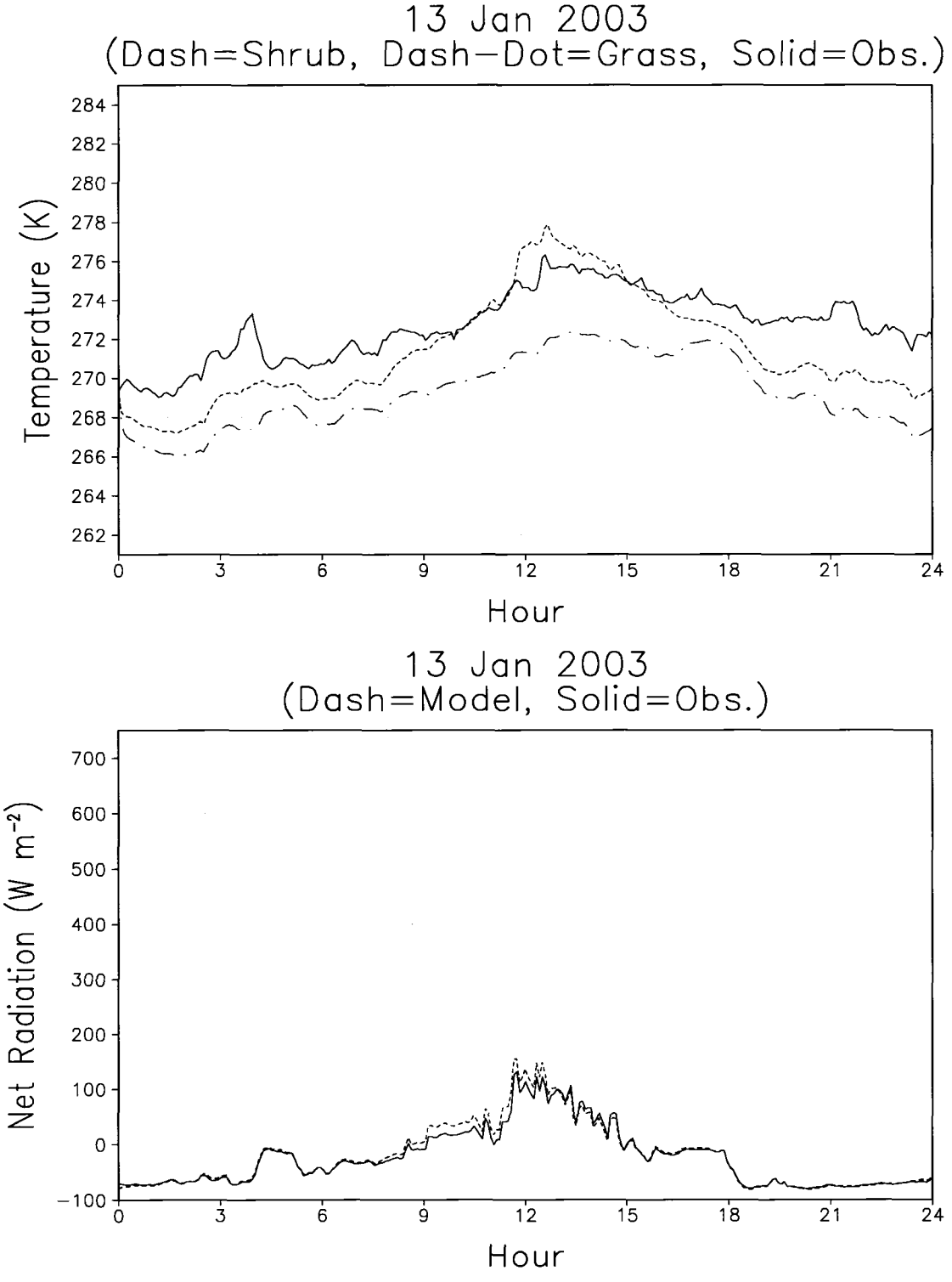

Figure 3.3: The top panel shows the modeled canopy air temperature for the shrubs (red dashed line) and grass (green dash-dot line) and the 10 m observed air temperature (black solid line). The bottom panel shows the modeled and simulated net radiation.

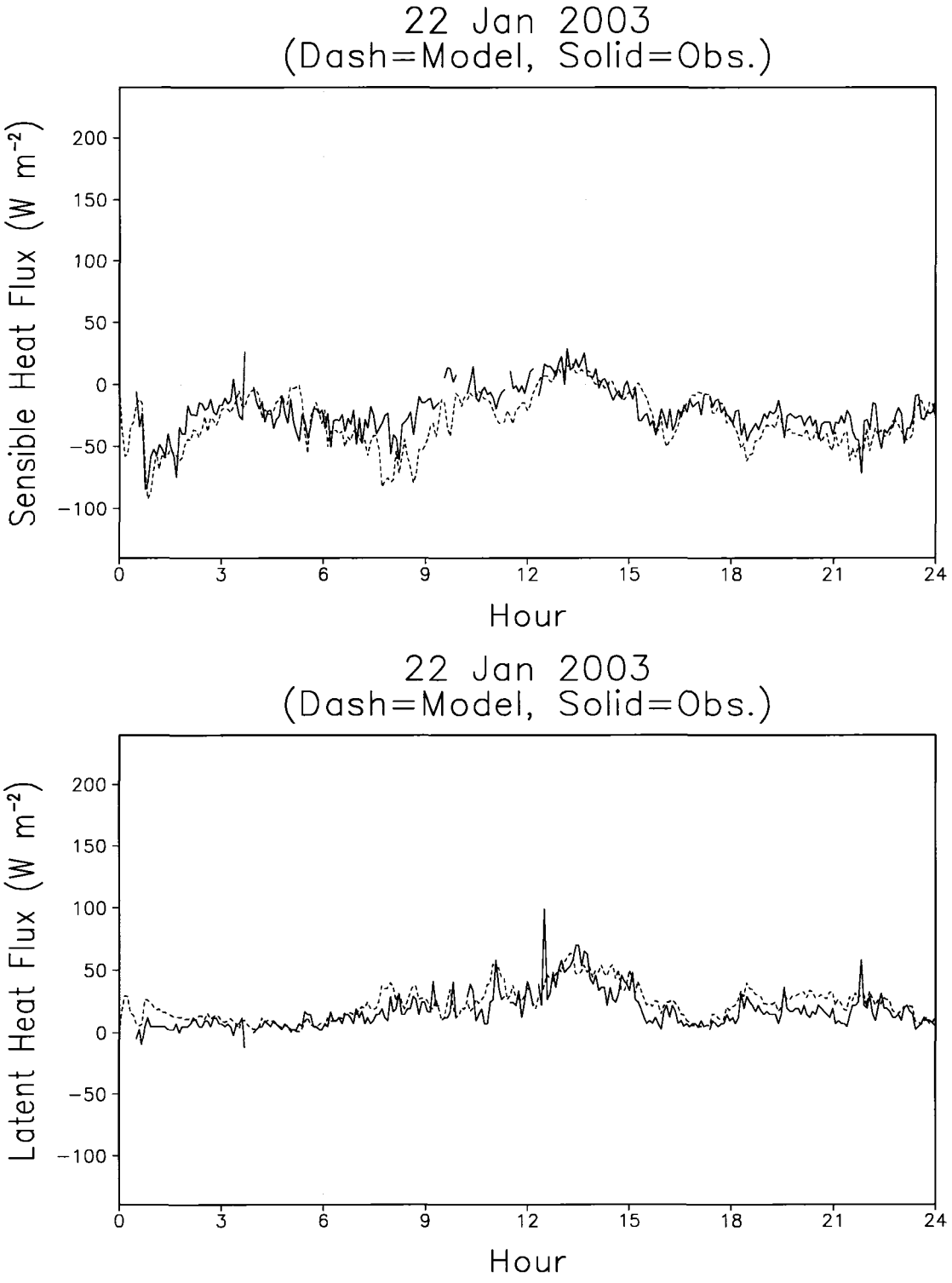

Figure 3.4: Same as Figure 3.2, except for 22 January 2003.

respectively. The top panel shows that the sensible heat flux ranged between 0 and -50 W m^{-2} for most of the simulation. During the middle of the day the sensible heat flux rose to 25 W m^{-2} as the protruding shrubs warmed the air above the snow; see Figure 3.5. As in the previous case, the model tended to overestimate the downward sensible heat flux. The average absolute difference between modeled and observed sensible heat fluxes was 14 W m^{-2} and the average percent difference was 110%. The bottom panel of Figure 3.4 shows that the latent heat flux was primarily positive with a weak mid-day maximum of 70 W m^{-2}. The model tended to overestimate the latent heat flux both night and day. The average absolute difference between modeled and observed latent heat fluxes was 9 W m^{-2} and the average percent difference was 82%.

The bottom panel of Figure 3.5 shows that the net radiation was generally between 0 and -100 W m^{-2} during the night and became positive with a peak value near 250 W m^{-2} during the middle of the day. The model simulated the net radiation well during the night time hours, but tended to underestimate the downward flux during the day. The average absolute difference between modeled and observed net radiation was 11 W m^{-2} and the average percent difference was 21%.

3.3.3 January 31, 2003

Figure 3.6 shows the sensible and latent heat fluxes for 31 January 2003. The average observed snow depths in the shrubs and grass were 0.11 and 0.12 m respectively. Average snow density in the shrubs and grass were 231 and 256 kg m^{-3} respectively. Finally, the fractions of shrub and grass areas covered with snow were 67 and 43% respectively. The sensible heat flux was negative most of the period with an exception of a brief occurrence of positive values in late morning. A weak diurnal cycle was apparent

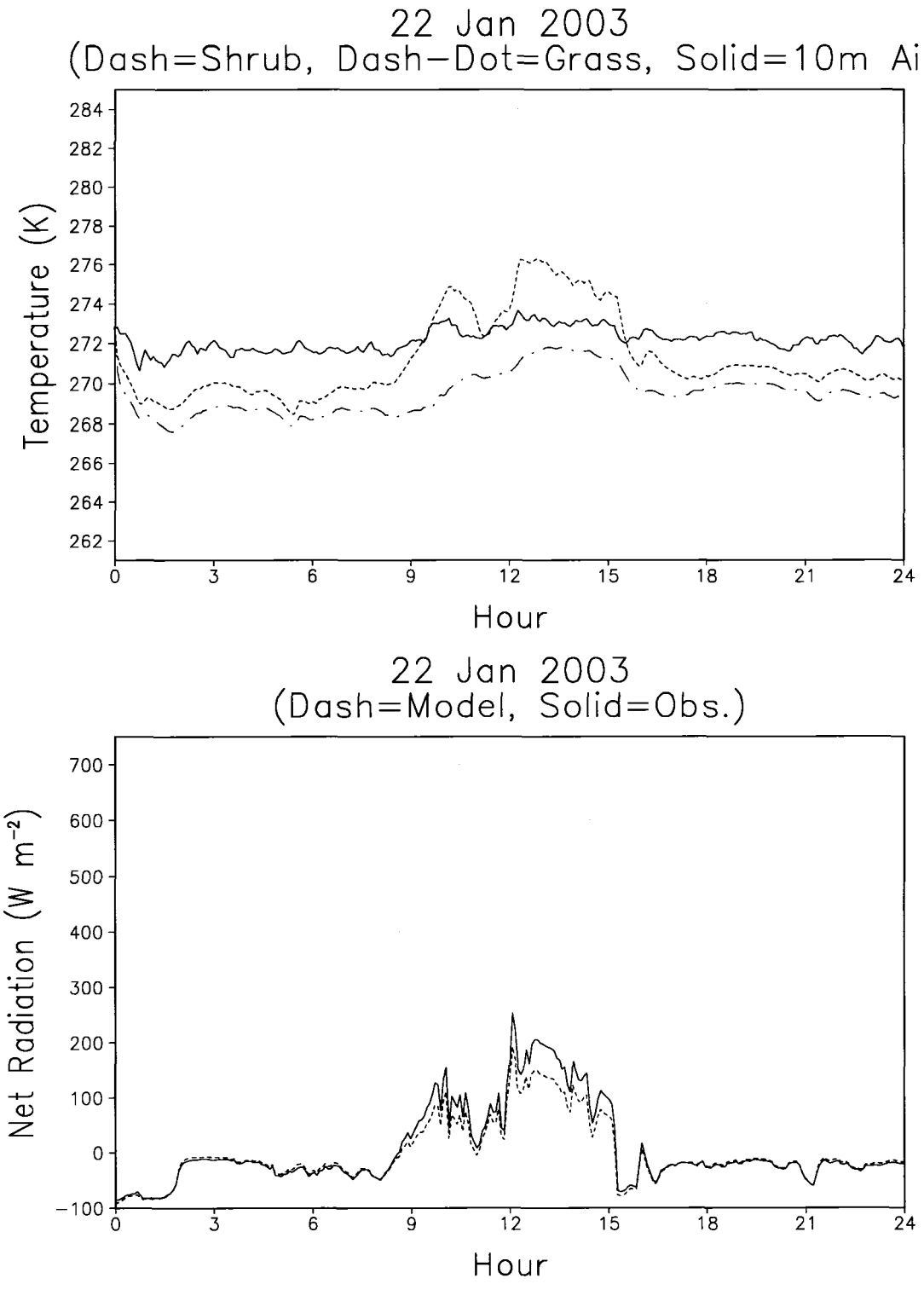

Figure 3.5: Same as Figure 3.3, except for 22 January 2003.

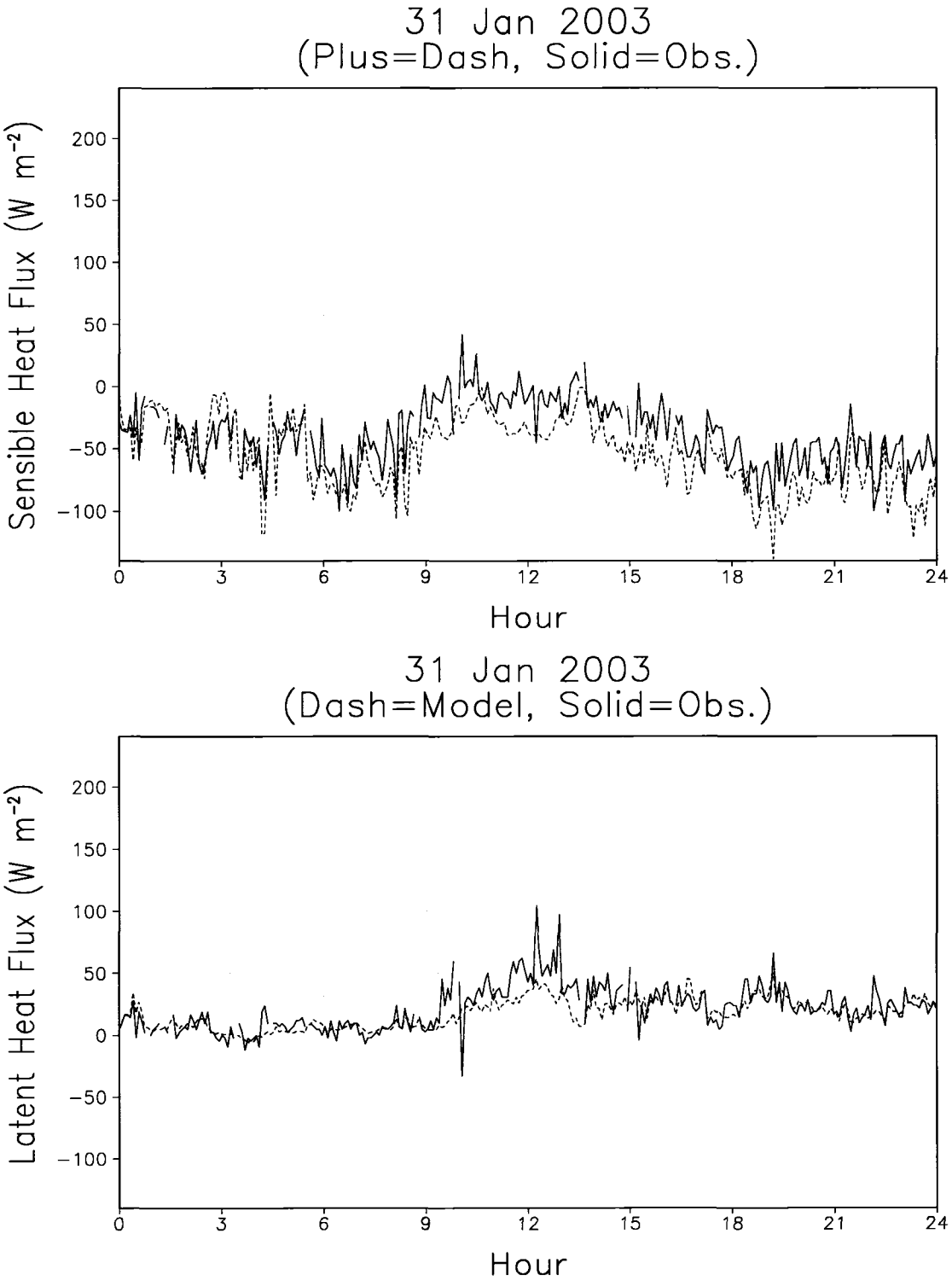

Figure 3.6: Same as Figure 3.2, except for 31 January 2003.

on this day with flux becoming less negative during the mid-day period. The model was able to capture this diurnal variation, but tended to overestimate the downward flux during most of the simulation. The average absolute difference between modeled and observed sensible heat fluxes was 22 W m^{-2} and the average percent difference was 169%. The bottom panel of Figure 3.6 shows that the latent heat flux was again mostly positive with a mid-day maximum around 100 W m^{-2}. The model was able to simulate the latent heat flux fairly well at night, but tended to underestimate during the daytime. Errors in the latent heat flux were greatest around mid-day. The average absolute difference between modeled and observed latent heat fluxes was 9 W m^{-2} and the average percent difference was 56%. The bottom panel of Figure 3.7 shows that the model underestimates the upward net radiation slightly during the nighttime and underestimates the downward net radiation by about 100 W m^{-2} during the middle of the day. The average absolute difference between modeled and observed net radiation was 22 W m^{-2} and the average percent difference was 24%.

3.3.4 February 10, 2003

Figure 3.8 shows the sensible and latent heat fluxes for 10 February 2003. The average observed snow depths in the shrubs and grass were 0.06 and 0.12 m respectively. Average snow density in the shrubs and grass were 263 and 210 kg m^{-3} respectively. Finally, the fractions of shrub and grass areas covered with snow were 92 and 26% respectively. On this particular day the sensible heat flux exhibited a strong diurnal cycle, ranging from as low as -75 W m^{-2} during the nighttime hours to as high as 175 W m^{-2} during the middle of the day. An inspection of Figure 3.9 reveals that the canopy air temperatures of the shrubs and grass both exceed the 10 m level air temperature during

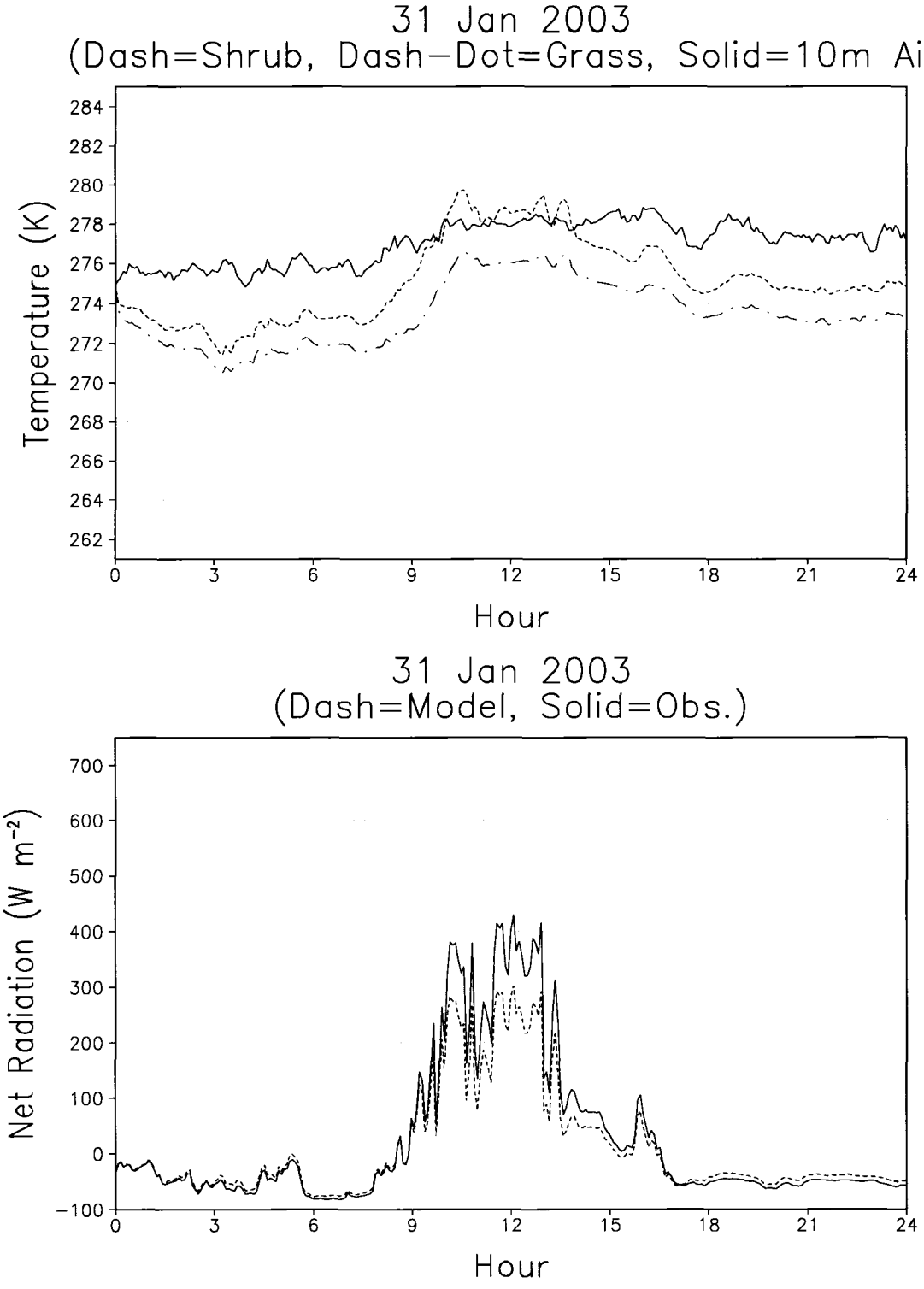

Figure 3.7: Same as Figure 3.3, except for 31 January 2003.

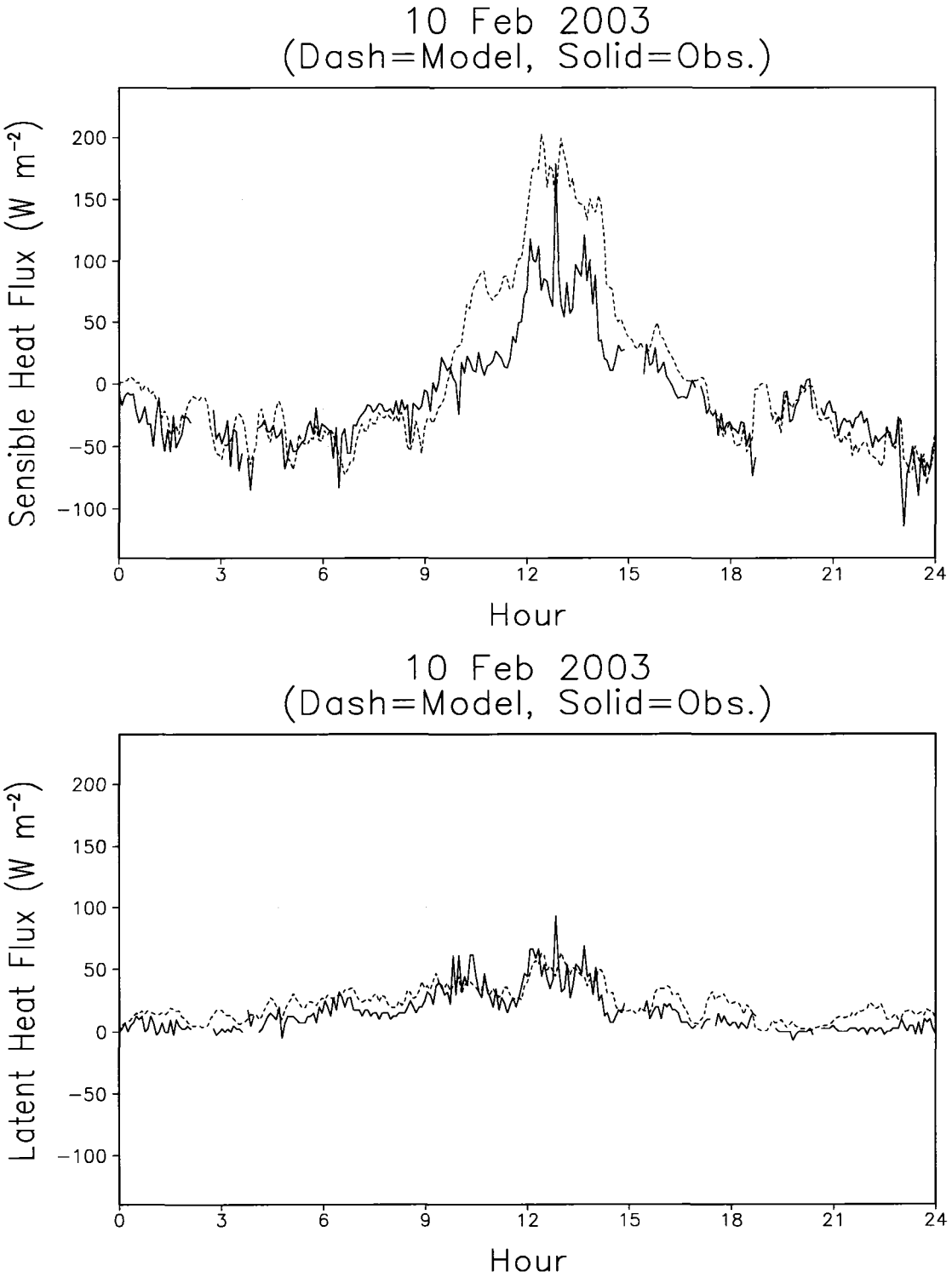

Figure 3.8: Same as Figure 3.2, except for 10 February 2003.

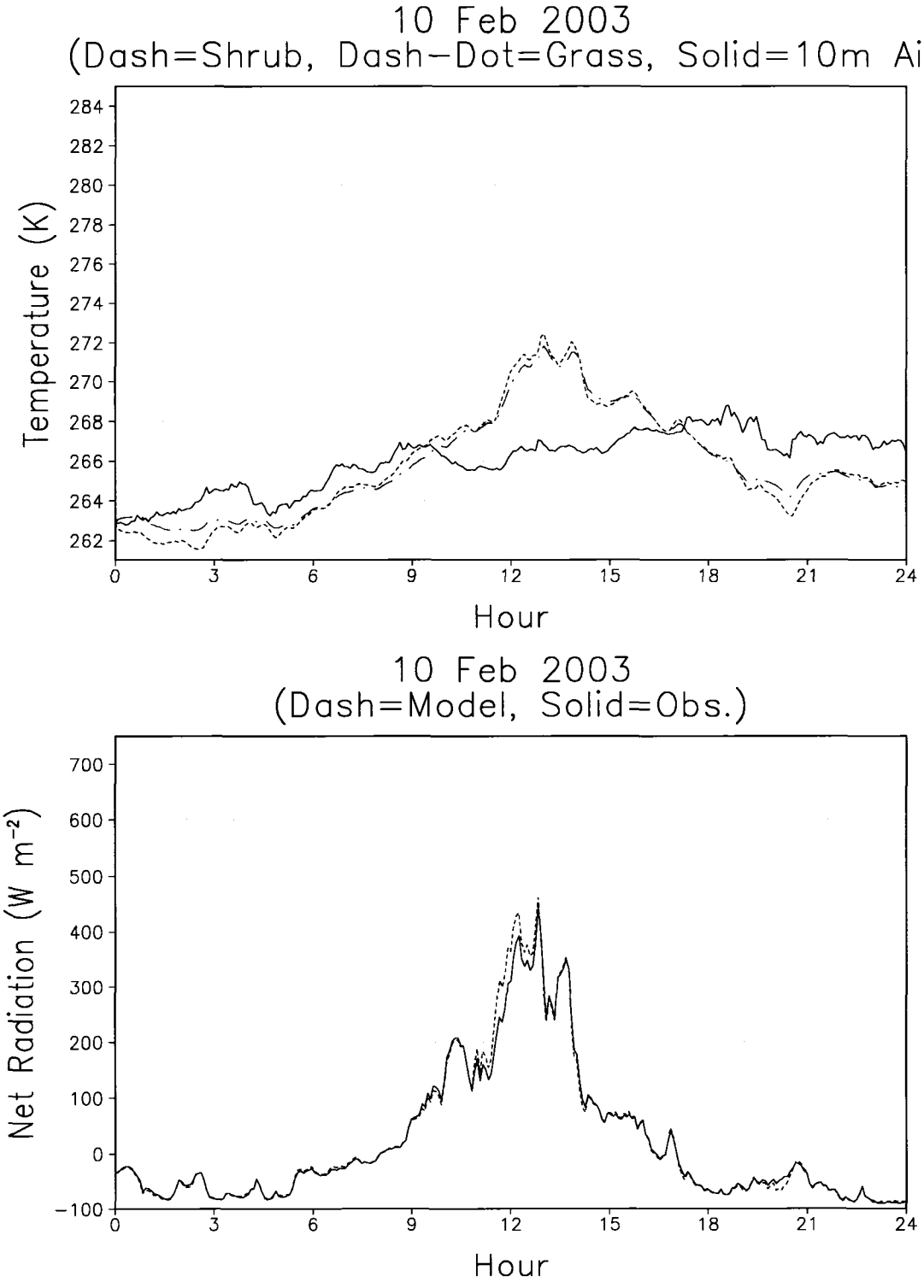

Figure 3.9: Same as Figure 3.3, except for 10 February 2003.

the middle of day, allowing for the strong upward sensible heat flux. The model was able to capture the sensible heat flux variation well; however, it tended to overestimate the magnitudes during both day and night. The average absolute difference between modeled and observed sensible heat fluxes was 26 W m^{-2} and the average percent difference was 147%. The latent heat flux followed a pattern similar those on the previous days. This time the model generally overestimated the nighttime latent heat flux and underestimated the daytime flux, but simulated the weak diurnal cycle fairly well. The average absolute difference between modeled and observed latent heat fluxes was 10 W m^{-2} and the average percent difference was 143%. Finally, the bottom panel of Figure 3.9 shows that the model simulated the diurnal cycle of net radiation fairly well with only a slight overestimation during the mid-day period. The average absolute difference between modeled and observed net radiation was 6 W m^{-2} and the average percent difference was 8%.

3.3.5 February 21, 2003

Figure 3.10 shows the sensible and latent heat fluxes for 21 February 2003. The average observed snow depths in the shrubs and grass were 0.05 and 0.08 m respectively. Average snow density in the shrubs and grass were 231 and 210 kg m^{-3} respectively. Finally, the fractions of shrub and grass areas covered with snow were 75 and 13% respectively. The sensible heat flux on this day climbed sharply during mid-day from near 0 W m^{-2} to around 175 W m^{-2} before dropping back to near 0 W m^{-2} during the evening. The sensible heat flux seldom dropped below -25 W m^{-2} during the time of this simulation. Modeled sensible heat fluxes closely approximated this cycle, but tended to be too small at night and too large during the day. The average absolute difference

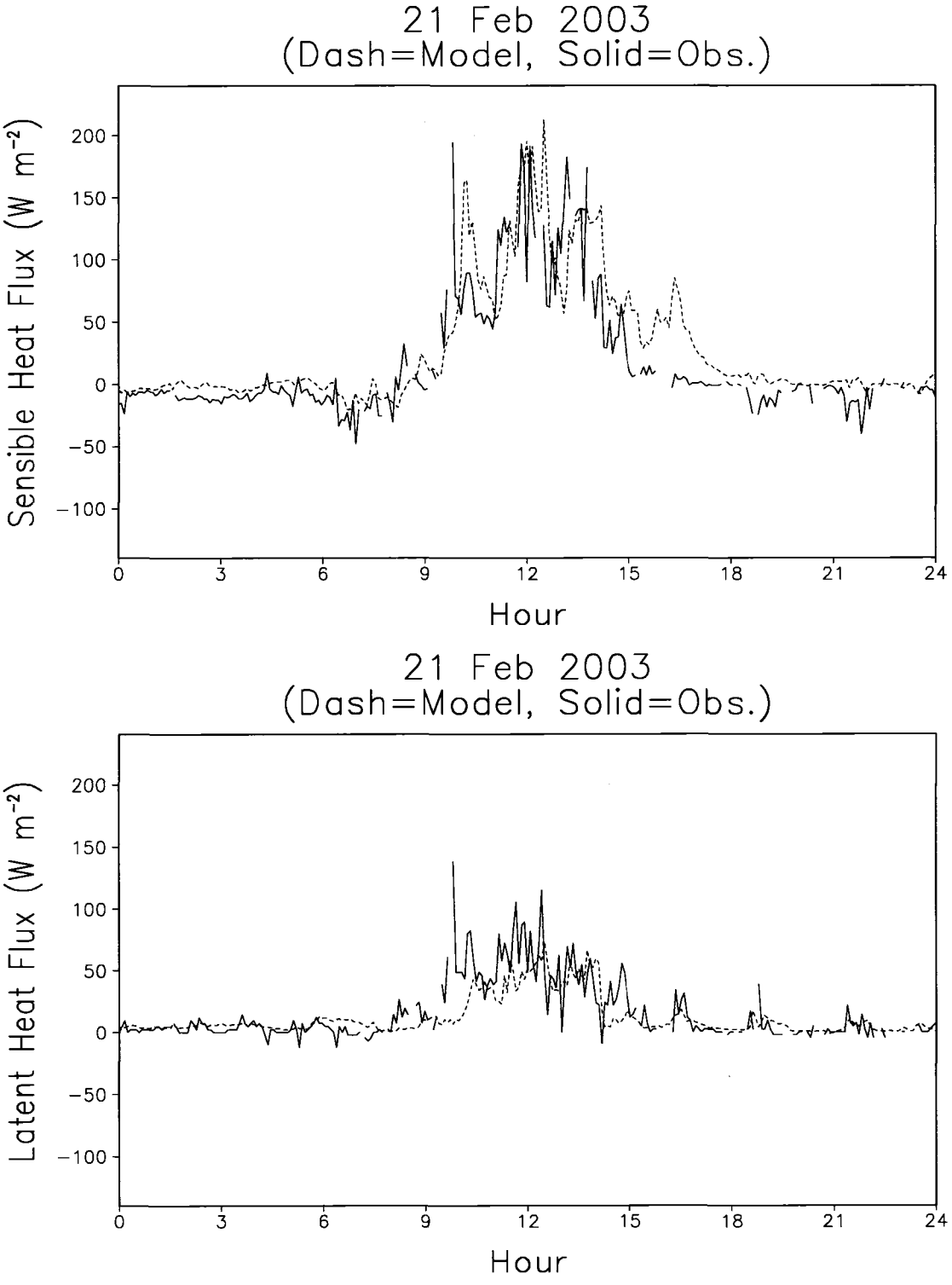

Figure 3.10: Same as Figure 3.2, except for 21 February 2003.

between modeled and observed sensible heat fluxes was 20 W m^{-2} and the average percent difference was 257%. The model was able to simulate the general pattern of latent heat flux on this day, but generated values that were too low during the day. The average absolute difference between modeled and observed latent heat fluxes was 10 W m^{-2} and the average percent difference was 92%. Finally, the bottom panel of Figure 3.11 shows that the model was once again able to reproduce the general pattern of net radiation. The average absolute difference between the modeled and observed net radiation was 11 W m^{-2} and the average percent difference was 79%.

3.3.6 March 3, 2003

Figure 3.12 shows the sensible and latent heat fluxes for 3 March 2003. The average observed snow depths in the shrubs and grass were 0.14 and 0.09 m respectively. Average snow density in the shrubs and grass were 258 and 234 kg m^{-3} respectively. Finally, the fractions of shrub and grass areas covered with snow were 100 and 94% respectively. This day had the greatest snow-covered area of any of the seven examined. The diurnal cycle of sensible heat flux was more muted than in the previous two days with a peak value near 50 W m^{-2}. The shrubs protruded through the snowpack and warmed the nearby air to above freezing, see Figure 3.13, producing positive sensible heat flux values during mid-day. The general cycle in sensible heat flux was captured by the model; however, the model's peak flux occurred slightly earlier than the observed peak. During much of period the downward sensible heat flux magnitudes were too large. The average absolute difference between modeled and observed sensible heat fluxes was 15 W m^{-2} and the average percent difference was 148%. Modeled latent heat fluxes were slightly too large, but the diurnal variation was handled fairly well. The average absolute

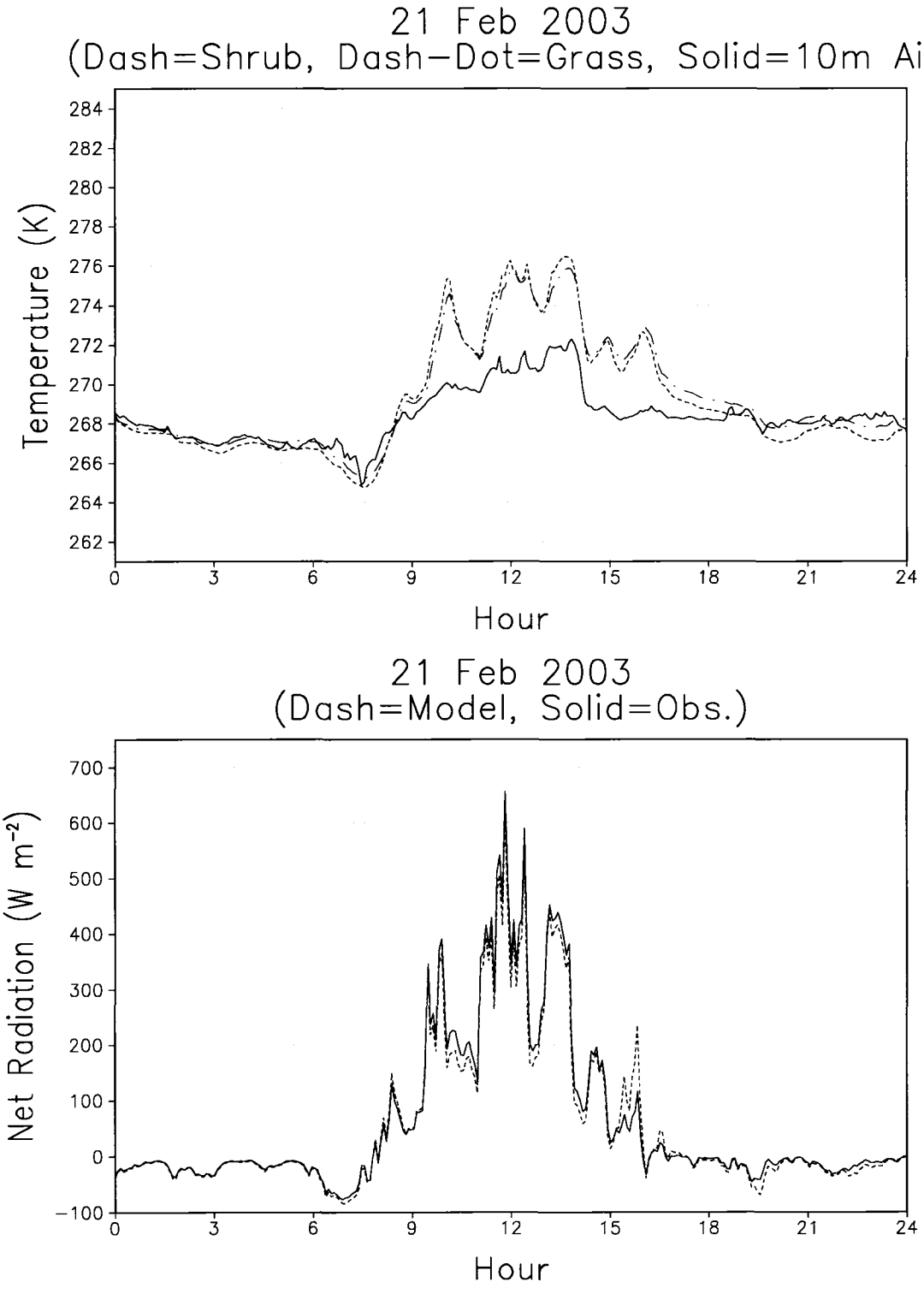

Figure 3.11: Same as Figure 3.3, except for 21 February 2003.

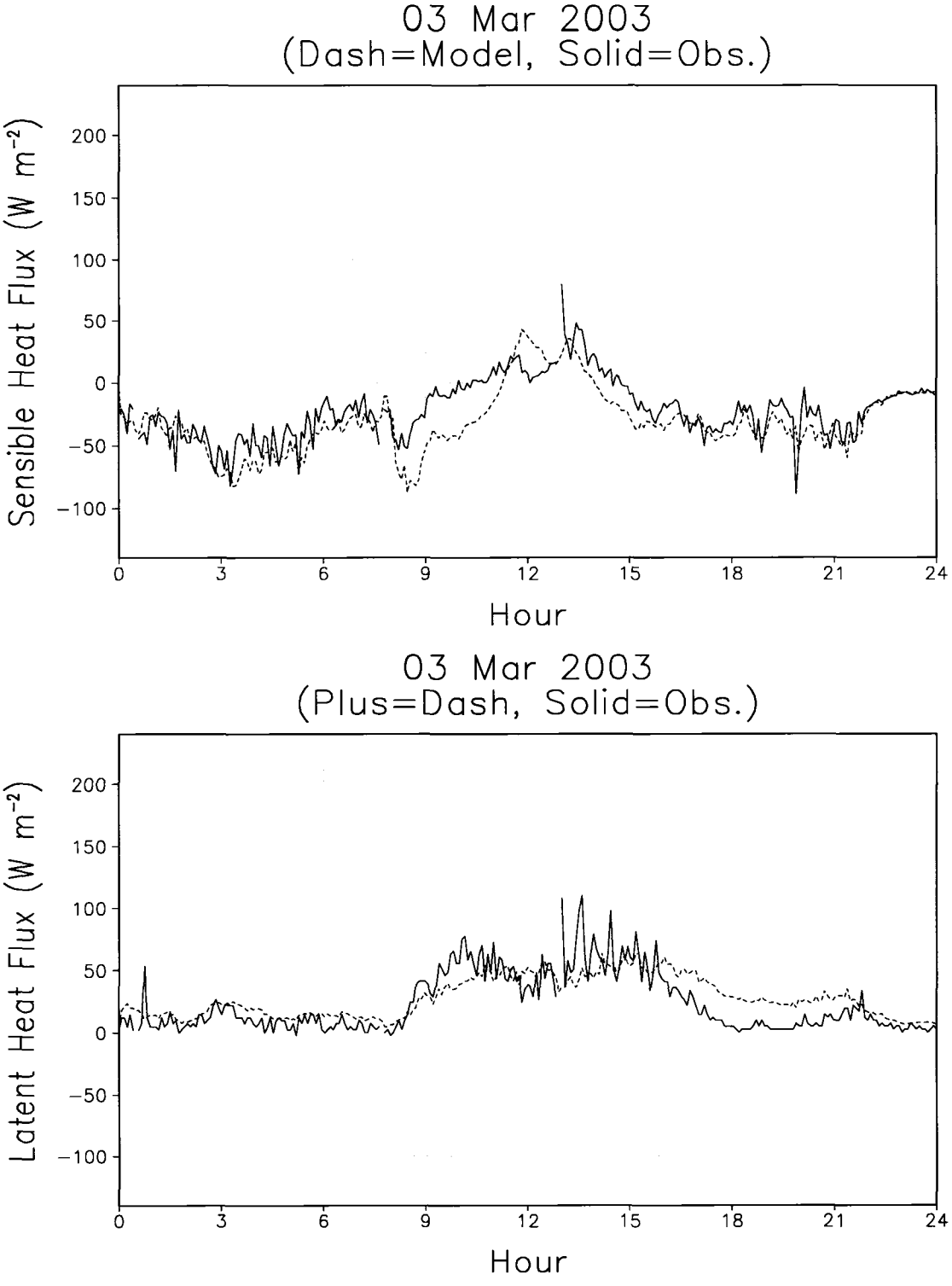

Figure 3.12: Same as Figure 3.2, except for 3 March 2003.

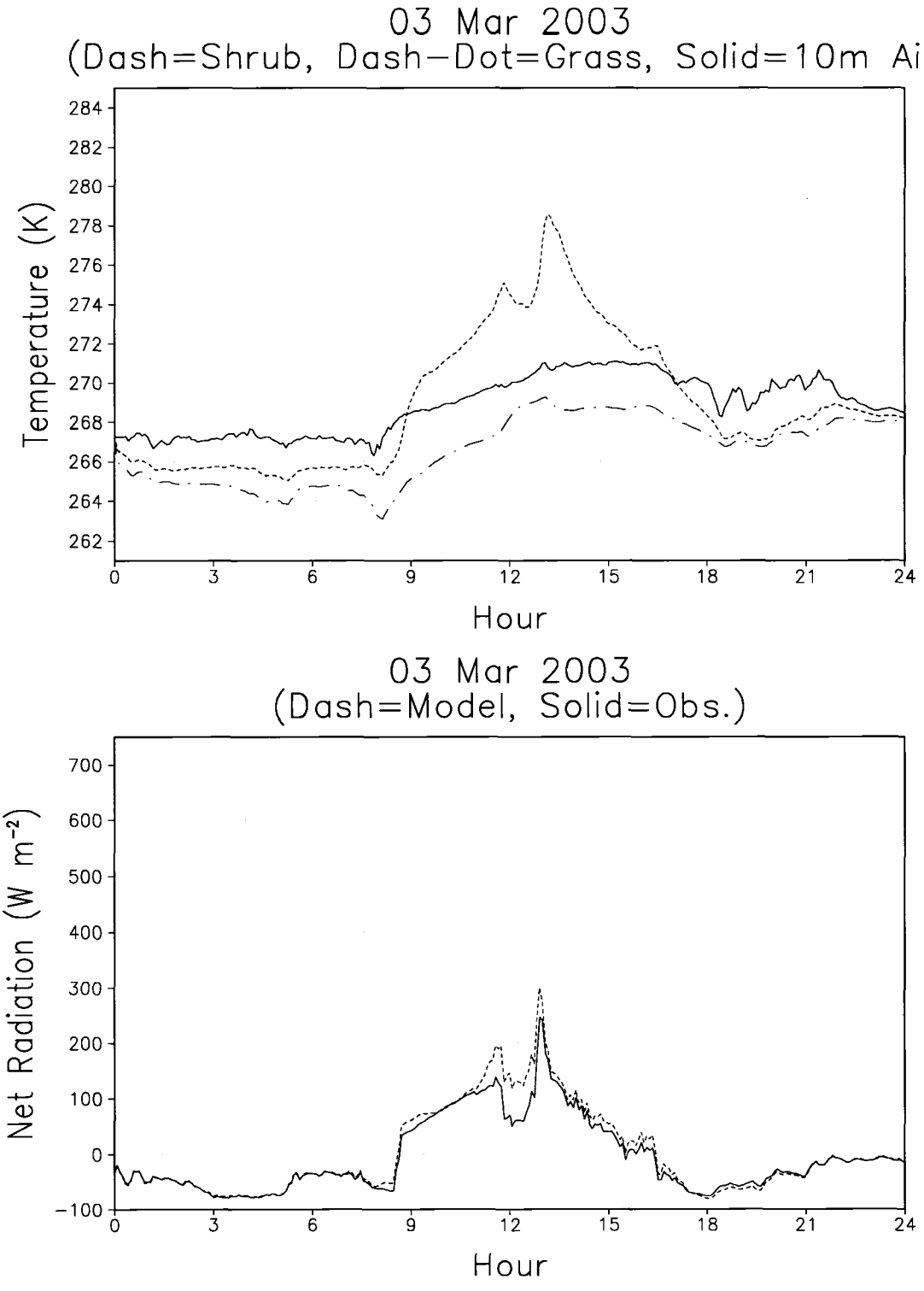

Figure 3.13: Same as Figure 3.3, except for 3 March 2003.

difference between modeled and observed latent heat fluxes was 12 W m^{-2} and the average percent difference was 150%. The net radiation, shown in Figure 3.13, featured a reduced mid-day maximum due to the increased snow cover. The model was able to match the observed net radiation fairly well, with an average absolute difference of 9 W m^{-2} and an average percent difference of 35%.

3.3.7 March 13, 2003

Figure 3.14 shows the sensible and latent heat fluxes for 13 March 2003. The average observed snow depths in the shrubs and grass were 0.14 and 0.12 m respectively. Average snow density in the shrubs and grass were 414 and 234 kg m^{-3} respectively. Finally, the fractions of shrub and grass areas covered with snow were 51 and 27% respectively. This day was handled more poorly than any other by the model. The sensible heat flux remained negative in the model for virtually the entire period, while the observations displayed a positive maximum around 100 W m^{-2} during the middle of the day. During the night the model overestimated the magnitude of the downward sensible heat flux. The average absolute difference between modeled and observed sensible heat fluxes was 38 W m^{-2} and the average percent difference was 260%. The observed latent heat flux exhibited a maximum near 200 W m^{-2} during the middle of the day, while the simulated flux peaked near 125 W m^{-2}. The average absolute difference between modeled and observed latent heat fluxes was 19 W m^{-2} and the average percent difference was 71%. Figure 3.15 shows that net radiation was underestimated by 100 W m^{-2} during the middle of the day. The average absolute difference between modeled and observed net radiation was 30 W m^{-2} and the average percent difference was 12%.

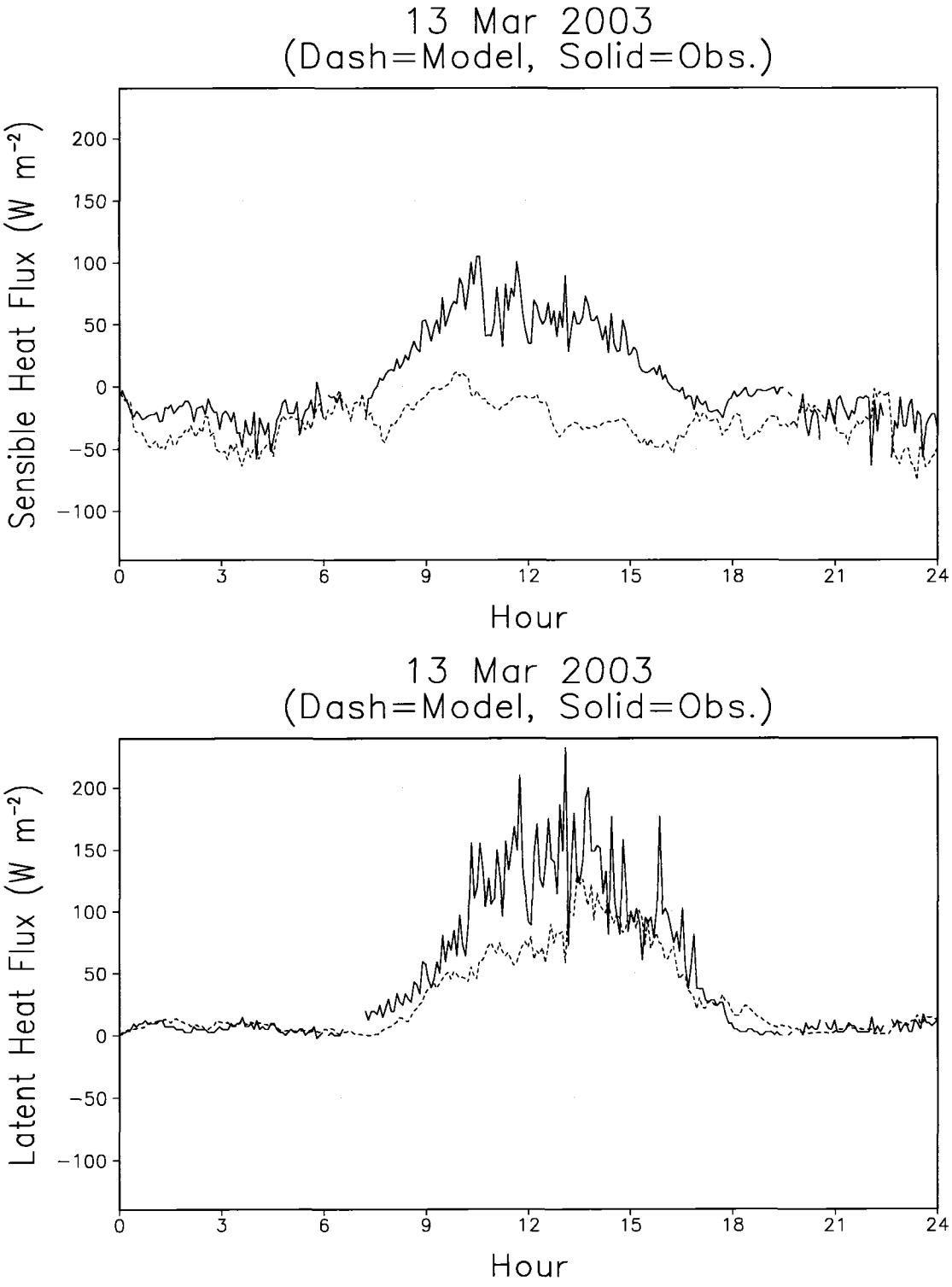

Figure 3.14: Same as Figure 3.2, except for 13 March 2003.

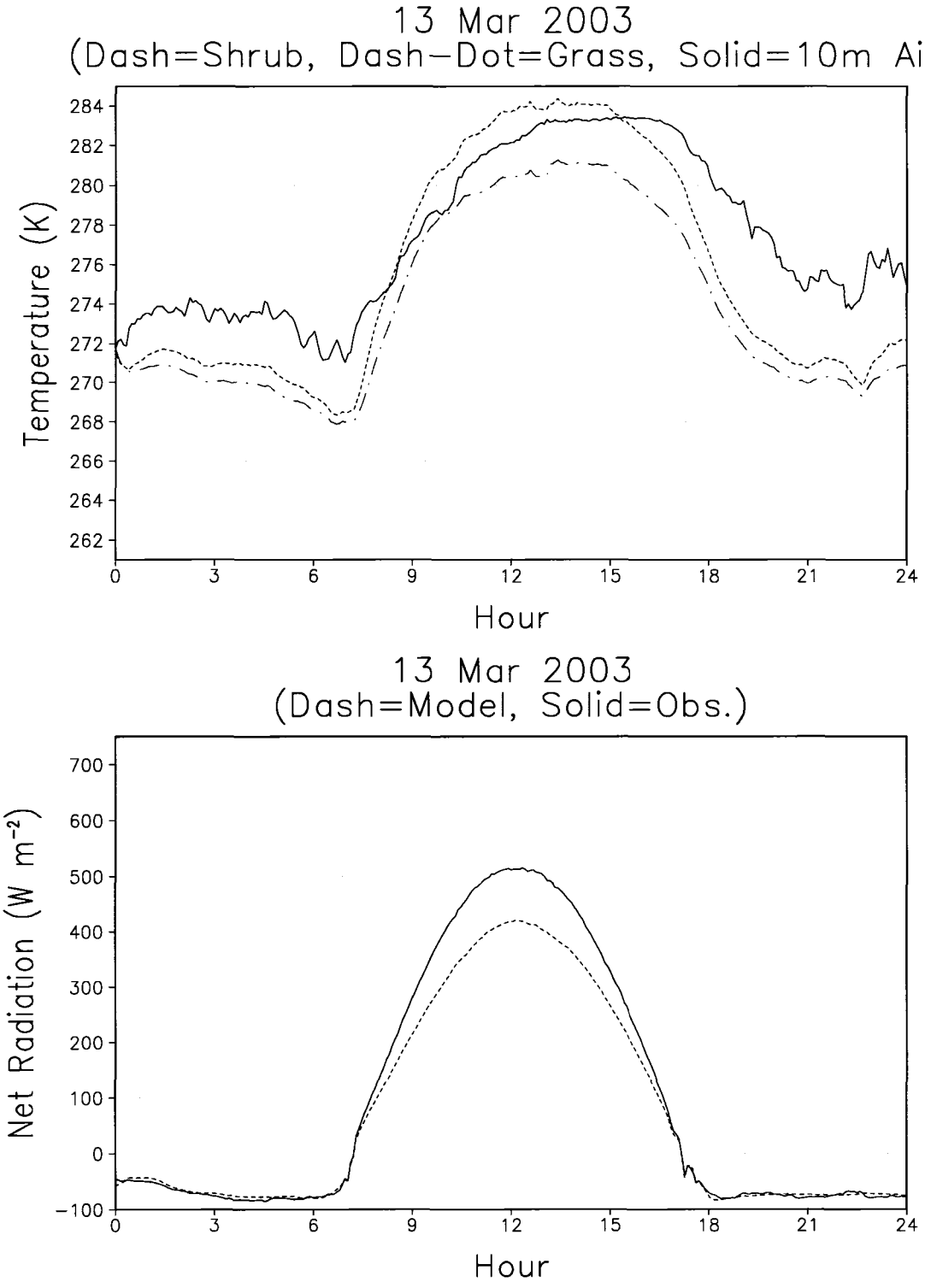

Figure 3.15: Same as Figure 3.3, except for 13 March 2003.

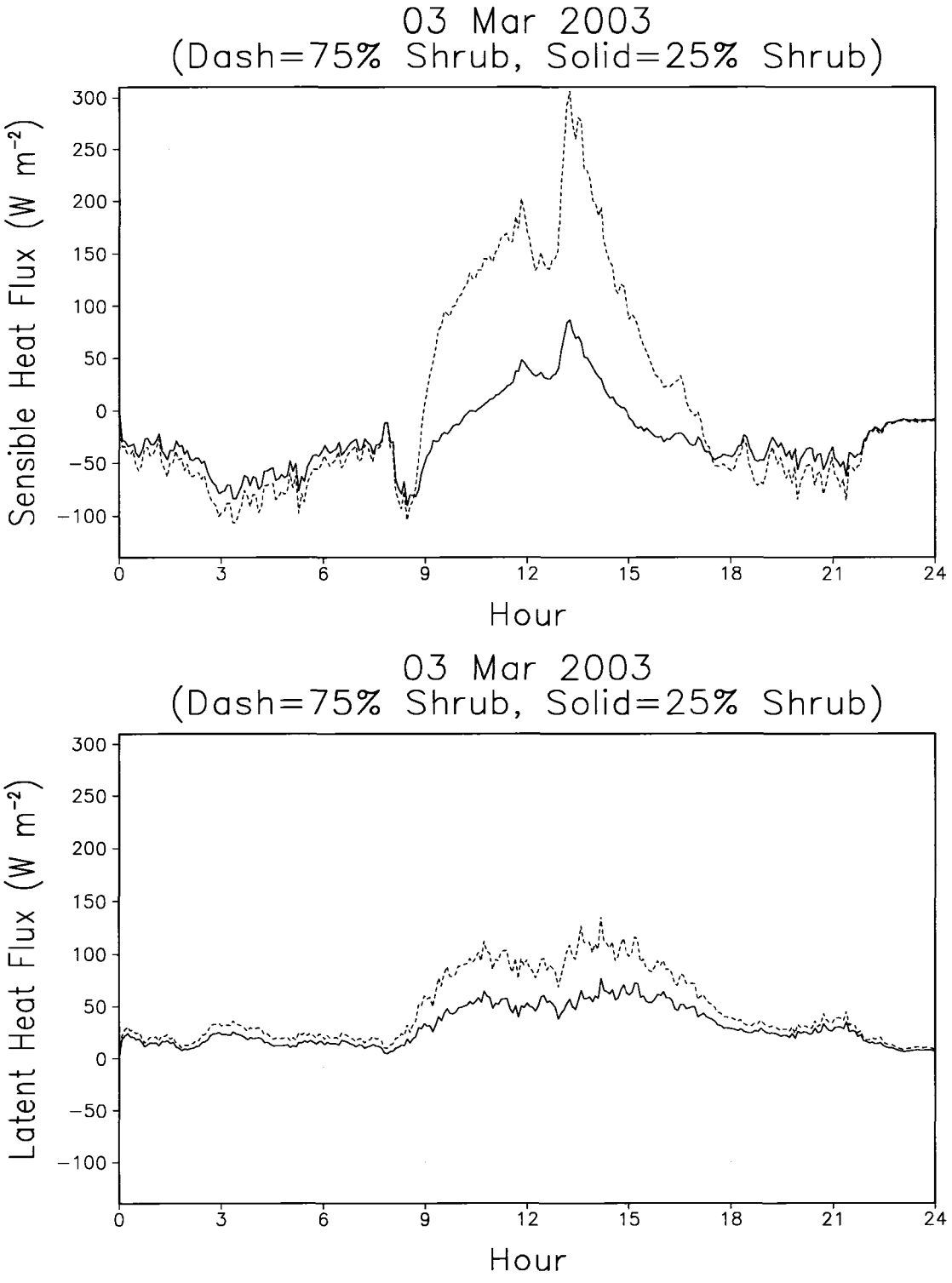

Figure 3.16: Modeled sensible and latent heat fluxes for case of 75% shrubs (red dashed line) and 25% shrubs (black solid line) on 3 March 2003.

3.4 Summary

In summary, the model captured the diurnal variation in the fluxes fairly well with the exception of the last day. The magnitudes, however, were in error quite often. One likely reason for the magnitude errors was the overly simplistic footprint used in this study. When the footprint is wrong the observations at the tower are not representative of the area being simulated by LEAF-2, and thus the model fluxes will not be expected to match the tower fluxes. An example of how sensitive the modeled fluxes are to the relative proportions of shrub and grass is shown on the previous page in Figure 3.16. These plots show the simulations for 03 March 2003 with the shrub fraction fixed at 25%, black solid line, and 75%, red dashed line. One can see that increasing the shrubs led to large increases in daytime sensible and latent heat fluxes. As a result, this fractional breakdown of the landcover must be known fairly accurately if the aggregate fluxes are to be simulated correctly. The development of a robust footprint theory for the FLOSS tower is beyond the scope of this study. The primary goal of this work was to see if LEAF-2 could reasonably simulate the fluxes of sensible and latent heat from a patchy snow-covered surface with heterogeneous vegetation.

Chapter 4

KUPARUK BASIN SIMULATIONS

4.1 Model Configuration

Three nested grids, as shown in Figure 4.1, were used in this study. The outer coarsest grid covered most of Alaska and had horizontal grid intervals of 72 km. The second grid covered a large part of north central Alaska and had horizontal intervals of 18 km, while the innermost grid was centered on the Kuparuk Basin with horizontal grid intervals of 4.5 km. On the two outer grids vertical grid intervals ranged from 300 m near the surface to 1000 m above the 12 km level. Vertical grid intervals on the fine grid ranged from 33 m near the surface to 1000 m above the 12 km level. The two coarse grids had a total of 27 levels reaching an altitude of about 18 km. The fine grid had 63 levels which also extended to about 18 km.

The model was initialized at 12 UTC 1 May for all three years, 1995, 1996, and 1997, with the NCAR-NCEP reanalysis (Kalnay et al. 1996). Surface observations in the Kuparuk Basin, provided by the University of Alaska Fairbanks Water and Environmental Research Center (WERC), were also incorporated into the atmospheric initialization fields. The simulations were all terminated in late June of each year after most of the significant snow had melted in the fine domain. The Smagorinsky (Smagorinsky et al. 1965) and Mellor-Yamada (Mellor and Yamada 1982) turbulence

schemes were used for horizontal and vertical diffusion, respectively. Both shortwave and longwave radiation were parameterized using the Chen and Cotton (Chen and Cotton 1983) routine. The boundaries of the outermost grid were nudged toward the NCAR-NCEP reanalysis every six hours during the course of the simulation.

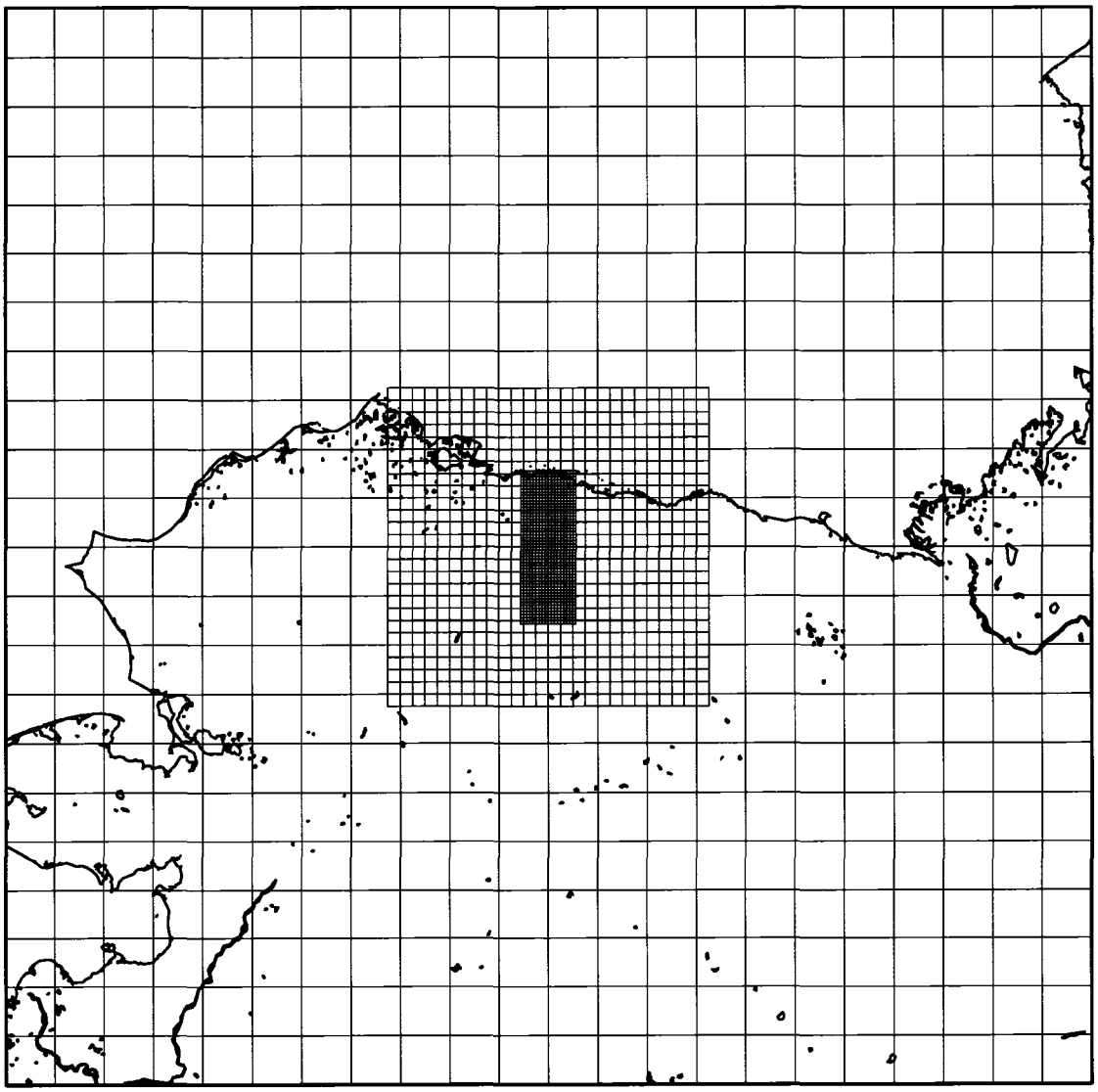

Figure 4.1: Atmospheric grid used for all three simulations.

4.2 Land-Cover Specification

For all simulations, the 1 km resolution Advanced Very High Resolution Radiometer (AVHRR) derived Olson Global Ecosystem (OGE) land-cover data (Olson 1994a; Olson 1994b) was used to specify the land cover in regions outside of the North Slope of Alaska. The land cover for the North Slope was specified from the 100 m resolution Northern Alaska-Multi-Spectral Scanner (NA-MSS) data set (Muller et al. 1999). For the shrub enhanced simulation, the moist and moist/wet tundra land-cover types were considered suitable for invasion by shrubs and were therefore replaced with the shrub category. The polluted snow simulation used the same vegetation as the control simulation.

In RAMS 4.4, LEAF-2 cross references all vegetation types to one of 18 Biosphere-Atmosphere Transfer Scheme (BATS) (Dickinson et al. 1986) categories for which physical parameters have been defined. The vegetation physical parameters used by LEAF-2 are albedo, LAI, vegetation fraction, emissivity, roughness length, displacement height, and root depth. In these simulations most of the North Slope was cross referenced to the deciduous shrub and tundra BATS categories. The displacement heights of tundra and shrubs were adjusted from their BATS values to correspond to canopy heights given in Liston and Sturm (2002). The resulting canopy heights for shrubs and tundra were 0.5 m and 0.1 m respectively. In addition, the LAI of shrubs was adjusted to zero since they are bare during most of the simulation period. The vegetation fraction of the shrubs was also adjusted to 0.7 due to lack of leaves. Finally, tundra vegetation fraction was adjusted to 0.9 to account for the thick organic mat which covers most of the soil. The default BATS values were used for all the other vegetation parameters. In the shrub enhanced

simulation the shrub canopy height was increased to 0.75 m and all other vegetation parameters remained the same as in the control. The vegetation parameters in the polluted snow simulation were the same as those in the control run.

4.3 Snow-Cover Initialization

The initial snow water equivalent (SWE) on the fine grid was derived by running the blowing snow model SnowTran-3D from 1 September to 30 April of each year as described in Liston and Sturm (2002). At regional scales the end-of-winter SWE in the Arctic is closely approximated by the difference between the total winter precipitation and the loss due to sublimation. Liston and Sturm (2002) used this principal to estimate the total winter precipitation for each of the years simulated in this study, namely 1995, 1996, and 1997. They iterated the model starting with a first guess for total winter precipitation equal to the observed north-south transect of end-of-winter SWE. The total precipitation was adjusted with each iteration until the average end-of-winter SWE at each latitude in the model was equal to the observed value. This SWE field was used for initialization of the fine grid in the control runs. The SWE on the fine grid for the enhanced shrub simulation was obtained by replacing the moist/wet tundra and moist tundra with shrubs on the SnowTran-3D domain and rerunning with the precipitation fields obtained above. In addition, since the shrubs were assumed to have become larger in the shrub enhanced simulation their snow holding capacity was increased by 50%. The initial SWE for the polluted snow simulation was the same as for the control.

The SWE for portions of the coarse grids located outside the fine grid region was initialized with the April values of the Global Monthly EASE-Grid Snow Water Equivalent Climatology dataset (Armstrong et al. 2005). This dataset is a 25 km grid of

Scanning Multichannel Microwave Radiometer (SMMR) and selected Special Sensor Microwave/Imagers (SSM/I) derived monthly mean SWE values.

Snow densities for the fine grid region were initialized from values observed by König and Sturm (1998) for each year. Each grid cell on the outer grids was assigned one of six snowcover classes from the Global Seasonal Snow Classification System (Liston and Sturm 1998b). Snow in these cells was then assigned a typical density (Liston et al. 1999a) based on its class. Coefficients of variation for use with SSNOWD were also assigned to each cell based on these classes.

Snow albedo was initialized based on time since last snowfall, as determined from the precipitation estimates generated by the SnowTran-3D simulations. New snow in the control and enhanced shrub runs was assigned an albedo of 0.85. The snow albedo decreases with time since last snowfall according to Equation 2.3. In the polluted snow simulation the new snow albedo was set 0.75. The decrease of 0.1 in this case represents the effect of black carbon contamination.

4.4 Soil Temperature and Moisture Initialization

There were eight soil layers extending down to 3 m depth. The soil layer thickness ranged from 0.05 m near the surface to 0.1 m at the deepest level. The soil types were specified from the Food and Agriculture Organization of the United Nations (FAO) dataset (FAO 1997). Soil temperature and moisture were specified from the 32 km National Center for Environmental Prediction North American Regional Reanalysis (NCEP-NARR) (Mesinger et al. 2006). The soil moisture was defined as all ice when the soil temperature was 0° C or less.

4.5 Simulation Specific Modifications to LEAF-2

The version of LEAF-2 used in these simulations was very similar to that used in the BOREAS and FLOSS testing projects, however, there were a few minor modifications. First of all, the blowing snow model had not been implemented for these simulations. The inclusion of the blowing snow model was not considered a priority for this study since very little blowing snow occurs during the May through June period of these simulations. Secondly, the fractional snow-covered area of the LEAF-2 patches was calculated with SSNOWD (Liston 2004) using the coefficients of variation assigned based on the Global Seasonal Snow Classification System. In the FLOSS study the snow-covered fraction was held constant and based on observations since the simulations were so short. In addition, the reduction in snow albedo with age has been decreased by 50% to better match the observed snow albedo in the region.

Finally, LEAF-2 in its present state can not accurately produce sensible heat fluxes from vegetation that is completely bare of leaves, since it is based on LAI. In order to get around this the sensible heat flux from the shrubs was modeled as being equal to the net radiation absorbed by the branches as in Otterman et al. (1993). This assumes that the heat capacity of the shrubs is very small and that there is no significant cooling due to the latent heat of evaporation. Cooling of the shrubs by latent heat of evaporation was negligible for most of this simulation since they were mostly dormant during the snow melt season. This is the same method used in Strack et al. (2003).

4.6 Control Run

In this section a discussion of the results of the control run is given. Observed values of snow water equivalent at Imnavait Basin and Betty Pingo, AK are compared

with those simulated by the model; see Figure 4.2 for station locations. In addition, observed 3 m air temperatures at the Imnavait Basin, West Kuparuk, UK Met, Franklin Bluffs, Sagwon, and Betty Pingo meteorological stations are compared with simulated values. These stations are all operated by the WERC. Finally, the observed incoming shortwave and longwave radiation, albedo, and net radiation at these stations are also compared with the model output. These comparisons will shed some light on how well the model can simulate the present day conditions in the Kuparuk Basin.

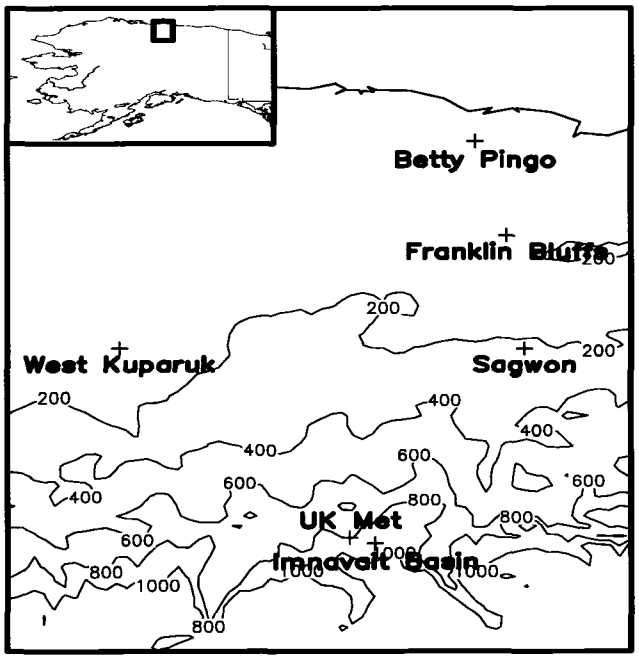

Figure 4.2: Map showing the locations of the Kuparuk meteorological stations. Topography is shown in 100 m intervals by the thin black contours.

4.6.1 Snow Water Equivalent

The observed evolution of snow water equivalent at the Imnavait research basin and Betty Pingo meteorological station are shown by the black circles in Figures 4.3-4.5. Imnavait Basin is an approximately 2.2 km^2 research watershed centered near 68.6° N and

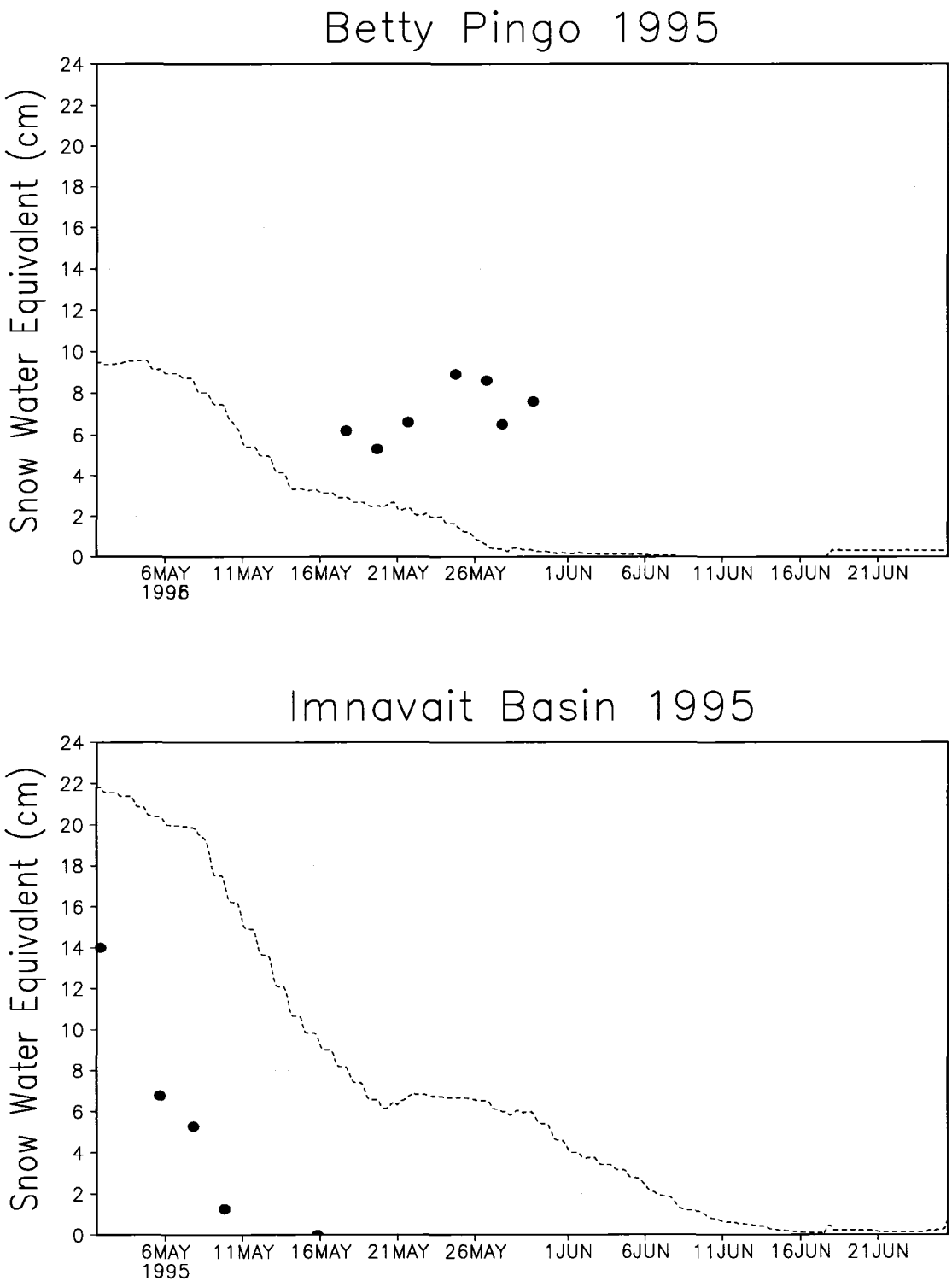

Figure 4.3: Observed and simulated SWE for Imnavait Basin and Betty Pingo (1995). Solid circles represent observations; red dashed line represents modeled values.

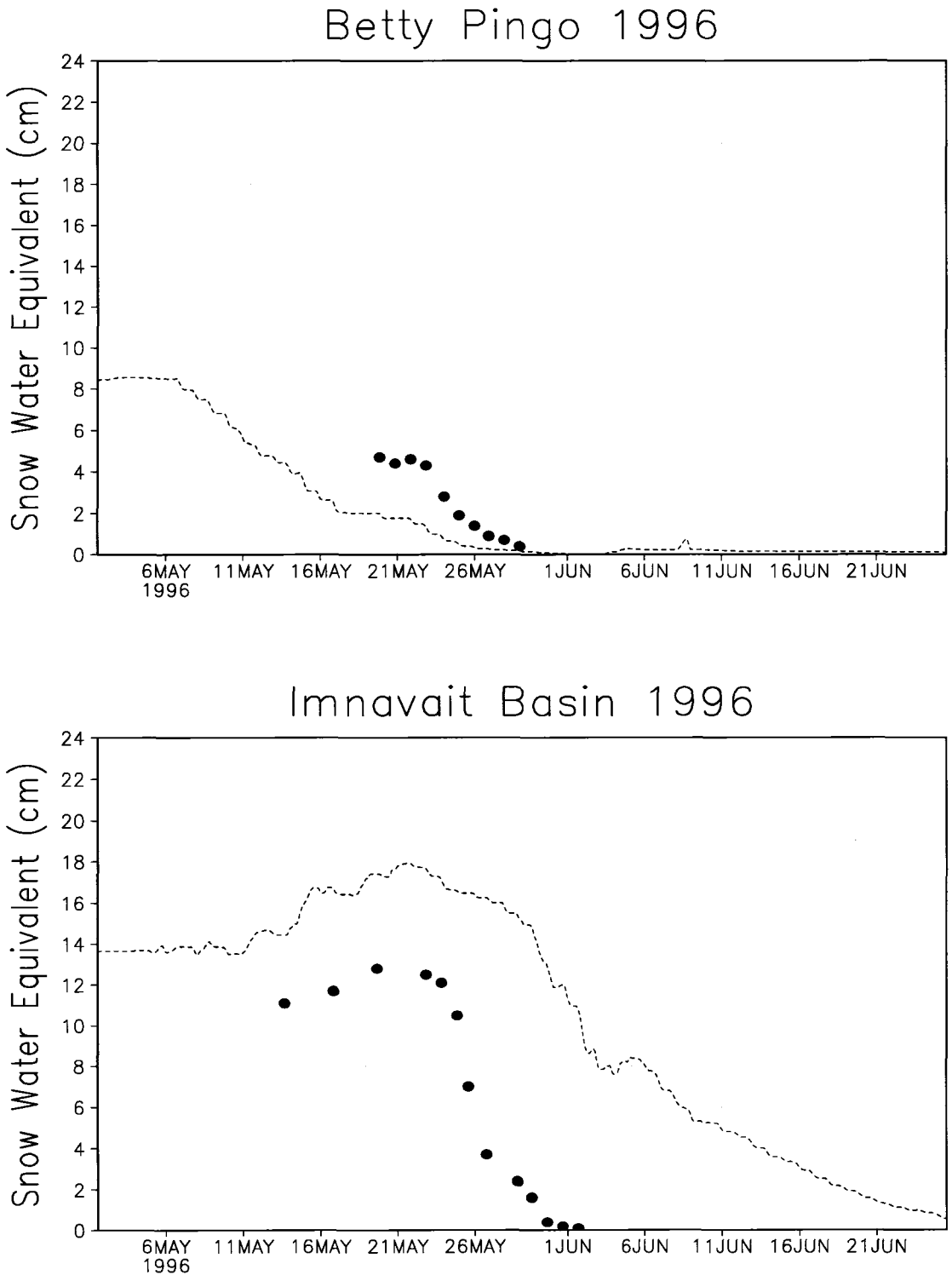

Figure 4.4: Same as Figure 4.3, except for 1996.

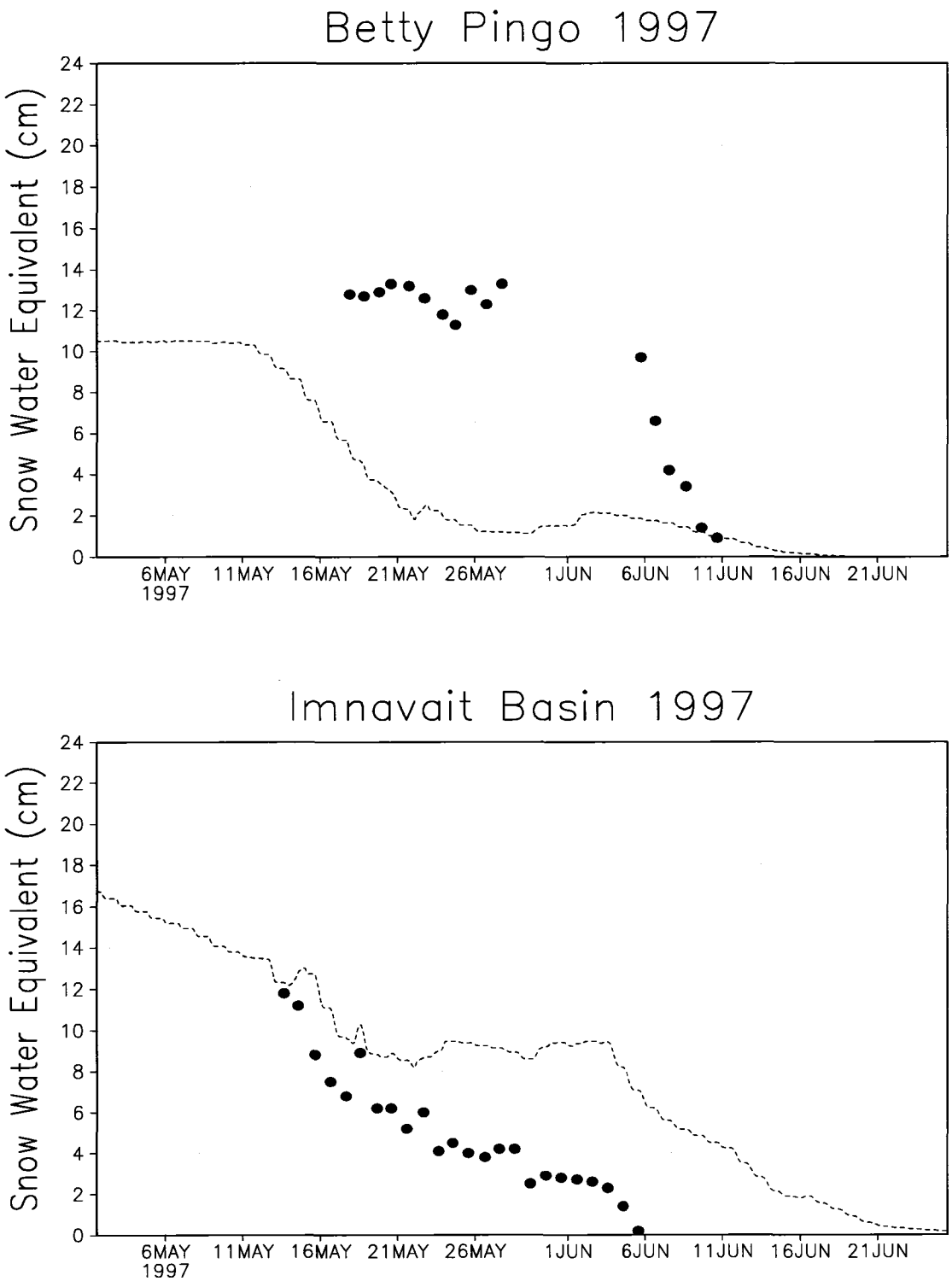

Figure 4.5: Same as Figure 4.3, except for 1997.

149.3° W (Kane et al. 1997). Betty Pingo is located on the Arctic coastal plain at the northern end of the Kuparuk Basin. Every few days during the melt period 50 snow depth and 5 snow density measurements were made at each of six sites along a transect across the Imnavait watershed. Four of the sites were located on the west facing slope of the basin, one on the valley bottom, and one on the east facing slope. The west facing slope represents about 78% of the basin while the east facing slope and valley bottom represent 17 and 5% of the basin respectively. The values shown in Figures 4.3-4.5 are area-weighted averages of the west and east facing slopes and the valley bottom. Every few days during the melt period 50 snow depth and 10 snow density measurements were also made at each of three sites located near the Betty Pingo station.

The red dashed lines in Figures 4.3-4.5 show the snow water equivalent evolution as simulated at the model grid cells containing Imnavait Basin and Betty Pingo. In all years the simulated snow melted too quickly at the Betty Pingo site. This could be due to excessively high incoming solar radiation, discussed in the next section, in the model. In contrast, the simulated snow at the Imnavait basin location persisted much longer than the observed values. However, it should be noted that the simulated snow depths are for the grid cell containing the observation stations. The values shown for Imnavait basin represent an area of 2.2 km^2 while the grid cell covers 20.25 km^2. It is possible that the snow remaining in the grid cell is located outside of the area of measurements. The grid cell containing Imnavait Basin was 35, 28, and 40% snow free at the time the observed snow in the watershed was gone in 1995, 1996, and 1997 respectively. A very small amount of snow persists until the end of the simulation in 1996 and 1997, but it covers less than 10% of the cell and represents a few deep drifts.

4.6.2 Air Temperatures and Radiative Fluxes

Figure 4.6 shows plots of the observed versus simulated net albedo for all six meteorological stations for 1995. No observations were available for Betty Pingo and Franklin Bluffs. The simulated albedo started around 0.85 for all the stations, except Betty Pingo which started at 0.72, and fell gradually to around 0.2 as the snow ablated. The observed albedo generally fell more rapidly during the snow melt period than in the model. This could be due to the fact that the meteorological towers see a smaller and more homogeneous region than the 4.5 km grid cells in the model. The snow will disappear from the footprint of the tower in a much shorter period of time than over the large grid cell which likely contains more heterogeneity in snow cover. The observed snow-free albedo was about 0.05 and 0.1 lower than the simulated values at the UK Met and West Kuparuk stations respectively. The observed snow-covered albedo appeared to be 0.1 to 0.2 higher than the modeled values at the UK Met station. Observed snow-covered albedo at the other stations was similar to those in the model. The diurnal pattern in the simulated albedo at Betty Pingo, Franklin Bluffs, and West Kuparuk was due to the presence of lakes and their associated zenith angle dependent albedo.

Figure 4.7 shows the observed and simulated albedo at the same stations in 1996. Again, the modeled albedo exhibited a more gradual transition to snow-free values than the observations. Initial albedo was too low at Betty Pingo, Franklin Bluffs and West Kuparuk while the snow-free albedo was too high. The model did fairly well at simulating both the snow-covered and snow-free albedo at Sagwon and the UK Met station. The results in 1997 were similar to those in 1996; see Figure 4.8.

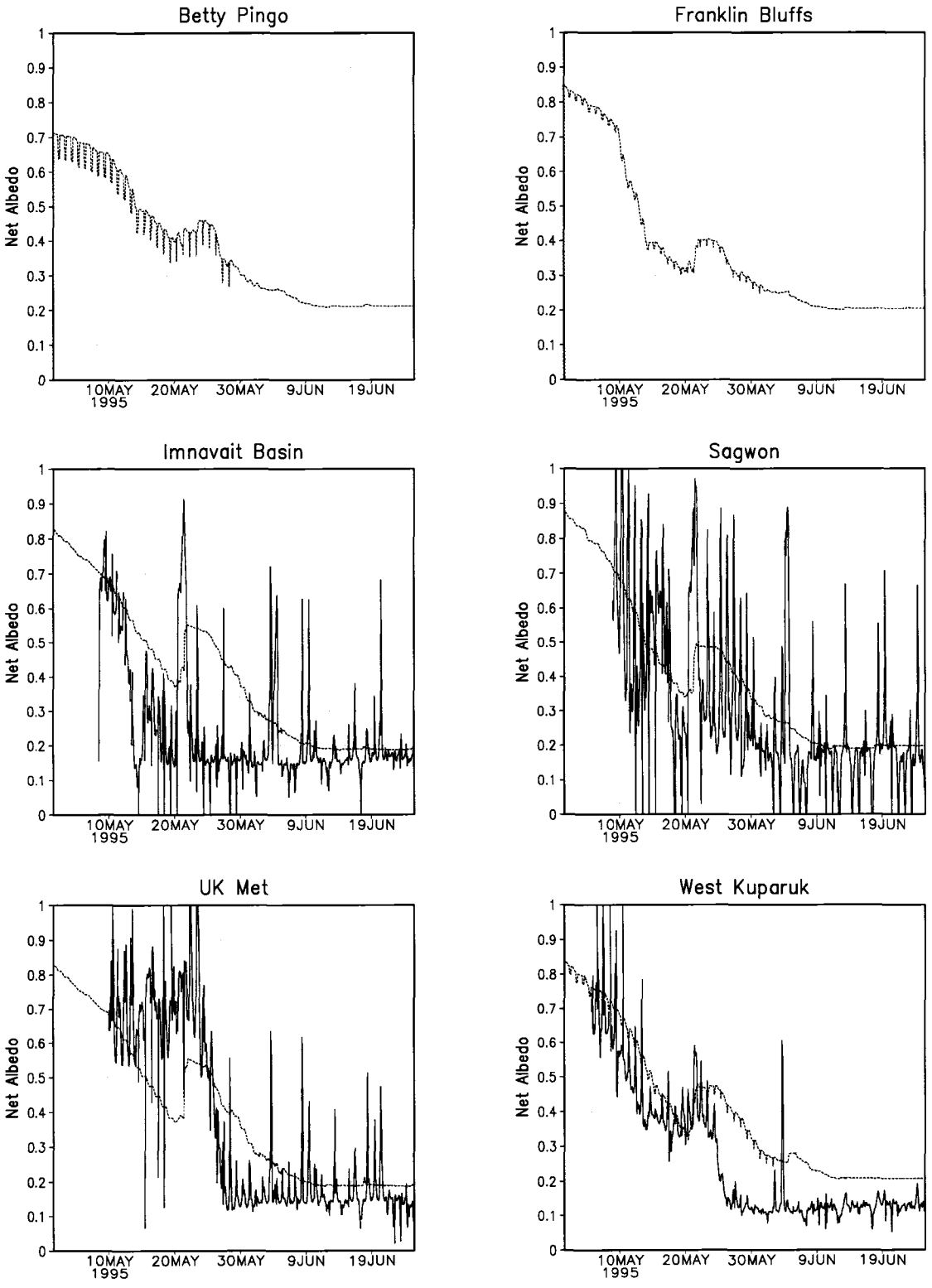

Figure 4.6: Simulated (red dashed line) and observed (black solid line) net surface albedo for 1995.

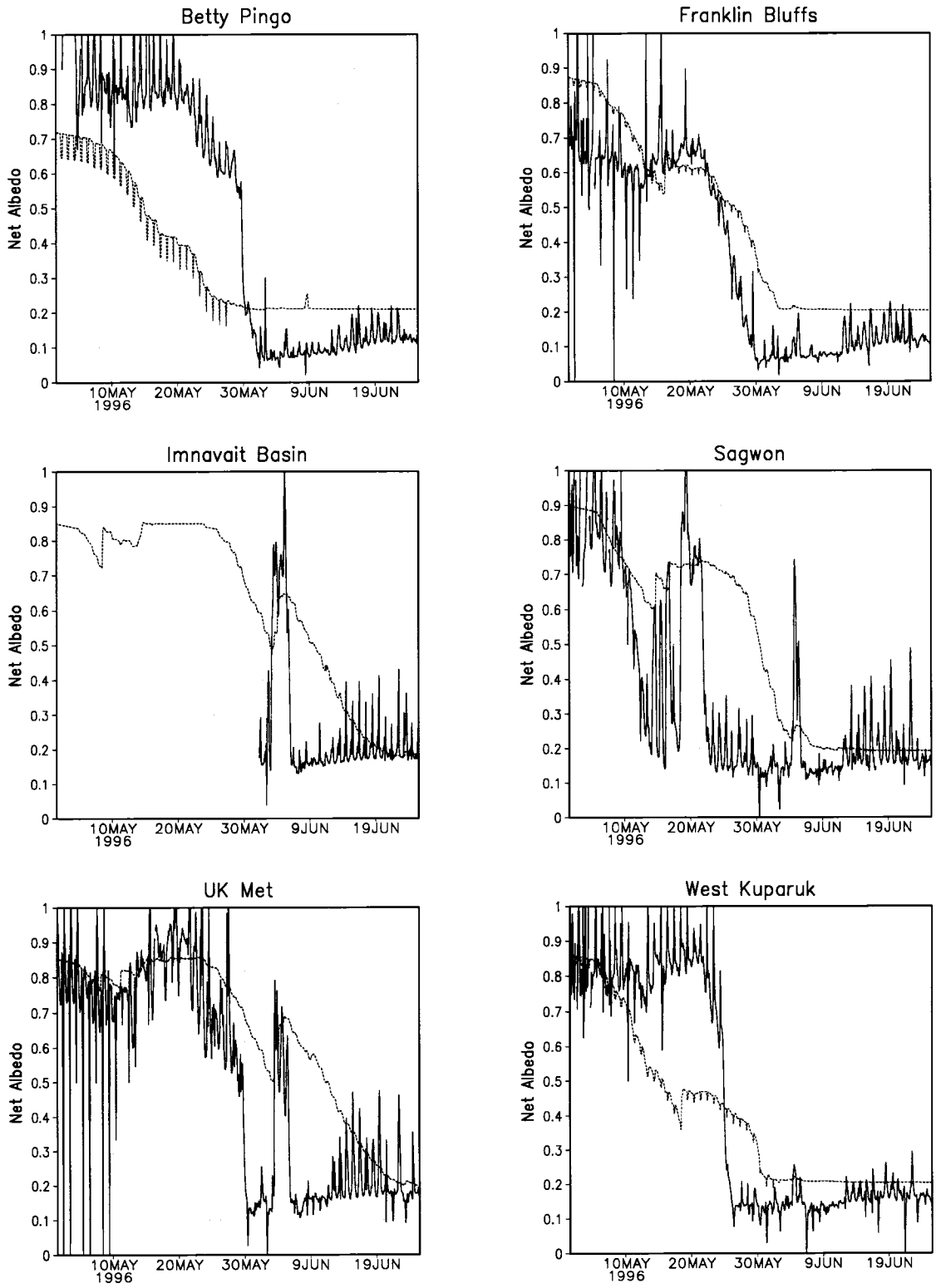

Figure 4.7: Same as Figure 4.6, except for 1996.

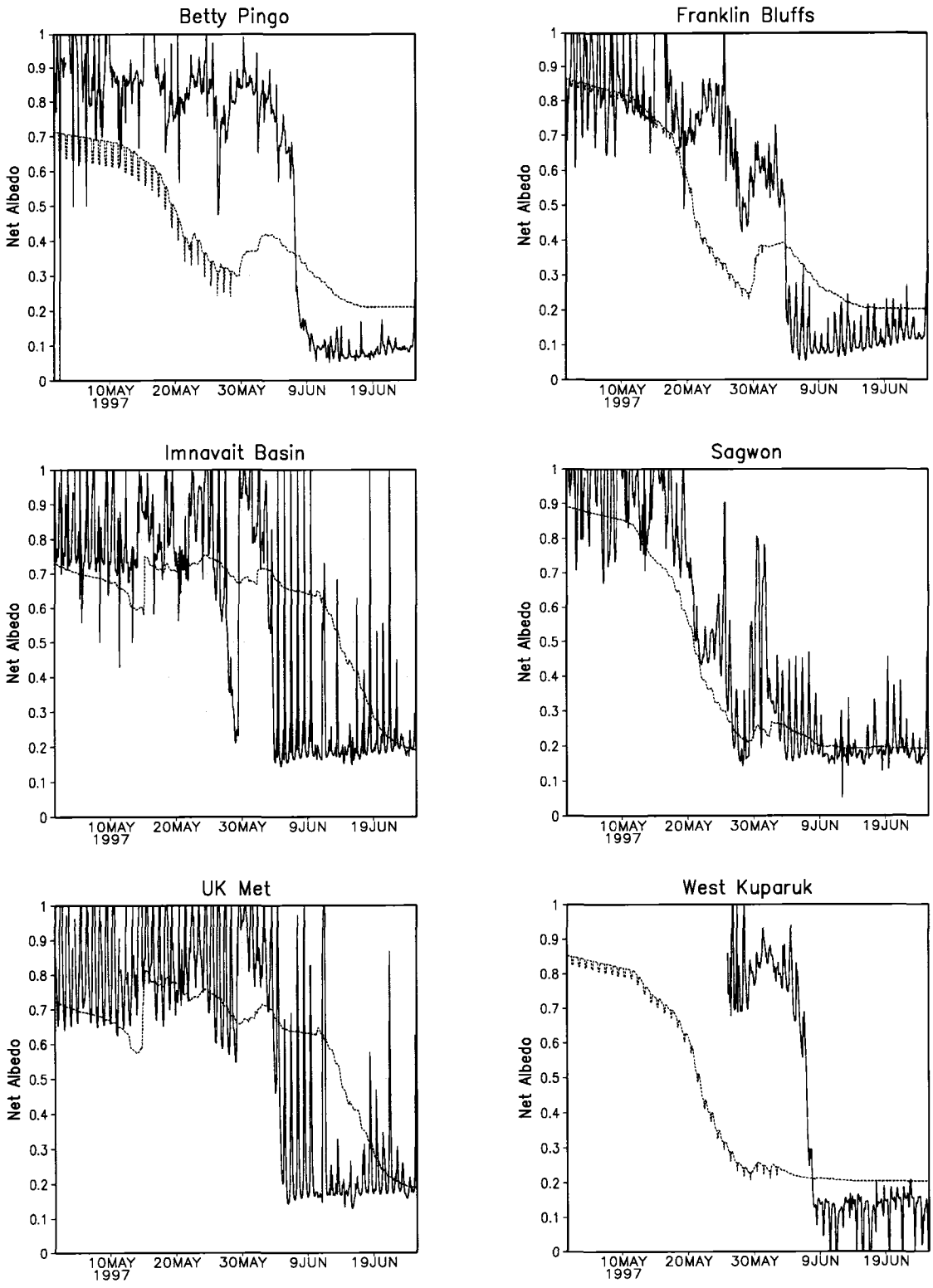

Figure 4.8: Same as Figure 4.6, except for 1997.

Figure 4.9 displays the differences in simulated and observed values of incoming solar radiation for 1995. At the stations where observations were available the simulated solar radiation often varied widely from the observed, often either over or underestimating by 200 W m^2 or more. Figures 4.10 and 4.11 show the incoming solar radiation for 1996 and 1997 respectively. The model generally varied widely from observations in these years as well.

Figure 4.12 shows the downwelling longwave radiation at the meteorological stations in 1995. The model underestimated the downward longwave radiation at Imnavait Basin and the UK Met station, often by 50 W m^2 or more. The model tended to overestimate the downwelling longwave radiation at West Kuparuk during the first part of the simulation, and alternated between over and underestimating during the latter part of the simulation.

The simulated downward longwave radiation in 1996 appeared to be too low most of the time at all the stations except West Kuparuk; see Figure 4.13. The flux at West Kuparuk tended too fluctuate between being too high and too low during much of the simulation. In 1997 the downwelling longwave radiation appeared to be too low at Betty Pingo and the UK Met station, but was generally too high at Franklin Bluffs; see Figure 4.14. The flux at Sagwon and West Kuparuk fluctuated between being too high and too low.

The frequently underestimated downward longwave radiation in the model may play a role in the delayed snow melt. Snow is a near perfect absorber of longwave radiation, and thus its rate of melt is very sensitive to changes in this quantity. The effects of the overestimation in incoming solar radiation discussed earlier could be more than

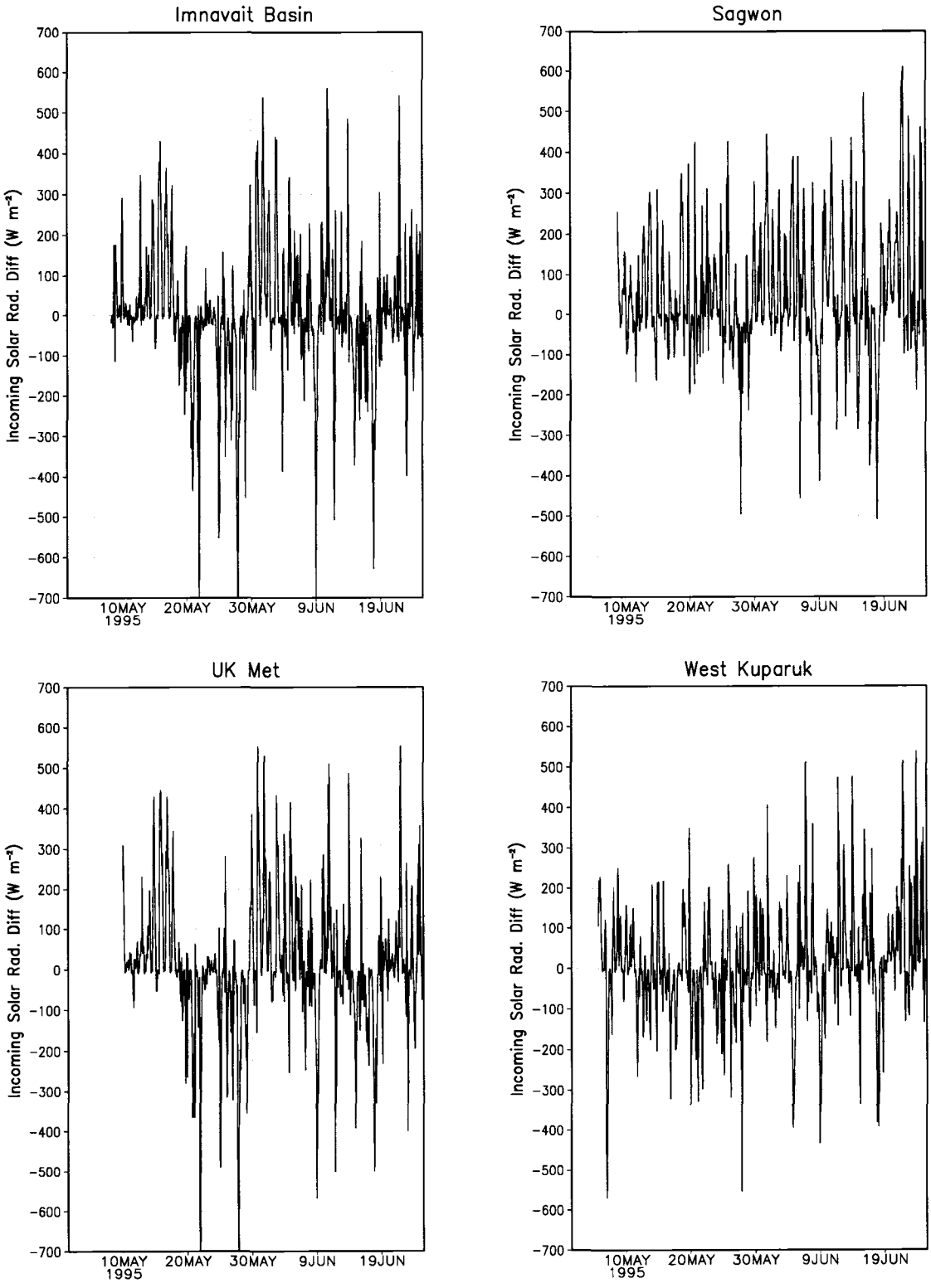

Figure 4.9: Difference between modeled and observed (Model-Observed) incoming solar radiation.

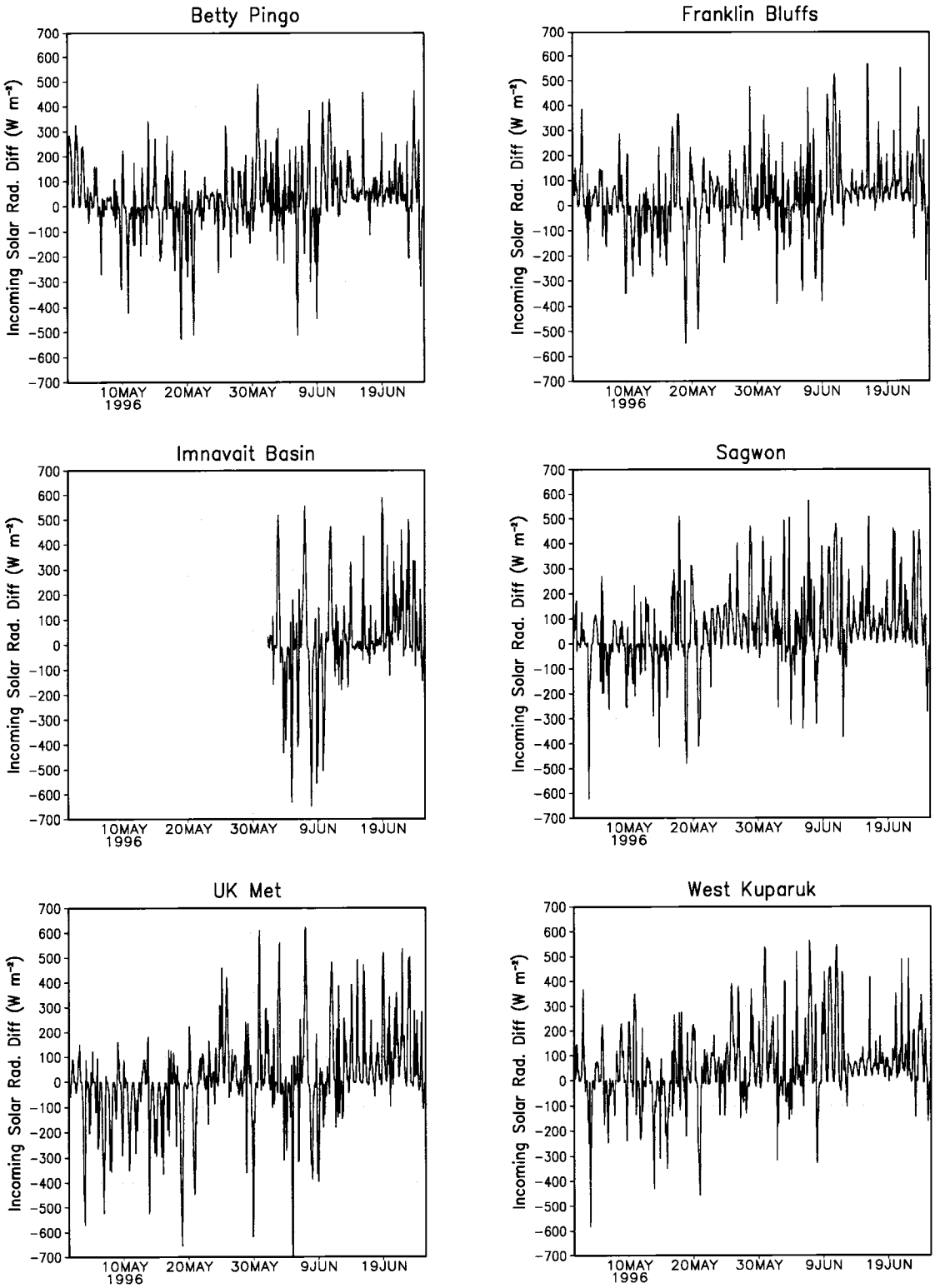

Figure 4.10: Same as Figure 4.9, except for 1996.

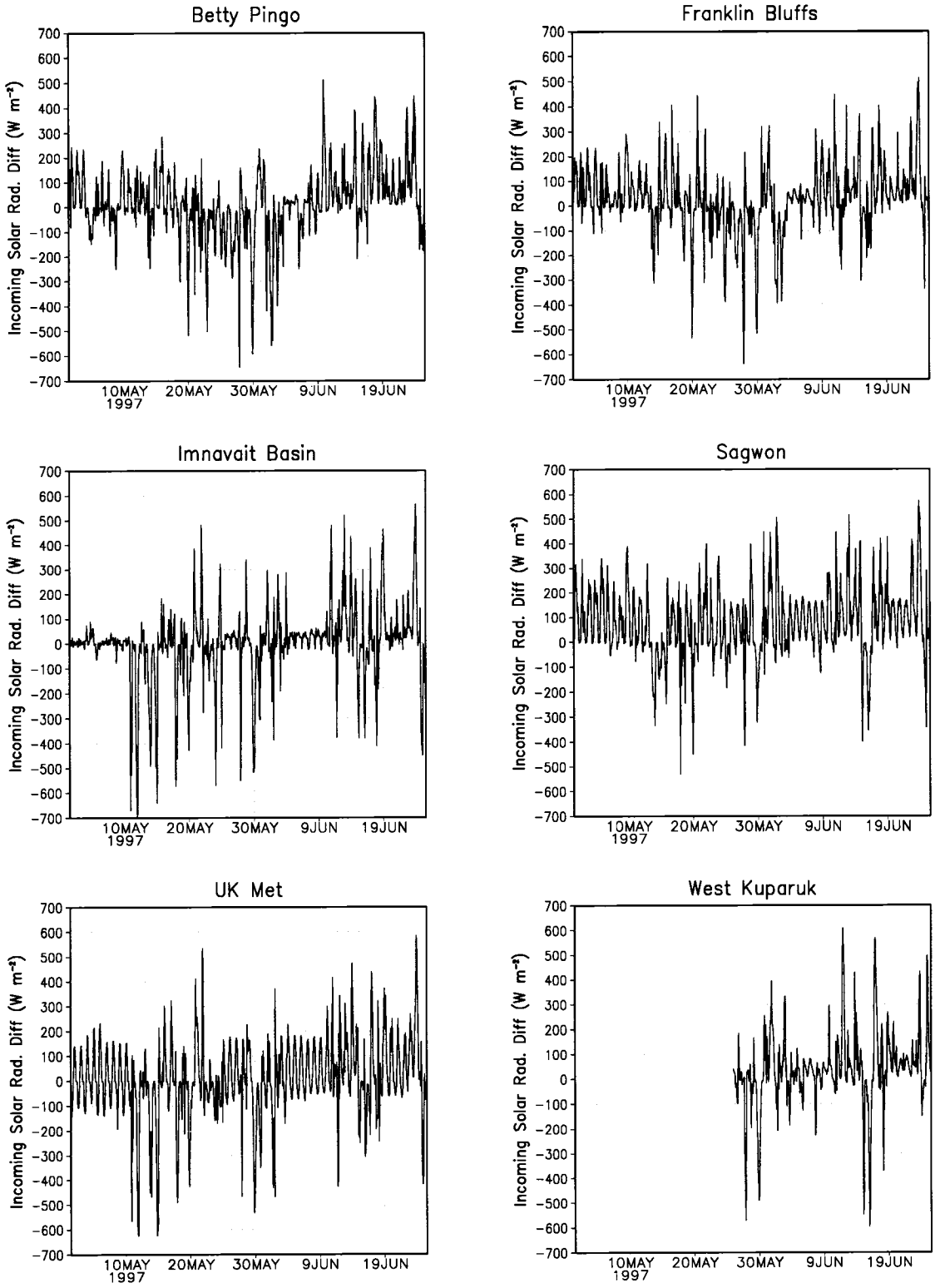

Figure 4.11: Same as Figure 4.9, except for 1997.

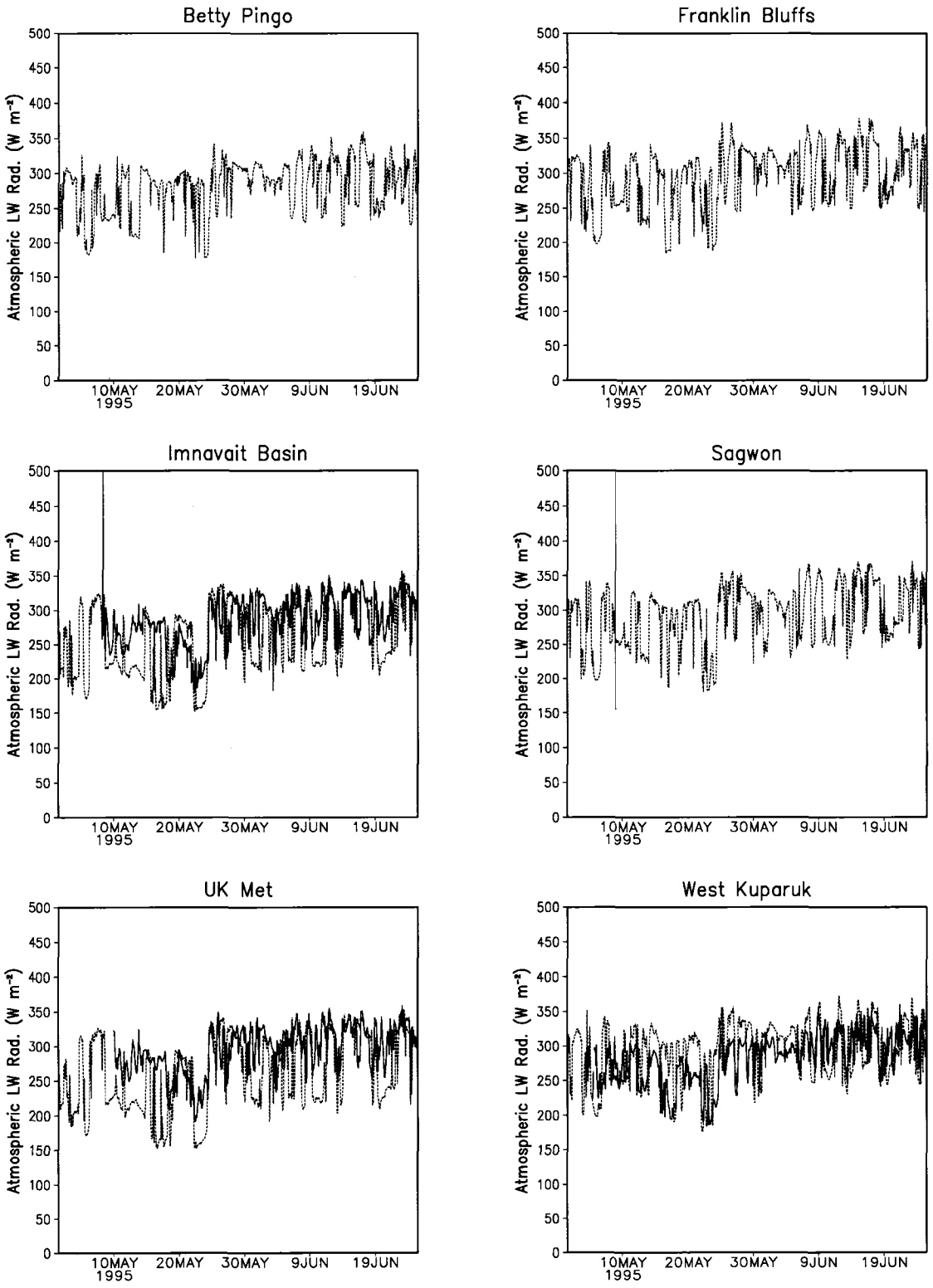

Figure 4.12: Simulated (red dashed line) and observed (black solid line) downwelling longwave radiation for 1995.

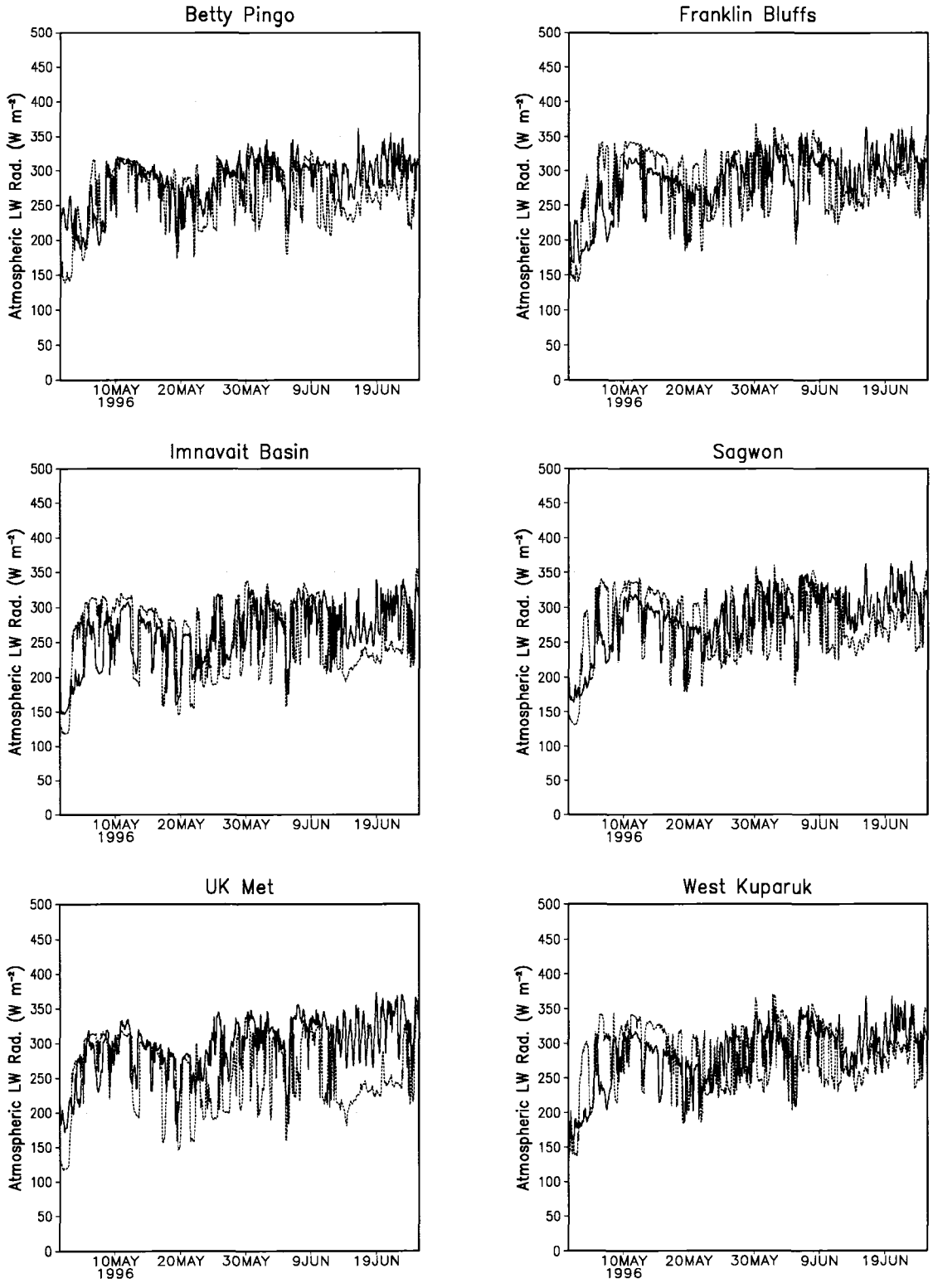

Figure 4.13: Same as Figure 4.12, except for 1996.

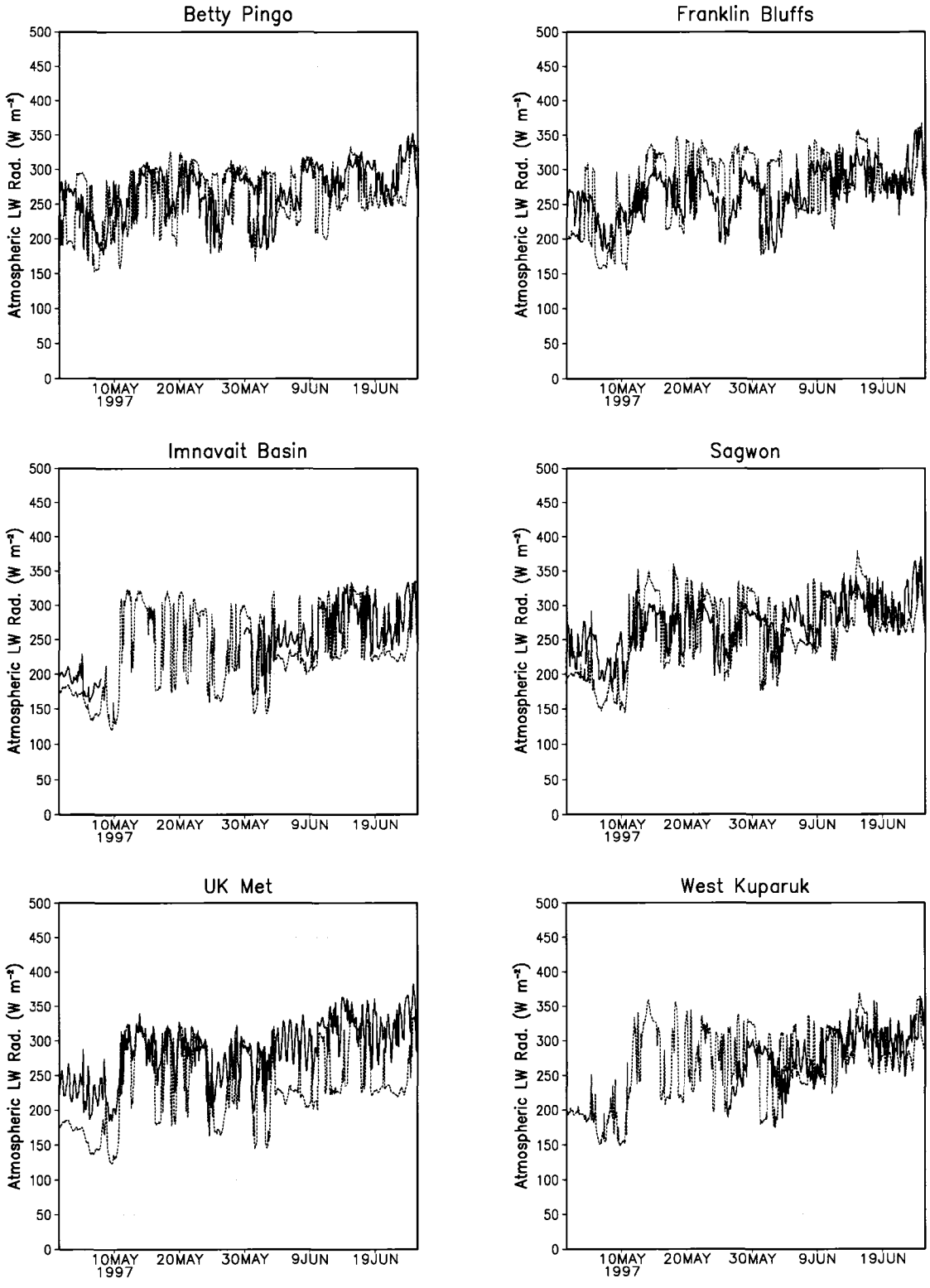

Figure 4.14: Same as for Figure 4.12, except for 1997.

offset by the reduced longwave radiative flux, leading to the overall sluggish snowmelt in these simulations.

Figure 4.15 shows the simulated and observed surface net radiation for 1995. The model tended to overestimate the downward net radiation during the daytime at Betty Pingo, especially during the first part of the simulation. On the other hand, the downward net radiation was often too small during the daytime at Imnavait Basin and Sagwon. In addition, the simulated upward net radiation appeared to be too large during the nighttime at these two stations. The modeled net radiation at West Kuparuk and the UK Met station appeared to be too large during most of the simulation. Although the magnitudes were off the model did capture some of the synoptic variability, such as the observed decrease in early May at Imnavait Basin and West Kuparuk. Figures 4.16 and 4.17 show the same general patterns hold for 1996 and 1997 respectively.

Finally, Figure 4.18 shows simulated and observed 3 m air temperatures for 1995. The model was able to capture the synoptic-scale variations in temperature fairly well at all stations. However, the temperatures were consistently too low at Imnavait Basin, West Kuparuk, and the UK Met station. The temperatures tended to be closer to the observations or slightly warmer at the northern stations. Part of the cool bias at the southern stations was likely due to the more persistent snow at these locations in the model. Figures 4.19 and 4.20 show the same general patterns hold for 1996 and 1997 respectively. When averaged over all years, the model averaged 0.9°C cooler than the observations during the month of May.

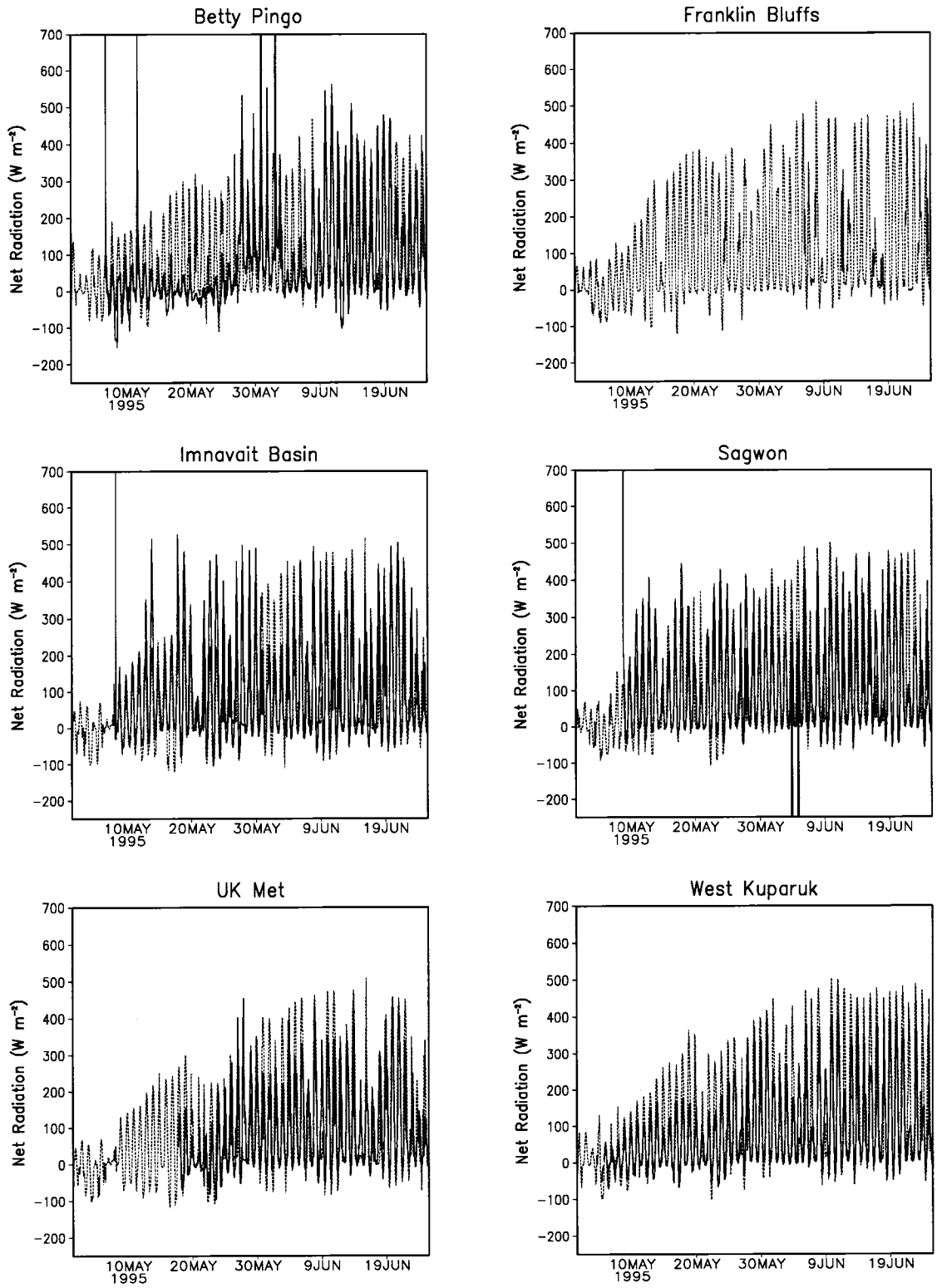

Figure 4.15: Simulated (red dashed line) and observed (black solid line) net radiation for 1995.

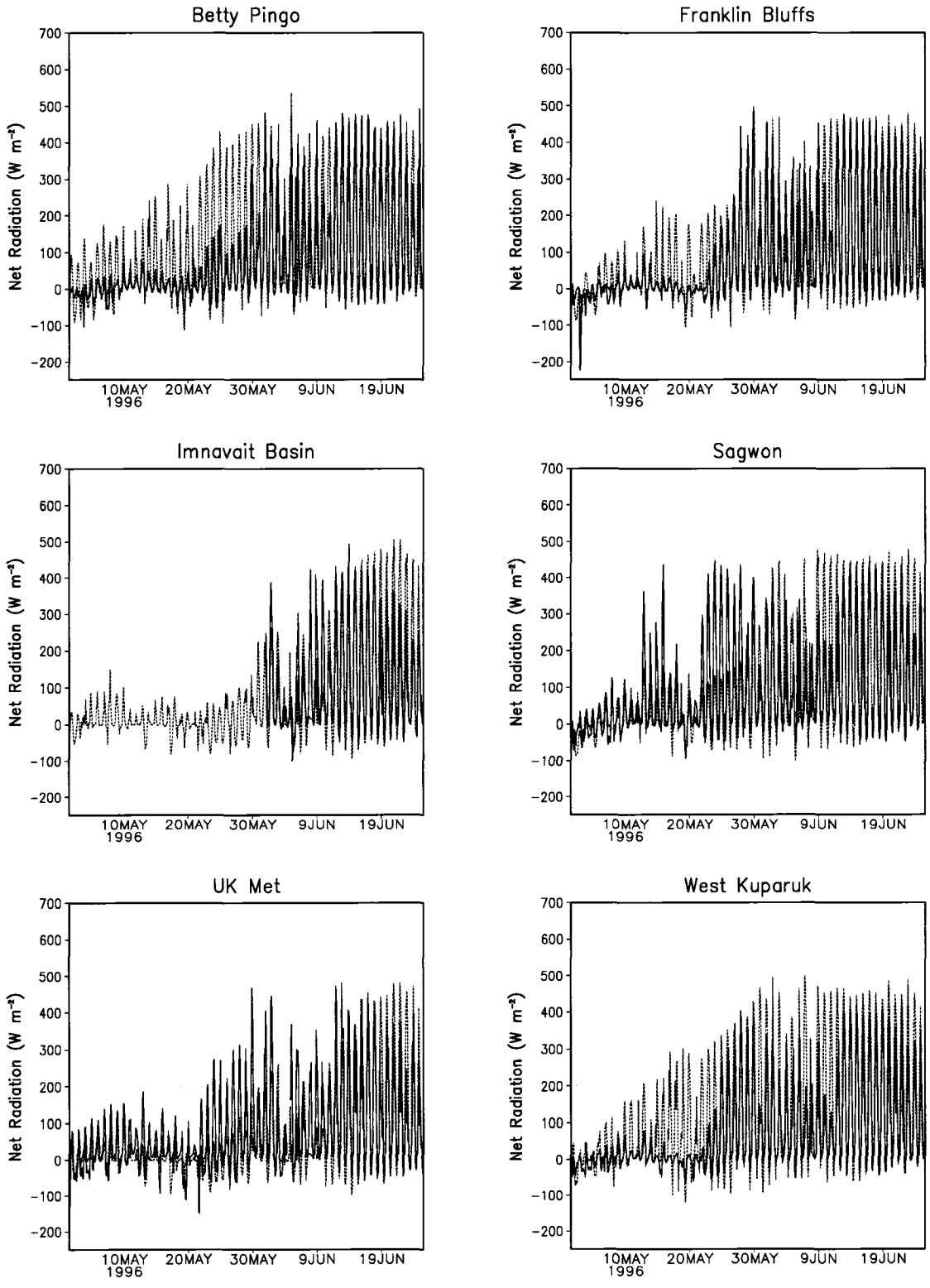

Figure 4.16: Same as for Figure 4.15, except for 1996.

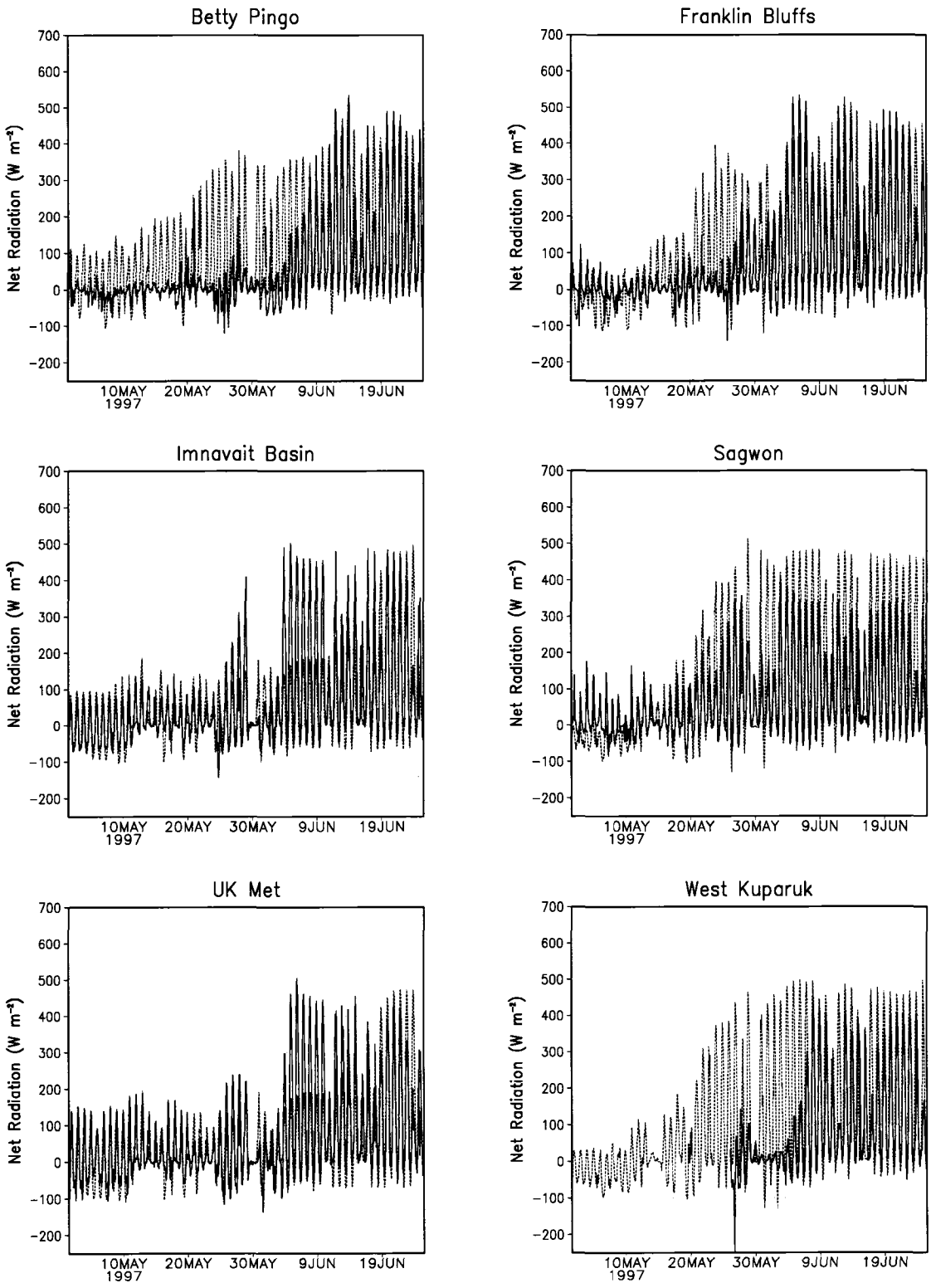

Figure 4.17: Same as for Figure 4.15, except for 1997.

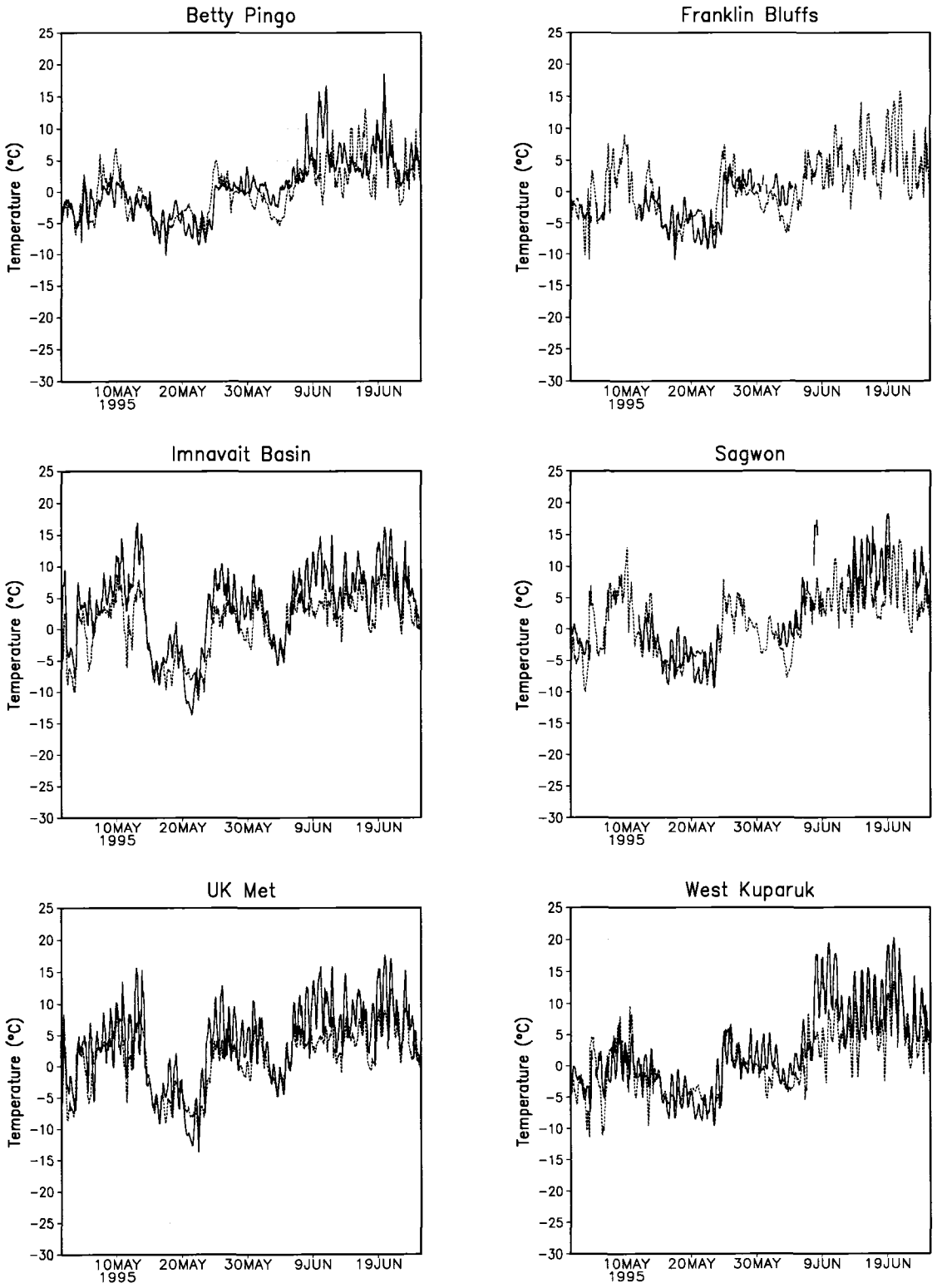

Figure 4.18: Simulated (red dashed line) and observed (solid black line) 3 m air temperature for 1995.

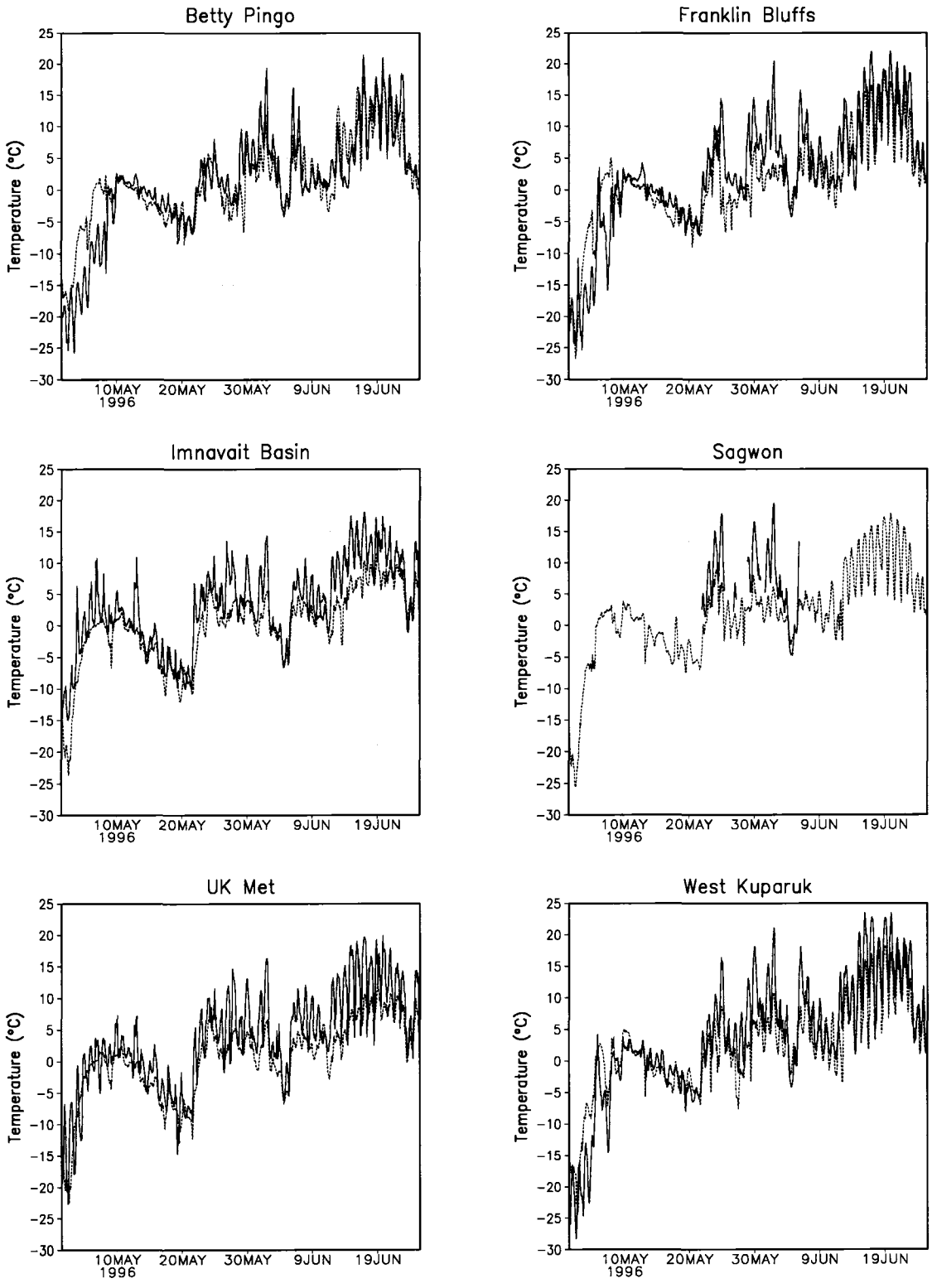

Figure 4.19: Same as for Figure 4.18, except for 1996.

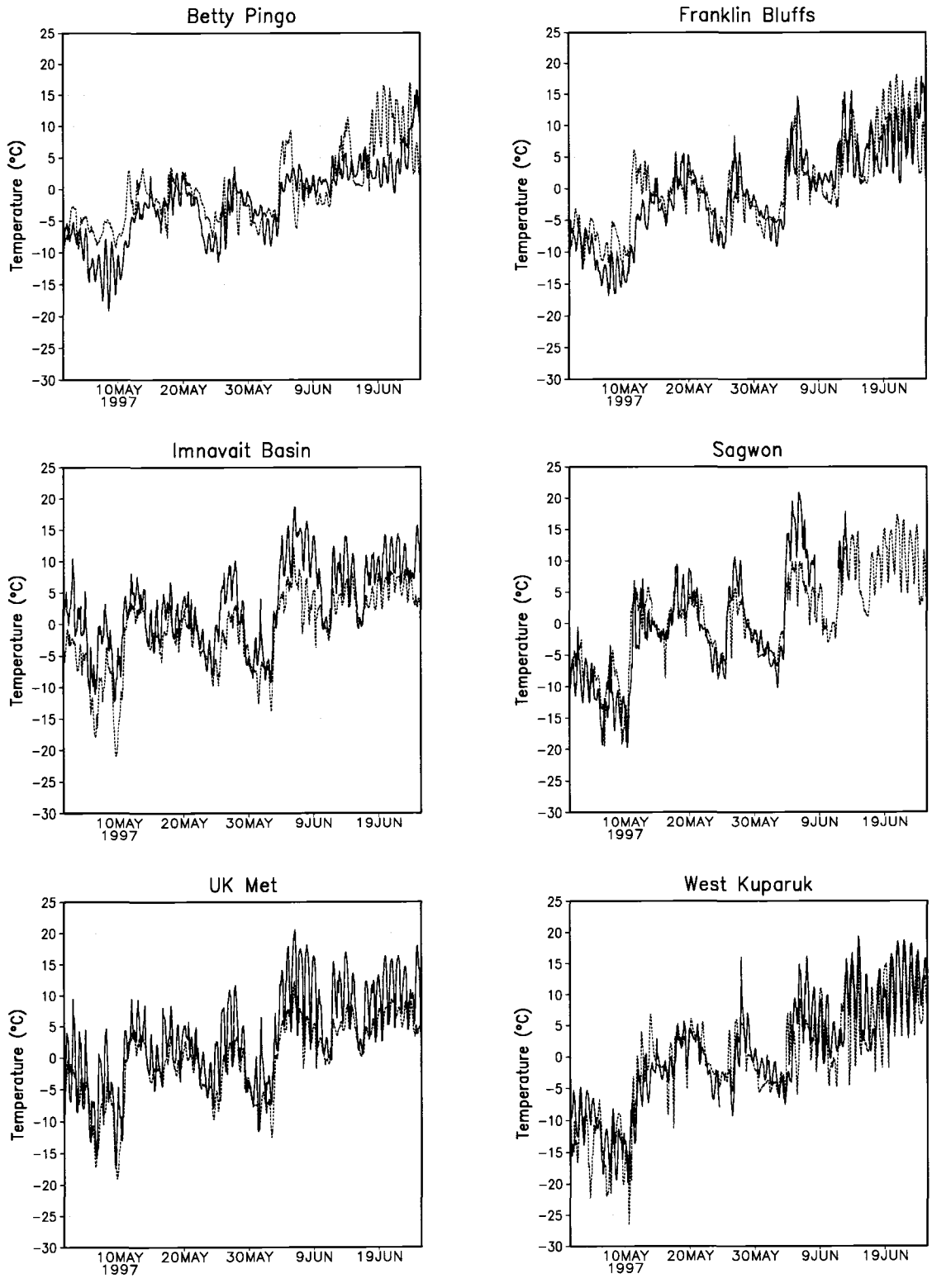

Figure 4.20: Same as for Figure 4.18, except for 1997.

4.6.3 Statistical Comparison of Control Run to Observations

The root mean square error (E), root mean square error with bias removed (EU), and the standard deviations of the predictions (σ) and observations (σ_{obs}) for the quantities mentioned above are listed in Table 4.1. All of these statistics were calculated using Equation 12.20 of Pielke (2002). According to Pielke (2002), a model demonstrates skill when $\sigma \approx \sigma_{obs}$, $E < \sigma_{obs}$, and $EU < \sigma_{obs}$. This study was most interested in the predominately snow-covered period, and so the following statistics were compiled only for the month of May when snow cover is most prominent.

Table 4.1 shows that the model appeared to have some skill in simulating the 3 m air temperatures, with a root mean square error of 4.3°C and σ_{obs} = 6.5°C. These results are comparable to the root mean square error in near-surface air temperatures in a snow modeling study by Narapusetty and Mölders (2005). They ran test simulations with the Hydro-Thermodynamic Soil-Vegetation Scheme (HTSVS) coupled to the Pennsylvania State University-National Center for Atmospheric Research (NCAR) Mesoscale Meteorological Model (MM5) and calculated root mean square errors around 11°C near the end of the 120 hour simulations. Even though their simulations are much shorter than those described in this dissertation, the results still suggest the E value of 4.3°C are reasonable for a mesoscale model such as RAMS. Since the E for modeled quantities tends to increase with the length of a simulation the average value of 4.3°C for the entire two month simulation is respectable, considering the E surpasses 10°C after just 120 hours of simulation in the MM5 study.

A review of the rest of Table 4.1 shows that the model appeared to have some skill in simulating net radiation and incoming solar radiation as well. However, the results for

the net surface albedo, downward longwave radiation, and snowmelt rates suggest lower skill levels for the model in predicting these quantities.

Parameter	3-m Air Temperature (°C)	Shortwave Radiation (W m^{-2})	Downward Longwave Radiation (W m^{-2})	Net Albedo	Net Radiation (W m^{-2})	Snowmelt Rate (cm hr^{-1})
E	4.3	149	51	0.39	87	0.095
EU	4.2	149	51	0.38	87	0.092
σ_{obs}	6.5	214	40	0.36	94	0.093
σ	5.2	247	60	0.19	102	0.044
N	5893	4782	4612	6157	4983	70

Table 4.1: The root mean square error (*E*), root mean square error with bias removed (*EU*), standard deviation of the observations (σ_{obs}), and standard deviation of the model (σ) for the listed parameter. The parameter N represents the number of comparisons for each parameter.

4.7 Perturbation Simulations

In this section the results of the perturbation simulations are compared with those of the control. The two perturbation simulations were the enhanced shrub and polluted snow cases. In the enhanced shrub simulation all the moist and moist/wet tundra categories on the North Slope were replaced with shrubs. This produced a 343% increase in the area of the fine grid covered by shrubs. In addition, the average shrub height was increased 50%. Figure 4.21 shows the distribution of shrubs in the control and enhanced shrub simulations. Also shown in Figure 4.21 is the initial SWE for the 1996 control and enhanced shrub simulations. It can be seen that the SWE was greater over much of the domain in the enhanced shrub simulation. The same general patterns held for the other two years. In the polluted snow simulation the initial snow albedo was decreased by 0.1. In all other respects the perturbation runs were identical to the control, and therefore any observed differences in the results can be attributed to the perturbations themselves.

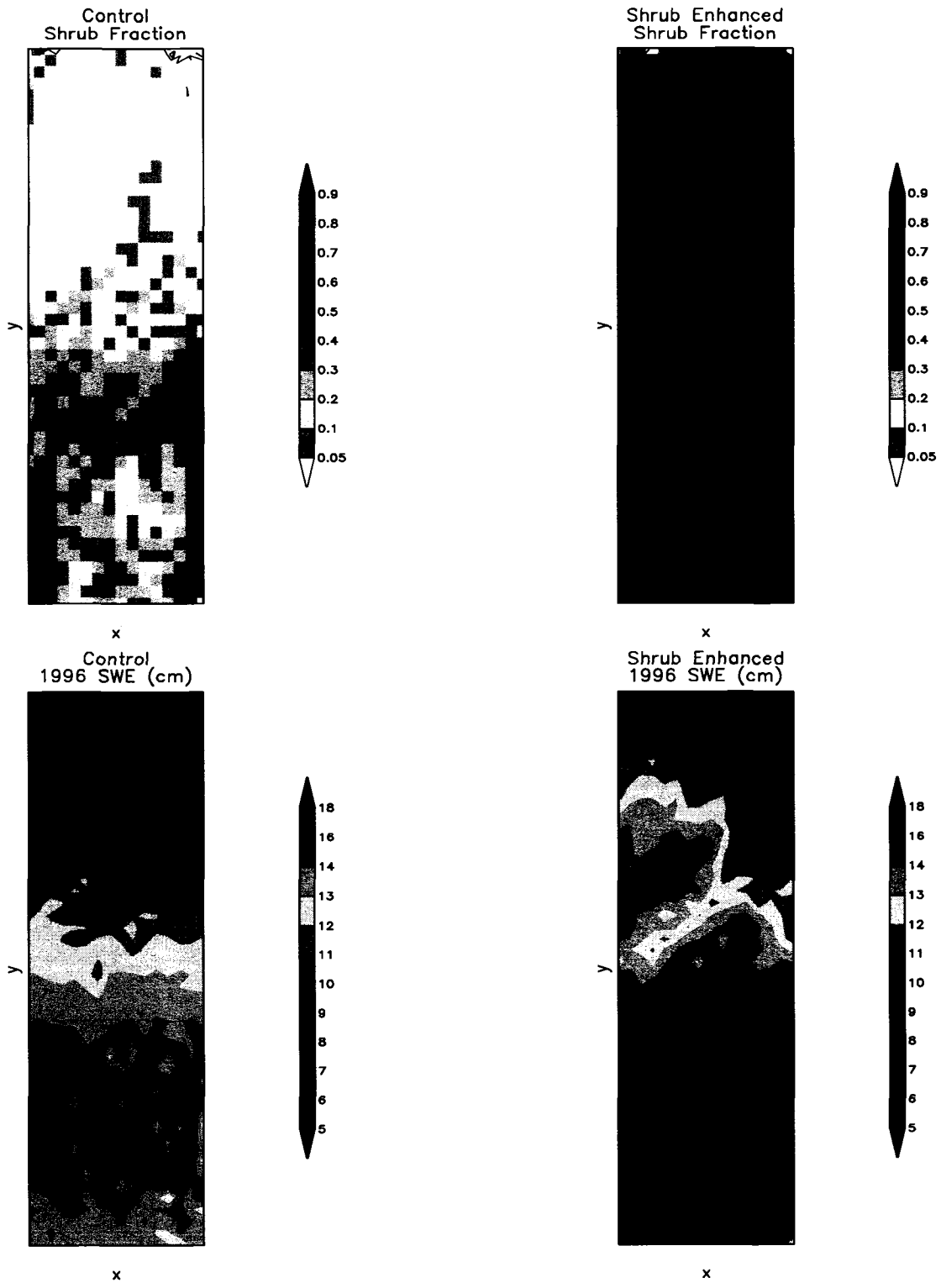

Figure 4.21: Top panels show the fraction of each grid cell covered with shrubs in control and enhanced shrub simulations. Bottom panels show the initial SWE for the 1996 control and enhanced shrub simulations.

Figure 4.22 shows the time evolution of domain average SWE in each year for all three simulations. Domain average in this discussion refers to the average over the fine grid. In each year the enhanced shrub simulation initially had more snow than the control. This is to be expected since the shrubs reduce blowing snow losses during the winter months. The melt rate in the enhanced shrub simulation proceeded more rapidly than in control, especially during the onset of melt, and the snow melted off 11 days earlier. This is due to the warming of the air and emission of longwave radiation by the protruding shrubs. The melt rate in the shrub simulation began to slow and approach that of the control simulation toward the end of the melt period. This is likely due to the shading effect of the shrubs becoming stronger as the snowpack decreased in depth.

The melt rate in the polluted snow case was also faster than the control, but not as fast as in the shrubs. However, since the initial snow depth was the same as in the control the differences in depth during the melt period are greatest in this simulation. The polluted snow also melted off about five days faster than in the control case.

Figure 4.23 shows domain-averaged surface sensible heat flux for the three simulations. The sensible heat flux started off small or negative with a weak diurnal cycle in all simulations. As more snow-free areas appeared daytime sensible heat flux grew larger in all the simulations. The sensible heat flux in the shrub simulation was much higher, often by 50 W m^2, during the snow-covered period of the simulation than in the control; see Figure 4.24. This is due to the relatively warm shrubs protruding through the snowpack. As the snow melted away the sensible heat flux in the shrub simulation became smaller than in the control. This was due to the greater amount of exposed soil in the modeled shrubs. The energy absorbed by the soil was used to melt the ice and

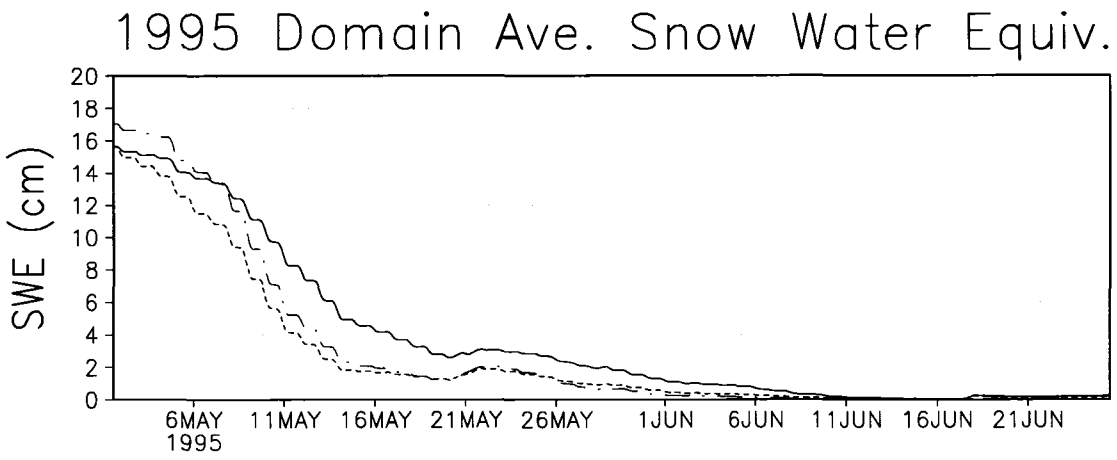

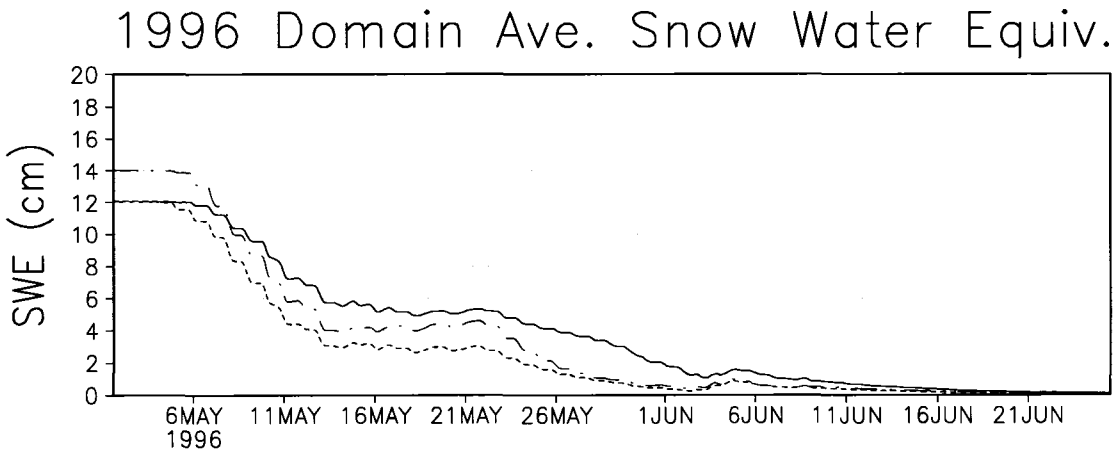

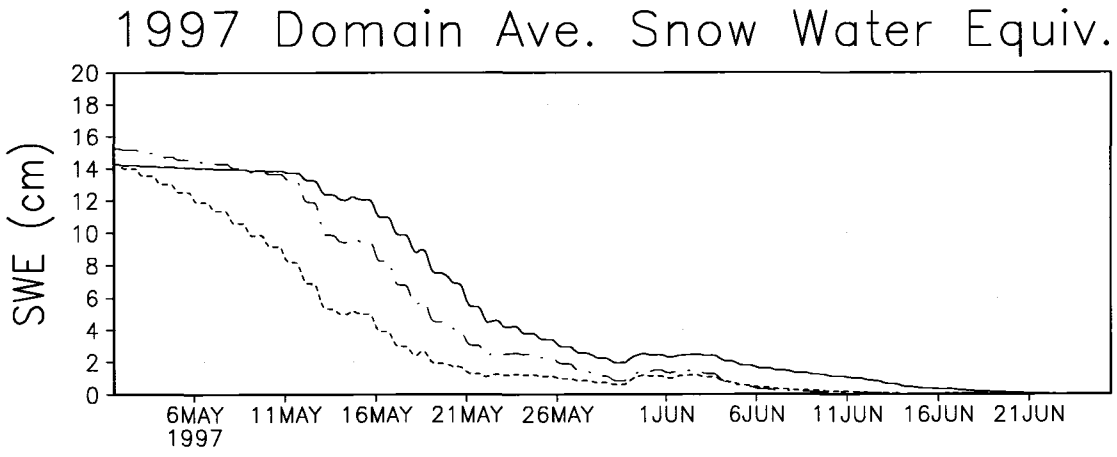

Figure 4.22: Domain-averaged SWE for the control (black solid) shrub enhanced (green dash-dot) and polluted snow (red dashed) runs.

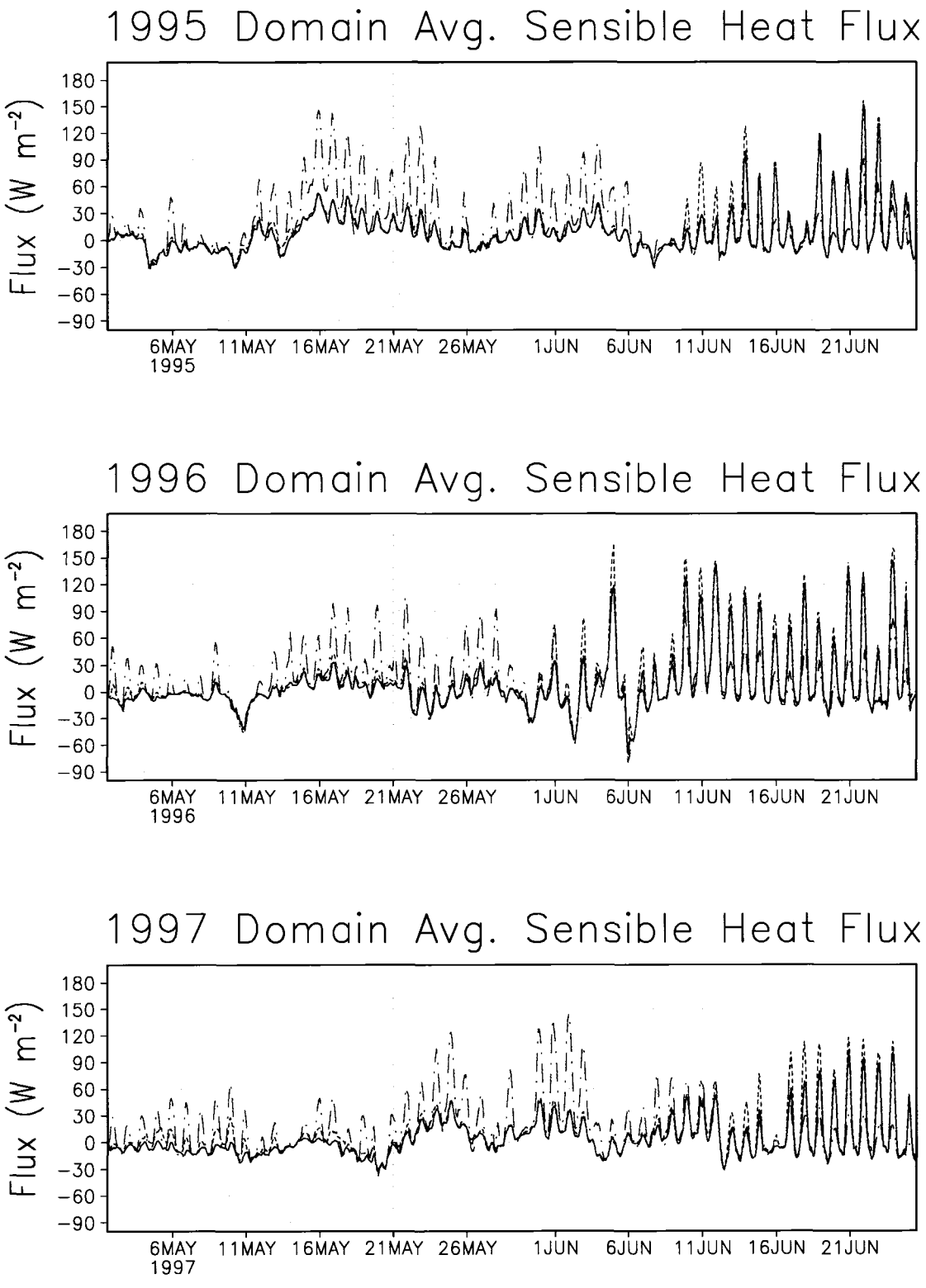

Figure 4.23: Domain-averaged sensible heat flux for the control (black solid) shrub enhanced (green dash-dot) and polluted snow (red dashed) runs.

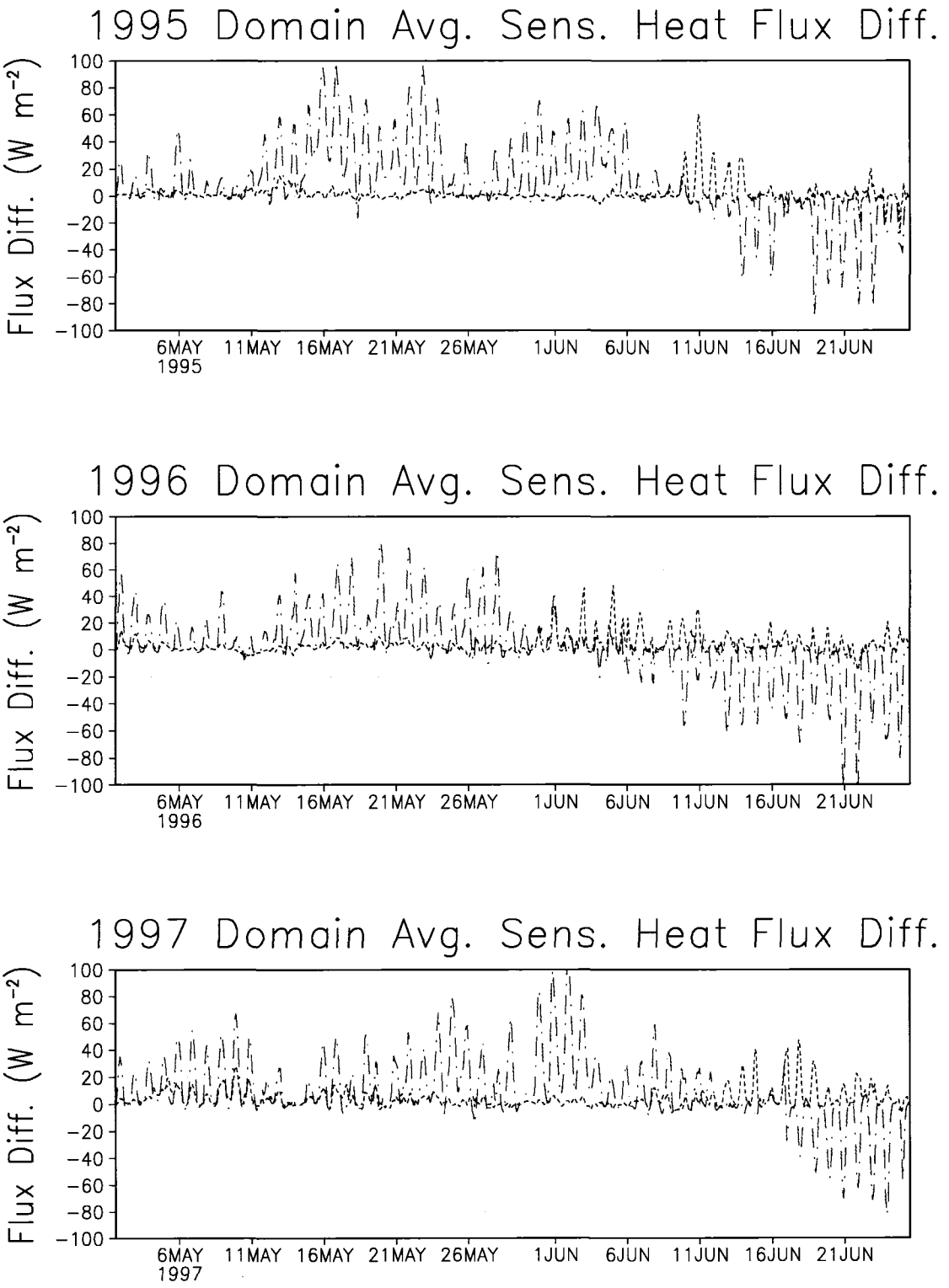

Figure 4.24: The differences in sensible heat flux from the control run for the enhanced shrub (green dash-dot line) and polluted snow (red dashed line) simulations. These values were obtained by subtracting the control run values from the values of the other two simulations.

therefore was not available to raise the surface temperature. The tundra vegetation covered more of the ground and cut off the cold soil from the overlying air. Since the tundra vegetation had a much lower heat capacity it could easily warm above ambient air temperature. However, it is not certain if this effect is seen in reality since in most cases the tundra organic mat lies beneath shrubs. In addition, observations by Chapin et al. (2000) do not suggest any strong depression in sensible heat fluxes over shrub tundra. LEAF-2 can not simulate such a double canopy in its present state so there was no choice but to have bare soil underlying the shrubs. The sensible heat flux averaged 17 W m^{-2} higher in the shrub run during May.

The sensible heat flux in the polluted snow simulation was closer to that in the control run. This is expected since the snow is limited to 0° C regardless of how low the albedo is. The main differences occur when the snow temperature is well below freezing and solar radiation is strong. In these cases the polluted snow can warm to greater temperatures than clean snow and produce a larger sensible heat flux. The sensible heat flux in the later part of the simulation was slightly greater in the polluted snow case. This is likely due to the slightly warmer soil from the earlier snow melt. The sensible heat flux averaged 2 W m^{-2} higher in the polluted snow run during the month of May.

Figure 4.25 shows the domain-averaged latent heat flux. It can be seen that in all the simulations the latent heat flux peaked during the snow melt period. The latent heat flux started off small and gradually increased as the amount of liquid water increased during the melt period. The latent heat flux tapered off late in the period as the amount of surface moisture declined. Higher peak values occurred in the enhanced shrub case due to the warmer air. Slightly higher peak values occurred in the polluted snow case when the

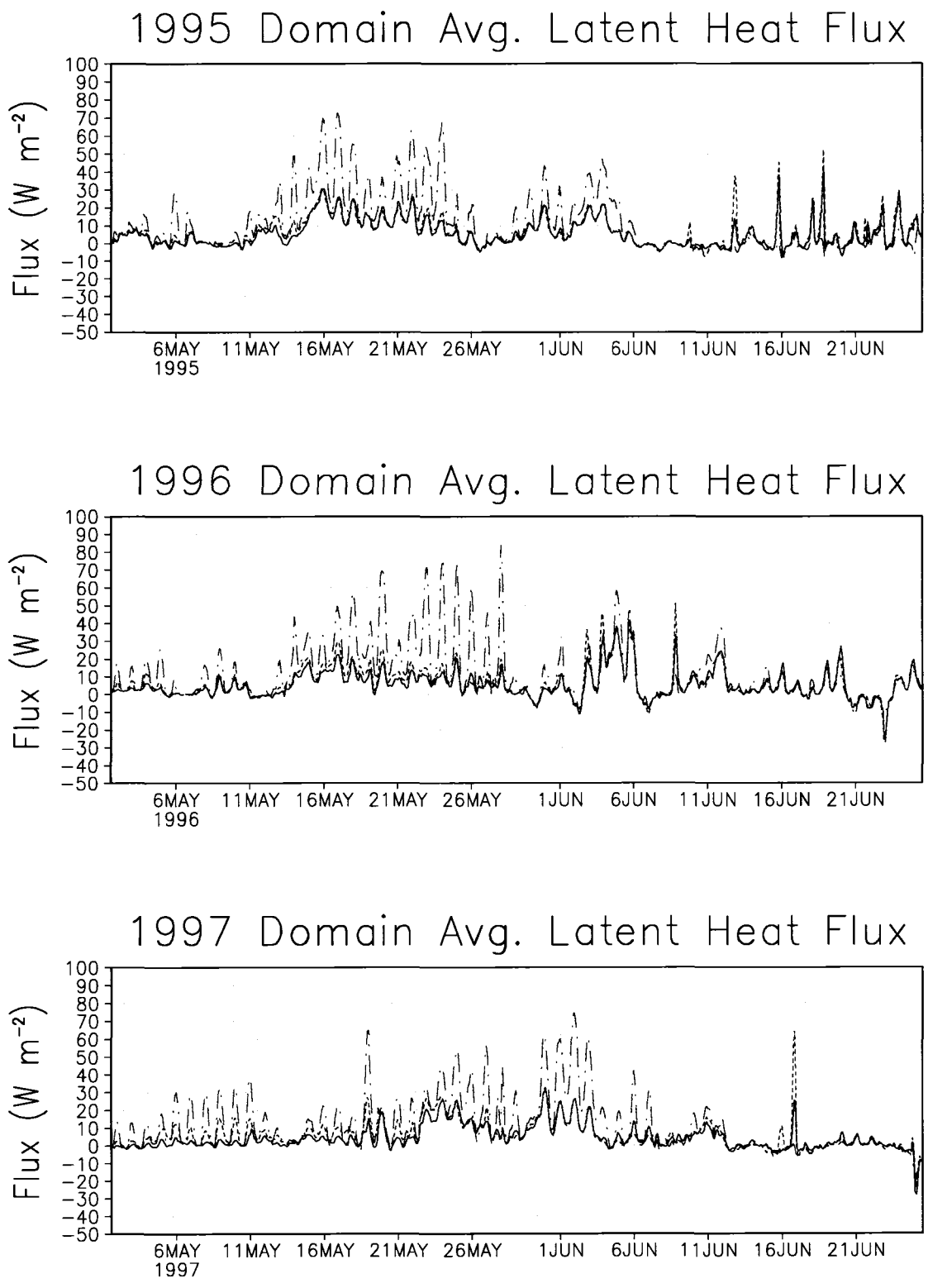

Figure 4.25: Domain-averaged latent heat flux for the control (black solid line) shrub enhanced (green dash-dot line) and polluted snow (red dashed line) runs.

polluted snow was able to warm the nearby air more than clean snow. Figure 4.26 shows the differences in latent heat flux between the different simulations. On average, during the month of May, the latent heat flux was 10 and 2 W m^{-2} higher in the shrub and polluted snow cases respectively.

Finally, Figure 4.27 shows the domain-averaged net radiation. The net radiation gradually increased toward the end of the simulations as the albedo decreased and incoming solar radiation increased. As expected, the net radiation was greater in both perturbation simulations during the snow-covered period due to the lower net surface albedo. The differences in net radiation between the various simulations are shown in Figure 4.28. The net radiation averaged 28 and 23 W m^{-2} higher during the month of May in the shrub and polluted snow simulations respectively.

Figure 4.29 shows the domain-averaged 2 m air temperature. The pattern of temperature closely followed the pattern of sensible heat fluxes discussed earlier. Figure 4.30 shows the differences in air temperatures between the perturbation and control runs. The largest differences occurred in the shrub enhanced simulation. During the month of May, the shrub enhanced simulation averaged 1.5°C warmer than the control. The temperatures in the polluted snow run averaged only 0.5°C warmer.

The domain-averaged planetary boundary layer height is shown in Figure 4.31. The planetary boundary layer height was generally less than 1000 m, but occasionally peaked around 1500 m. The deepest boundary layer occurred in the shrub enhanced simulation, and is a result of the greater sensible heat flux generated by the protruding shrubs. Differences in the boundary layer depths between the perturbation and control runs are shown in Figure 4.32. The planetary boundary depth in the shrub enhanced simulation

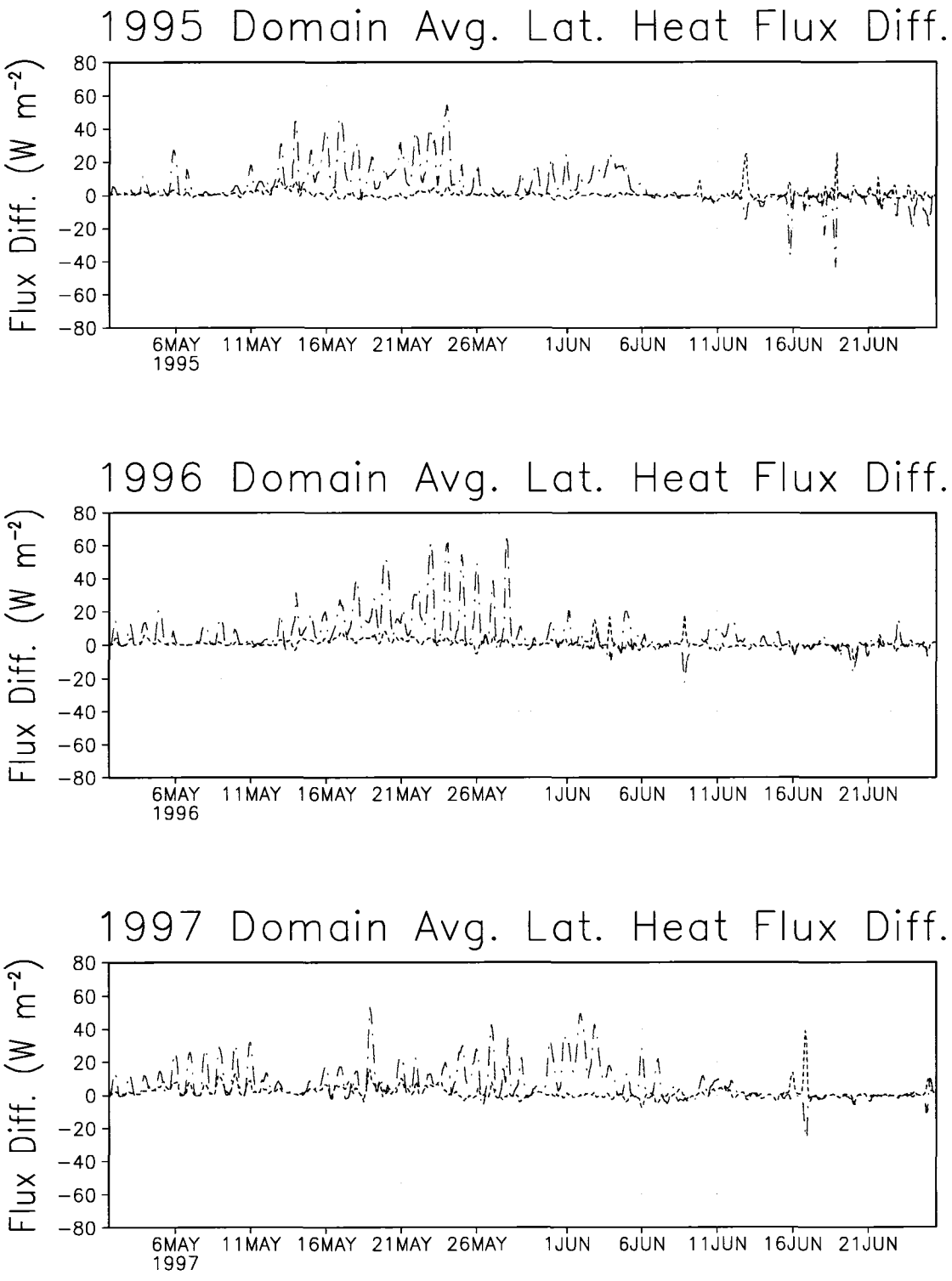

Figure 4.26: The differences in latent heat flux from the control run for the enhanced shrub (green dash-dot line) and polluted snow (red dashed line) simulations. These values were obtained by subtracting the control run values from the values of the other two simulations.

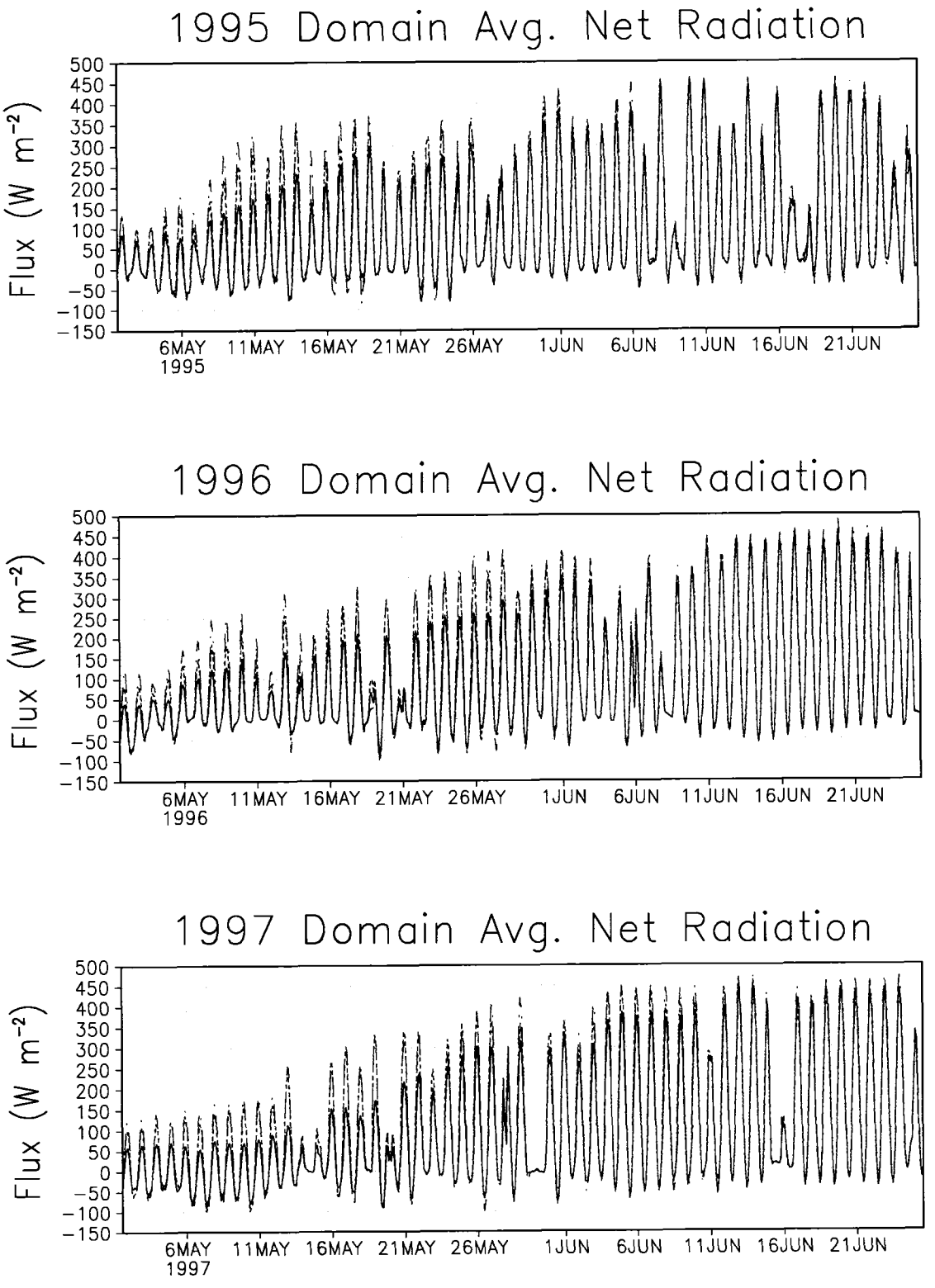

Figure 4.27: Domain-averaged net radiation for the control (black solid line) shrub enhanced (green dash-dot line) and polluted snow (red dashed line) runs.

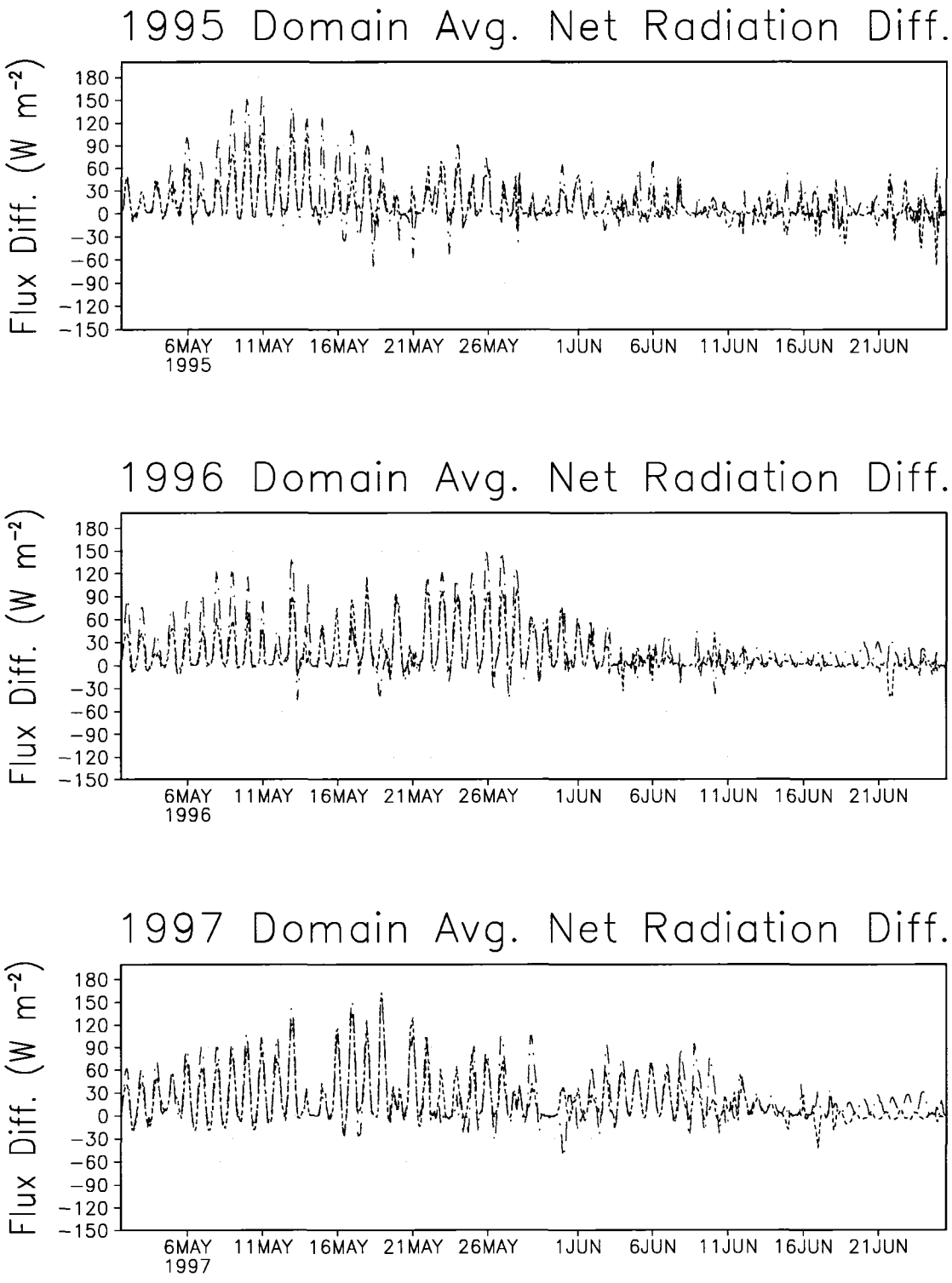

Figure 4.28: The differences in net radiation from the control run for the enhanced shrub (green dash-dot line) and polluted snow (red dashed line) simulations. These values were obtained by subtracting the control run values from the values of the other two simulations.

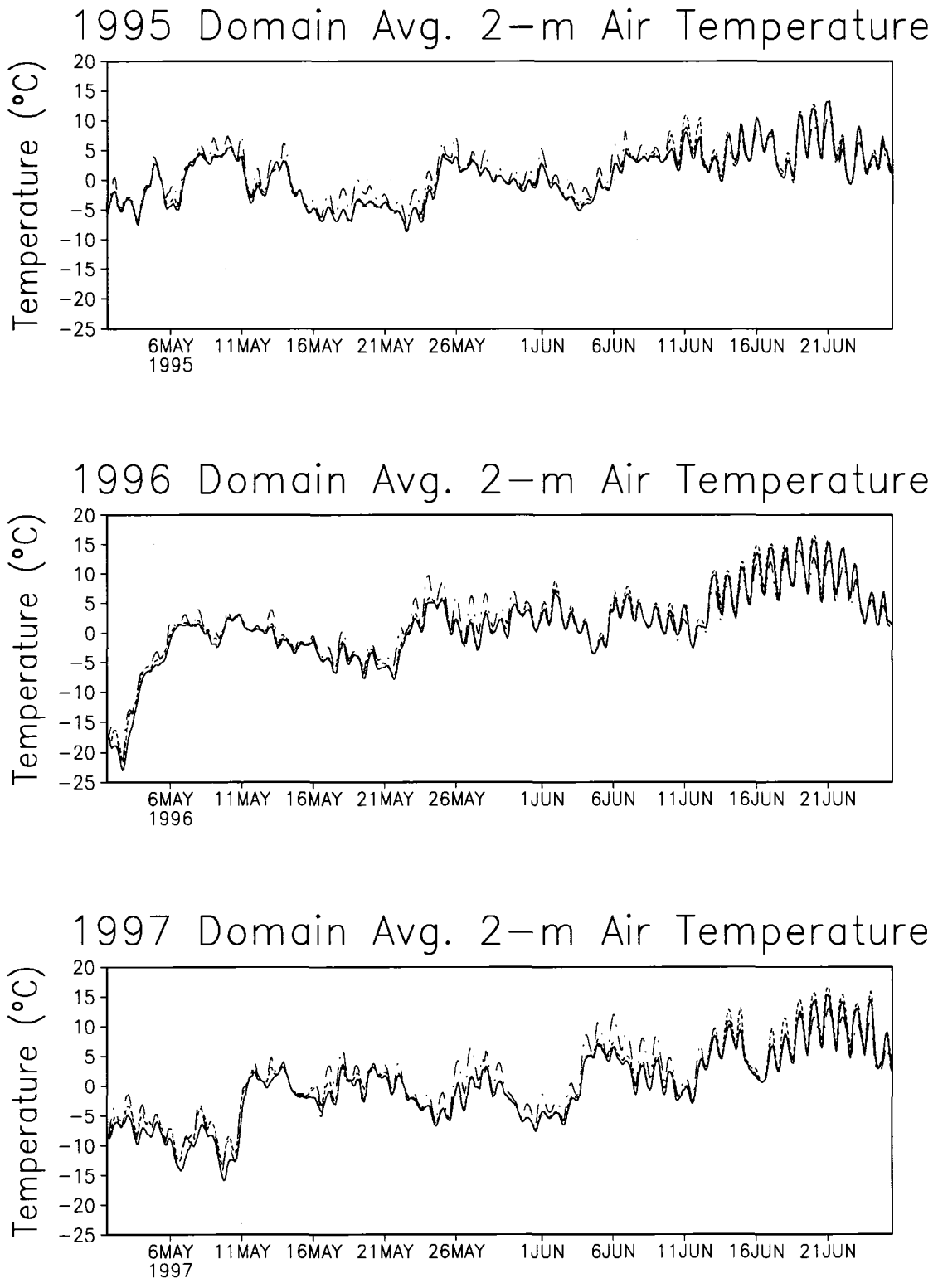

Figure 4.29: Domain-averaged 2 m air temperature for the control (black solid line) shrub enhanced (green dash-dot line) and polluted snow (red dashed line) runs.

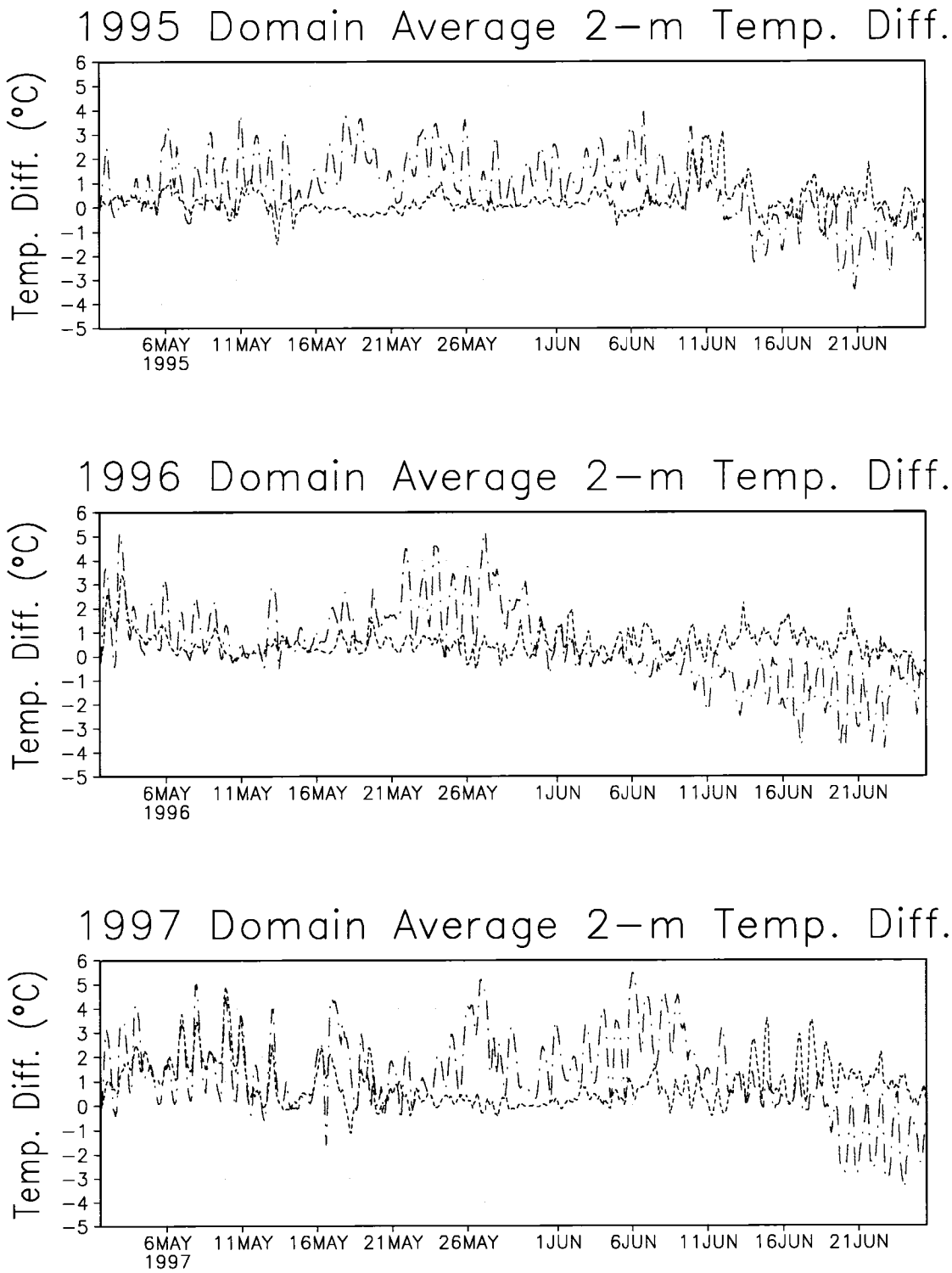

Figure 4.30: The differences in 2 m air temperature from the control run for the enhanced shrub (green dash-dot line) and polluted snow (red dashed line) simulations. These values were obtained by subtracting the control run values from the values of the other two simulations.

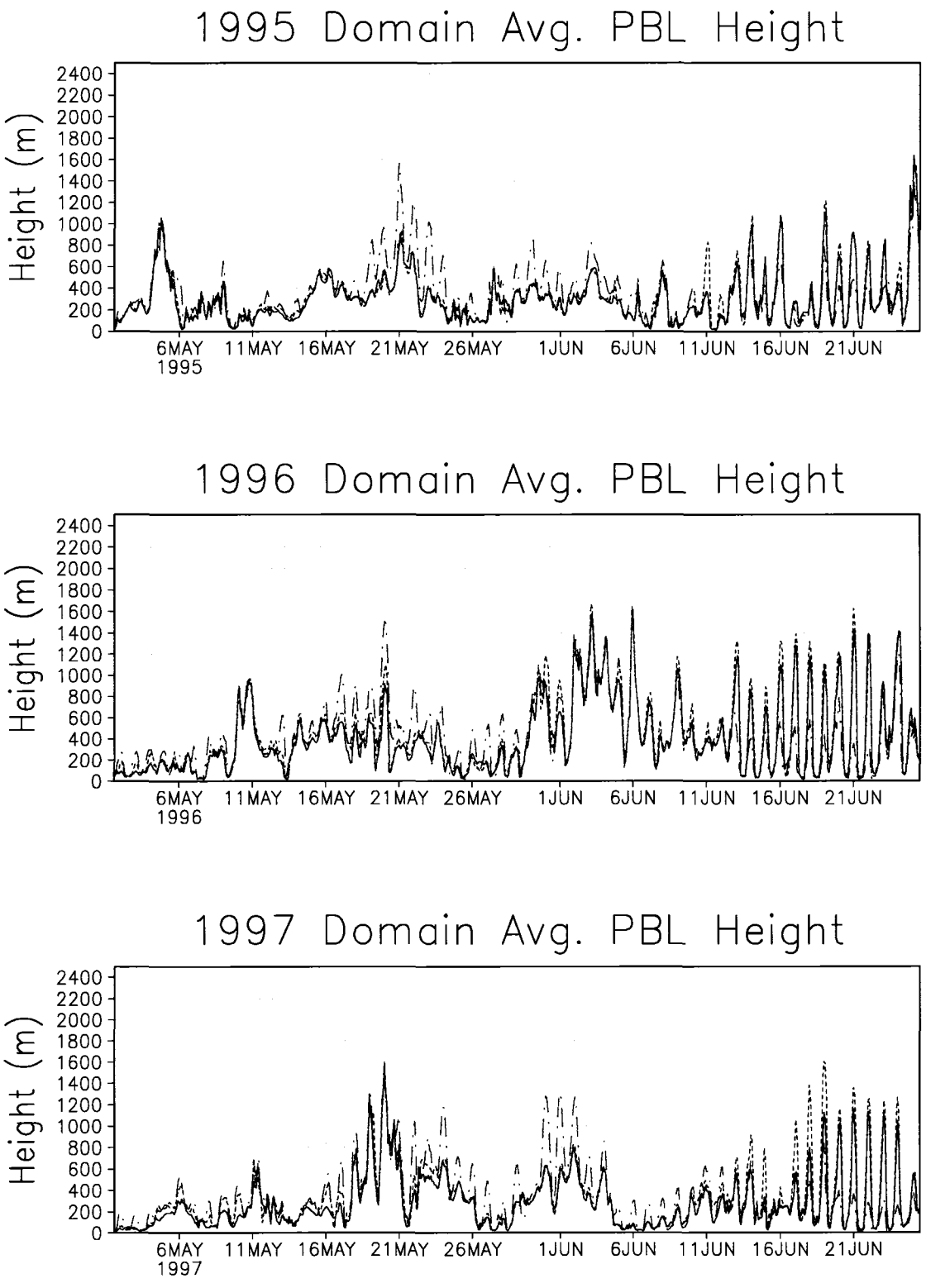

Figure 4.31: Domain-averaged planetary boundary layer height for the control (black solid line) shrub enhanced (green dash-dot line) and polluted snow (red dashed line) runs.

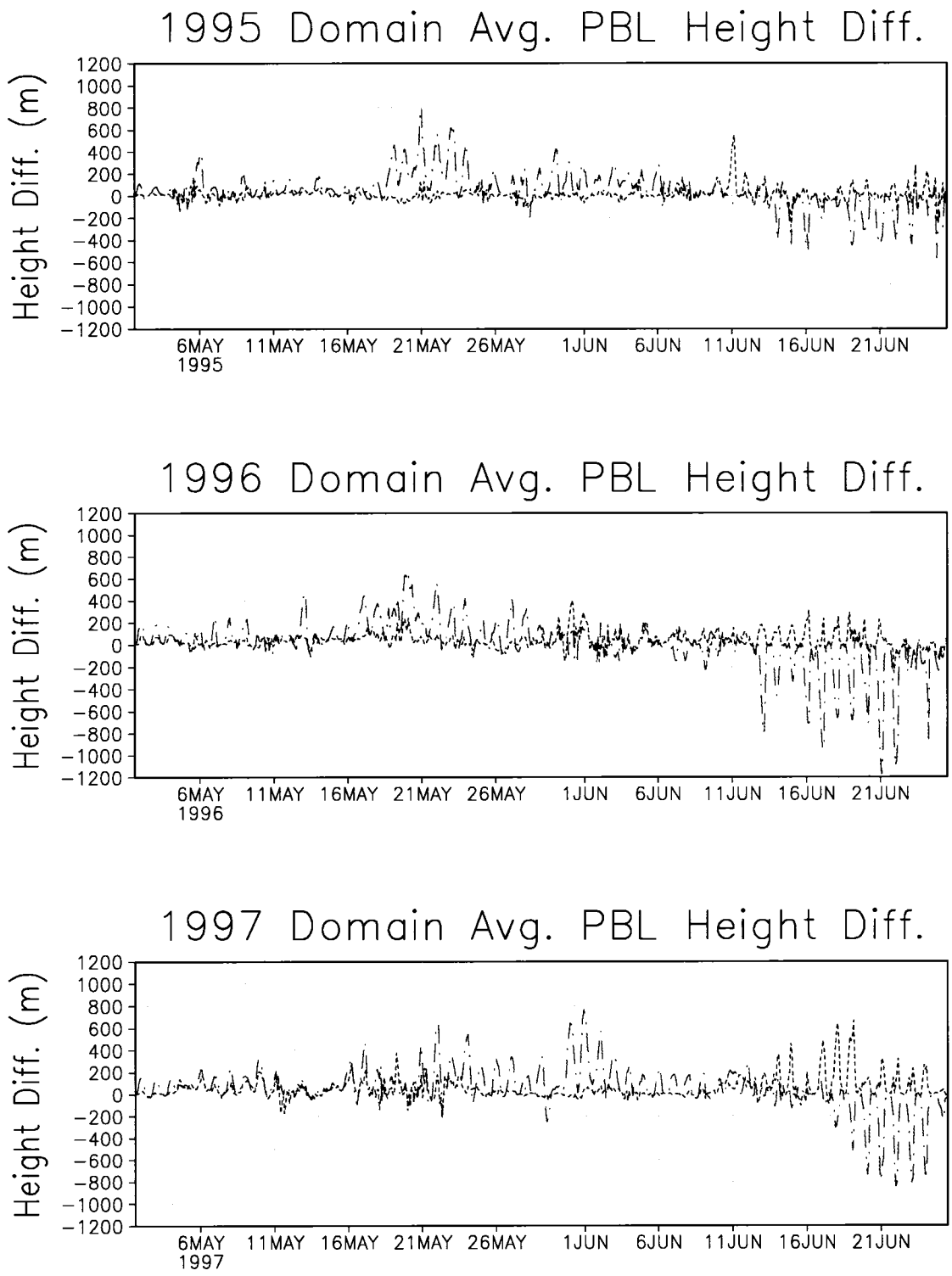

Figure 4.32: The differences in planetary boundary layer height from the control run for the enhanced shrub (green dash-dot line) and polluted snow (red dashed line) simulations. These values were obtained by subtracting the control run values from the values of the other two simulations.

often grew several hundred meters deeper than in the control during the month of May, and on average was 108 m deeper when snow was present. The difference between the polluted snow case and the control run was generally smaller, averaging 25 m deeper in the polluted snow run when the snow was present.

4.8 Statistical Comparison of the Perturbation Runs to the Control Run

In order to determine the significance of these perturbations paired t-tests were used to construct confidence intervals for the mean differences in the variables mentioned in the previous section. Table 4.2 displays the 99.9% confidence intervals for the mean differences between 2 m air temperature, sensible heat flux, latent heat flux, net radiation, snowmelt rate, planetary boundary layer height, and snow-free date. These values were determined by calculating the mean difference over all grid points for each time step during May of each year examined.

Parameter	Shrub-Control	Carbon-Control
2-m Air Temperature (°C)	$1.5 \pm < 0.1$	$0.5 \pm < 0.1$
Sensible Heat Flux (W m^{-2})	16.8 ± 0.1	$2.3 \pm < 0.1$
Latent Heat Flux (W m^{-2})	10.1 ± 0.1	$1.6 \pm < 0.1$
Net Radiation (W m^{-2})	28.4 ± 0.2	22.8 ± 0.2
Planetary Boundary Layer Height (m)	108 ± 1	25 ± 1
Snow Melt Rate (cm hr^{-1})	0.004 ± 0.002	0.002 ± 0.002
Snow-free Date (days)	11 ± 1	$5 \pm < 1$

Table 4.2: The mean difference between the shrub and control (shrub-control) and carbon and control (carbon-control) simulations with 99.9% confidence interval. There were N=695520 comparisons for each parameter.

The confidence intervals show that all the differences were significant at the 99.9% confidence level except for the snow melt rate in the carbon simulation. The 99.9% confidence interval for the snow melt rate in the carbon case includes zero, and so is not significantly different from the rate in the control run. However, this analysis shows that most of the parameters of interest in the perturbation runs are significantly different at a

very high level of confidence. Furthermore, these results strengthen the theory that shrub expansion and black carbon deposition can have a significant impact on near-surface weather and climate during the snowmelt period and should be accounted for in long-term simulations of global climate.

Chapter 5

CONCLUDING REMARKS

5.1 Summary and Conclusions

Shrub encroachment in the Arctic increases the amount of snow retained through the winter by reducing the amount lost through sublimation of blowing snow. The shrubs break the force of the wind, making it more difficult for snow particles to become airborne. As a result, less snow particle surface area is exposed to the air and the loss due to sublimation is reduced. The net result is a deeper end-of-winter snowpack given the same amount of over-winter precipitation.

Although shrub invasion leads to a deeper end-of-winter snowpack, the spring melt season is accelerated and shortened due to the increase in net radiation created by the shrubs. The shrubs, which are typically much taller than the lichens and mosses of the tundra, are capable of protruding through the snowpack earlier in the melt season. The dark protruding shrubs absorb incoming solar radiation much more efficiently than the high albedo snow and warm to higher temperatures. The relatively warm shrubs then emit longwave radiation to the snow and turbulent sensible heat flux to the surrounding air. The longwave radiation emitted by the shrubs is readily absorbed by the snow, a near blackbody. In addition, the warming of the air above the snow by the shrubs allows for warming of the snowpack through turbulent sensible heat transfer. The shrubs thus

convert incoming shortwave radiation, a form of energy poorly absorbed by snow, to longwave radiation and sensible heat, forms which are readily absorbed by snow. These warming effects more than offset the reduction of shortwave radiation by shading during the primary melt period.

The reduction of snow albedo by soot deposition also leads to enhanced snow ablation during the melt season. The soot allows the snowpack to absorb more of the incoming solar radiation directly. However, soot has relatively less influence on sensible heat flux and air temperatures since, unlike in the case of shrubs, the surface is limited to the freezing point. The temperature of polluted snow only exceeds that of clean snow when the ambient temperature is well below freezing and solar radiation is strong.

In this study RAMS 4.4 was used to simulate the effects of a shrub invasion and soot deposition on snow melt and near-surface air temperature in the Kuparuk Basin of Alaska. First, enhancements were made to the RAMS 4.4 snow model and it was tested offline against observations of snow depth and sensible and latent heat fluxes. In the next step control simulations spanning the tundra snowmelt period form May through late June for three years were run using the present day vegetation distribution and clean snow. The results of these simulations were compared with available observations to see how well the model could simulate reality. Lastly, two perturbation simulations were run, one with most of the present day tundra replaced with shrubs, and another with present day vegetation but snow polluted with soot. The snow melted off 11 days earlier in the shrub enhanced and 5 days earlier in the polluted snow simulation. Near-surface air temperatures averaged 1.5 and 0.5°C warmer during the snowmelt period in the shrub enhanced and polluted snow simulations respectively. In addition, planetary boundary

layer heights averaged 108 m deeper in the shrub enhanced simulation, and 25 m deeper in the polluted snow simulation.

5.2 Future Work

One direction for future work is to run annual simulations which would allow for the exploration of the net effect of the shrubs over the annual cycle. Previous modeling work by Chapin et al. (2000) suggests that invasion of Arctic tundra by shrubs also leads to warming during the summer season due to reduction in albedo. Little is known about how the shrubs affect the winter atmosphere. Due to the fact that solar radiation is small to non-existent in the Arctic during the winter the radiation effects of the shrubs will be inconsequential during this season. However, the reduction in blowing snow will lead to reduced atmospheric moisture which could influence cloud cover, and hence longwave radiation exchange during the winter months. Finally, it would be interesting to run the annual simulations on a global domain to determine if the shrub effects on the Arctic atmosphere teleconnet to other parts of the globe.

REFERENCES

Anderson, E.A., 1976: A point energy and mass balance model of a snow cover, NOAA, 150 pp.

Armstrong, R.L., M.J. Brodzik, K. Knowles, and M. Savoie, 2005: Global monthly EASE-Grid snow water equivalent climatology, National Snow and Ice Data Center, Boulder, CO, USA.

Auer, A.H., 1974: The rain versus snow threshold temperature. *Weatherwise*, **27**, 67.

Baker, D.G., D.L. Ruschy, R.H. Skaggs, and D.B. Wall, 1992: Air temperature and radiation depression associated with a snow cover. *J. Appl. Meteor.*, **31**, 247-254.

Brun, E., E. Martin, V. Simon, C. Gendre, and C. Coleou, 1989: An energy and mass balance model of snowcover suitable for operational avalanche forecasting. *J. Glaciol.*, **35**, 333-342.

Chapin, F.S., III, W. Eugster, J.P. McFadden, A.H. Lynch, and D.A. Walker, 2000: Summer differences among Arctic ecosystems in regional climate forcing. *J. Climate*, **13**, 2002-2010.

Chen, C. and W.R. Cotton, 1983: A one-dimensional simulation of the stratocumulus-capped mixed layer. *Bound.-Layer Meteor.*, **25**, 289-321.

Cohen, J. and D. Rind, 1991: The effect of snow cover on the climate. *J. Climate*, **4**, 689-706.

Cotton, W.R., R.A. Pielke, Sr., R.L. Walko, G.E. Liston, C.J. Tremback, H. Jiang, R.L. McAnelly, J.Y. Harrington, M.E. Nicholls, G.G. Carrio, and J.P. McFadden, 2003: RAMS 2001: Current status and future directions. *Meteor. Atmos. Phys.*, **82**, 5-29.

Dickinson, R.E., A. Henderson-Sellers, P.J. Kennedy, and M.F. Wilson, 1986: Biosphere-Atmosphere Transfer Scheme (BATS) for the NCAR Community Climate Model: Technical Report NCAR/TN-275+STR, National Center for Atmospheric Research, Boulder, CO, USA.

Douville, H., J.-F. Royer, and J.-F. Mahfouf, 1995a: A new snow parameterization for the Meteo-France climate model. Part I: Validation in stand alone experiments. *Climate Dyn.*, **12**, 21-35.

Douville, H., J.-F. Royer, and J.-F. Mahfouf, 1995b: A new snow parameterization for the Météo-France climate model. Part II: Validation in a 3-D GCM experiment. *Climate Dyn.*, **12**, 36-52.

Ellis, A.W. and D.J. Leathers, 1998: A quantitative approach to evaluating the effects of snow cover on cold airmass temperatures across the U.S. Great Plains. *Wea. Forecasting*, **13**, 688-701.

Essery, R.L.H., E. Martin, H. Douville, A. Fernandez, and E. Brun, 1999: A comparison of four snow models using observations from an alpine site. *Climate Dyn.*, **15**, 583-593.

FAO, 1997: Digital soil map of the world and derived soil properties. Version 3.5. FAO.

Fernandez, A., 1998: An energy balance model of seasonal snow evolution. *Phys. Chem. Earth*, **23**, 661-666.

Goetz, S.J., A.G. Bunn, G.J. Fiske, and R.A. Houghton, 2005: Satellite-observed photosynthetic trends across boreal North America associated with climate and fire disturbance. *Proc. Natl. Acad. Sci. USA*, **102**, 13521-13525.

Hansen, J., and L. Nazarenko, 2004: Soot climate forcing via snow and ice albedos. *Proc. Natl. Acad. Sci. USA*, **101**, 423-428.

Hardy, J.P., R.E. Davis, R. Jordan, W. Ni, and C.E. Woodcock, 1998: Snow ablation modelling in a mature aspen stand of the boreal forest. *Hydrol. Process.*, **12**, 1763-1778.

Jin, J., X. Gao, S. Sorooshian, Z.-L. Yang, R. Bales, R.E. Dickinson, S.-F. Sun, and G.-X. Wu, 1999: One-dimensional snow water and energy balance model for vegetated surfaces. *Hydrol. Process.*, **13**, 2467-2482.

Jordan, R., 1991: A one-dimensional temperature model for a snow cover: Technical documentation for SNTHERM.89, U.S. Army Cold Regions Research and Engineering Lab, Hanover, NH, 49 pp.

Jordan, R.E., E.L. Andreas, and A.P. Makshtas, 1999: Heat budget of snow-covered sea ice at the North Pole 4. *J. Geophys. Res.*, **104**, 7785-7806.

Kalnay, E., M. Kanamitsu, R. Kistler, W. Collins, D. Deaven, L. Gandin, M. Iredell, S. Saha, G. White, J. Woollen, Y. Zhu, M. Chelliah, W. Ebisuzaki, W. Higgins, J. Janowiak, M. K.C., C. Ropelewski, J. Wang, A. Leetmaa, R. Reynolds, R. Jenne, and D. Joseph, 1996: The NCEP/NCAR 40-year reanalysis project. *Bull. Amer. Meteor. Soc.*, **77**, 437-471.

Kane, D.L., R.E. Gieck, and L.D. Hinzman, 1997: Snowmelt modeling at small Alaskan Arctic watershed. *J. Hydrol. Eng.*, **2**, 204-210.

König, M. and M. Sturm, 1998: Mapping snow distribution in the Alaskan Arctic using air photos and topographic relationships. *Water Resour. Res.*, **34**, 3471–3483.

Leathers, D.J. and D.A. Robinson, 1993: The association between extremes in North American snow cover extent and United States temperatures. *J. Climate*, **6**, 1345-1355.

Link, T. and D. Marks, 1999: Distributed simulation of snowcover mass- and energy-balance in the boreal forest. *Hydrol. Process.*, **13**, 2439-2452.

Liston, G.E., 1995: Local advection of momentum, heat, and moisture during the melt of patchy snow covers. *J. Appl. Meteor.*, **34**, 1705-1715.

Liston, G.E., 2004: Representing subgrid snow cover heterogeneities in regional and global models. *J. Climate*, **17**, 1381-1397.

Liston, G.E. and M. Sturm, 1998a: A snow-transport model for complex terrain. *J. Glaciol.*, **44**, 498-516.

Liston, G.E. and M. Sturm, 1998b: Global seasonal snow classification system, National Snow and Ice Data Center, Boulder, CO, USA.

Liston, G.E. and M. Sturm, 2002: Winter precipitation patterns in Arctic Alaska determined from a blowing-snow model and snow-depth observations. *J. Hydrometeor.*, **3**, 646-659.

Liston, G.E. and K. Elder, 2006: A meteorological distribution system for high-resolution terrestrial modeling (Micromet). *J. Hydrometeor.*, **7**, 217-234.

Liston, G.E., R.A. Pielke, Sr., and E.M. Greene, 1999a: Improving first-order snow-related deficiencies in a regional climate model. *J. Geophys. Res.*, **104**, 19559-19567.

Liston, G.E., J.P. McFadden, M. Sturm, and R.A. Pielke, Sr., 2002: Modelled changes in arctic tundra snow, energy and moisture fluxes due to increased shrubs. *Glob. Change Biol.*, **8**, 17-32.

Liston, G.E., J.-G. Winther, O. Bruland, H. Elvehoey, and K. Sand, 1999b: Below-surface ice melt on the coastal Antarctic ice sheet. *J. Glaciol.*, **45**, 273-285.

Louis, J.F., M. Tiedtke, and J.F. Geleyn, 1981: A short history of the operational PBL parameterization at ECMWF. *Workshop on Planetary Boundary Layer Parameterization*, Shinfield Park, Reading, United Kingdom, ECMWF, 59-80.

Mellor, G.L. and T. Yamada, 1982: Development of a turbulence closure model for geophysical fluid problems. *Rev. Geophys. Space Phys.*, **20**, 851-875.

Mesinger, F., G. DiMego, E. Kalnay, K. Mitchell, P.C. Shafran, W. Ebisuzaki, D. Jovic, J. Woollen, E. Rogers, E.H. Berbery, M.B. Ek, Y. Fan, R. Grumbine, W. Higgins, H. Li, Y. Lin, G. Manikin, D. Parrish, and W. Shi, 2006: North American Regional Reanalysis. *Bull. Amer. Meteor. Soc.*, **87**, 343-360.

Muller, S.V., A.E. Racoviteanu, and D.A. Walker, 1999: Landsat MSS-derived land-cover map of northern Alaska: Extrapolation methods and a comparison with photo-interpreted and AVHRR-derived maps. *Int. J. Remote Sens.*, **20**, 2921-2946.

Namias, J., 1985: Some empirical evidence for the influence of snow cover on temperature and precipitation. *Mon. Wea. Rev.*, **113**, 1542-1553.

Narapusetty, B. and N. Mölders, 2005: Evaluation of snow depth and soil temperatures predicted by the Hydro-Thermodynamic Soil-Vegetation scheme coupled with the Fifth-Generation Pennsylvania State University-NCAR Mesoscale Model. *J. Appl. Meteor.*, **44**, 1827-1843.

Olson, J.S., 1994a: Global ecosystem framework-definitions: USGS EROS Data Center Internal Report, Sioux Falls, SD, 37 pp.

Olson, J.S., 1994b: Global ecosystem framework-translation strategy: USGS EROS Data Center Internal Report, Sioux Falls, SD, 39 pp.

Otterman, J., M.D. Novak, and D.O.C. Starr, 1993: Turbulent heat transfer from a sparsely vegetated surface: two-component representation. *Bound.-Layer Meteor.*, **64**, 409-420.

Pielke, R.A., Sr., 2002: *Mesoscale Meteorological Modeling*. 2nd ed. Vol. 78, *International Geophysics Series*, Academic Press, 676 pp.

Sellers, P.J., F.G. Hall, R.D. Kelly, A. Black, D. Baldocchi, J. Berry, M. Ryan, K.J. Ranson, P.M. Crill, D.P. Lettenmaier, H. Margolis, J. Cihlar, J. Newcomer, D. Fitzjarrald, P.G. Jarvis, S.T. Gower, D. Halliwell, D. Williams, B. Goodison, D.E. Wickland, and F.E. Guertin, 1997: BOREAS in 1997: Experiment overview, scientific results, and future directions. *J. Geophys. Res.*, **102**, 28731-28769.

Shewchuk, S.R., 1997: Surface mesonet for BOREAS. *J. Geophys. Res.*, **102**, 29077-29082.

Smagorinsky, J., S. Manabe, and J.L. Holloway, Jr., 1965: Numerical results from a nine-level general circulation model of the atmosphere. *Mon. Wea. Rev.*, **93**, 727-798.

Strack, J.E., R.A. Pielke, Sr., and J. Adegoke, 2003: Sensitivity of model-generated daytime surface heat fluxes over snow to land-cover changes. *J. Hydrometeor.*, **4**, 24-42.

Strack, J.E., G.E. Liston, and R.A. Pielke, Sr., 2004: Modeling snow depth for improved simulations of snow-vegetation-atmosphere interactions. *J. Hydrometeor.*, **5,** 723-734.

Sturm, M. and C. Racine, 2005: A Half-Century of change in arctic Alaskan shrubs: a photographic-based assessment, National Snow and Ice Data Center, Boulder, CO, USA.

Sturm, M., J. Holmgren, and G.E. Liston, 1995: A seasonal snow cover classification system for local to global applications. *J. Climate*, **8**, 1261-1283.

Sturm, M., C. Racine, and K. Tape, 2001a: Increasing shrub abundance in the Arctic. *Nature*, **411**, 546-547.

Sturm, M., T. Douglas, C. Racine, and G.E. Liston, 2005: Changing snow and shrub conditions affect albedo with global implications. *J. Geophys. Res.*, **110**.

Sturm, M., J.P. McFadden, G.E. Liston, F.S. Chapin, III, C.H. Racine, and J. Holmgren, 2001b: Snow-shrub interactions in Arctic tundra: A hypothesis with climate implications. *J. Climate*, **14**, 336-344.

Tape, K., M. Sturm, and C. Racine, 2006: The evidence for shrub expansion in Northern Alaska and the Pan-Arctic. *Glob. Change Biol.*, **12**, 686-702.

Walko, R.L., L.E. Band, J. Baron, T.G.F. Kittel, R. Lammers, T.J. Lee, D. Ojima, R.A. Pielke, Sr., C. Taylor, C. Tague, C.J. Tremback, and P.L. Vidale, 2000: Coupled atmosphere-biophysics-hydrology models for environmental modeling. *J. Appl. Meteor.*, **39**, 931-944.

Yang, Z.-L., R.E. Dickinson, A. Robock, and K.Y. Vinnikov, 1997: Validation of the snow submodel of the Biosphere-Atmosphere Transfer Scheme with Russian snow cover and meteorological observational data. *J. Climate*, **10**, 353-373.